CODEN:LUTEDX/(TEIE-5424)/1-116(2019)

Industrial Electrical Engineering and Automation

Elbow Design, Servo Motor Selection and Control Implementation of the Agile Parallel Kinematic Manipulator

Felix Lundblad

Hampus Farmängen

Division of Industrial Electrical Engineering and Automation
Faculty of Engineering, Lund University

Lund University
Faculty of Engineering

Division of Industrial
Electrical Engineering and Automation

Division of Industrial Production

Elbow design, servo motor selection and control implementation of the Agile Parallel Kinematic Manipulator

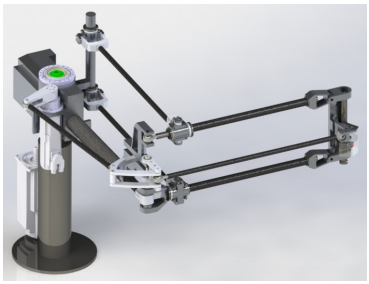

Authors
Felix Lundblad
Hampus Farmängen

Industrial Supervisors
Magnus Olsson
Adam Nilsson

Academic Supervisors
Gunnar Lindstedt
Hans Walter

Examiners
Johan Björnstedt
Carin Andersson

Opponent
Piotr Czernicki
Mathias Kallmert

May, 2019

Abstract

The purpose of this work was to contribute to the creation of a prototype of a new type of robot called Agile Parallel Kinematic Manipulator or AgilePKM for short. Designing, building and controlling a new type of robot is a task which goes beyond the scope of any master thesis project, but there are subtasks which are more suitable to handle within the available time frame. A principle design will be handled, meaning no actual hardware will be available or constructed. There are three subtasks that are addressed as described below.

The AgilePKM consists of many joints and links where one of the most crucial joints is the elbow joint. The first subtask was to construct this joint to efficiently meet the requirements and advantages of the new robot structure. The elbow joint is a very exposed joint as it exclusively actuates vertical movements, carrying not only the payload but the forearm structure as well. This was to be done while facilitating sufficient movement for the extensive working space and minimizing weight and cost for the proof-of-concept prototype. To ensure that these targets were fulfilled an adapted needs identification process was carried out followed by benchmarking and concept generation. From this the most promising concept was chosen and further developed to reach the most suitable design.

The second subtask was to select servo motors. This task involved making a lot of assumptions and asking for specifications which was far from final due to the lack of a mechanical design. This was the reason to present a general recipe on how to select a servo motor, in addition to presenting the final selection for the prototype. The specifications as well as the motor and driver are subject to change when building a second prototype. This thesis will then form a good base of knowledge for such changes.

The third task was to implement kinematic transformations for the robot, and to integrate those in an available automation software platform. The selected platform was TwinCAT3 by Beckhoff using the integrated CNC kernel provided by ISG Stuttgart. The kinematics was already developed in Python for easy prototyping and debugging. It was manually translated to C++ for performance and then imported to TwinCAT via a C++ module. The ISG kernel takes care of the trajectory planning. It was experienced that after several hours with the tool one notices the restrictions of the tools, such as the inability to dynamically limit the acceleration of each axis.

The report forms a good basis for the design of many types of robots. In the case of the AgilePKM, the selections and implementations made in this thesis will be directly built upon and the prototype will be realized in the year following this thesis work. As mentioned, no hardware is available at the time of writing.

Preface

As our interests have always been geared towards automation and optimization, the thought of writing a master thesis within robotics has been on our minds for a long time. Cognibotics AB and Torgny Brogardh filed a patent for the AgilePKM which became the seed which grew this thesis. Because of the nature of robotics and its need of many different engineering disciplines to be incorporated in the developing process, the work was somewhat divided between the two of us. As Felix is leaning more towards the software aspects and Hampus towards hardware, the split was natural. Felix has been developing the automation platform and selecting servo motors while Hampus has been developing elbow design. All else have been a collaboration. Felix will be supervised and examined by the division of *Industrial Electrical Engineering and Automation* and Hampus by the division of *Industrial Production*, which is why this thesis will be published on both institutions.

It has been an incredible journey of our academic as well as professional knowledge and a joy to be able to go into depth in each of our separate subjects, and still touch upon all other disciplines which are needed in the design of a new robot.

Cognibotics

Cognibotics is located in Lund, Sweden and is dedicated to driving the next wave of wide-spread robot use by improving accuracy and programmability. They will from here be referred to as "the company".

Acknowledgements

We would like to thank Klas Nilsson and everyone at Cognibotics for giving us the opportunity to develop the AgilePKM. Our official supervisors Adam Nilsson and Magnus Olsson, and Tommy Olofsson and and Olof Sörnmo for their tireless help.

LTH and its wonderful staff has prepared us well for this task, and we would like to thank our supportive academic supervisors Gunnar Lindstedt and Hans Walter.

Furthermore we would like to thank our family and friends, especially Anna Dantorp and Anna Andersson, who has supported us throughout this master thesis and the years leading up to it.

"It is faster to make a four-inch mirror then a six-inch mirror than to make a six-inch mirror."

Thomson's Rule for First-Time Telescope Makers

Abbreviations

2D - Two dimesions
3D - Three dimensions
AgilePKM - Agile Parallel Kinematic Manipulator CNC - Computer Numerical Control
CoG - Center of Gravity
DoF - Degrees of Freedom
FEM - Finite Element Method
HTM - Homogenous Transformation Matrix
I/O - Inputs/Output
ISG - MCP - ISG Motion Control Platform
ISO - International Organization for Standardization
M1 - Motor driving the bicep around the Z-axis
M2 - Motor driving the forearm around the Z-axis
M3 - Motor driving the arm in the Z-axis
NC - Numerical Control
RMS - Root Mean Square
RPM - Revolutions Per Minute
SCARA - Selective Compliance Assembly Robot Arm
TCP - Tool Center Point
UML - Unified Modeling Language

Contents

Chapter 1

Introduction

To initiate the development of the AgilePKM some basic understanding of robotics needs to be established along some insight into workings of the AgilePKM and the competing robot types. From this a good framework can then be established, with clear goals and limitations, for the development of the prototype.

1.1 Background

The idea of automation is very old and some researchers say that it all began in Alexandria during the first century BC. An engineer called Heron had ideas of creating automated doors powered by the lit altar in a temple and a device which converted energy from steam to rotational movement. The earliest application of robot mechanisms, called automatons, originated in Greece. This technology spawned from liturgy and was not intended for automating labour. The exploration of automation came to a hold for the Greeks, but during the 9th century the Arabs came in possession of the preserved Greek texts and continued their work. As the Arabs where more interested in the practical uses of automation they applied their mind-set to the Greek texts and described and depicted over one hundred devices in the book "The Science of Ingenious Mechanisms". [7][25]

During the Renaissance the interest in automation were reignited and one of the great intellectuals who explored the technology was Leonardo da Vinci. He tried to implement and develop upon the old thoughts. Some two hundred years later Swiss craftsmen challenged the limits of their current technology by building automatons in the form of dolls. The insights gained during this time was very important when implementing the first automatic machines in the industry.[7]

During and following the industrial revolution humanity has continued to develop on the technology and increased automation is almost always mentioned when there is a desire to increase efficiency and profitability. Nowadays there are a handful different types of robots which are used in the industry daily. A brief explanation of some of the most common ones, which this thesis will develop upon, follows.

1.1.1 SCARA

SCARA robots, shown in Figure 1.1, consists of two joints in series with parallel axes, one in the base and one in the arm. Its workspace is cylindrical, with an unreachable area in the center where the base is, in the horizontal plan and the end effector moves vertically. The robot is built on the principal of serial kinematics, which means that

Figure 1.1: ABB's versions of SCARA, articulated robot and delta robot

joints are chained. Some of its advantages are the large workspace, its high speed and thanks to a very rigid design, good repeatability and precision. However, it is limited to work with planar surfaces. It is commonly used in applications such as assembling and packaging.[34]

1.1.2 Articulated Robot

Articulated robots, shown in 1.1, is one of the most common types of industrial robots and resembles the human arm. This robot is, like the SCARA, constructed on the principal of serial kinematics. The axis for each joint is usually placed either in parallel or orthogonal to the previous joint axis and the arm is connected to the base with a twisting joint. The number of joints in the robot may range from two to ten and each joint adds another degrees of freedom. The most common version of articulated robots has six Degrees of Freedom (DoF) since this allows any Tool Center Point (TCP) position and orientation within the workspace. Thanks to the DoF the workspace is very large compared to the floor space occupied, which is what makes this type of robot ideal where lots of movement is desired in applications such as painting, welding and assembling.[34]

1.1.3 Delta Robot

As shown in Figure 1.1 the delta robot's appearance differs significantly from the other two. Both SCARA and articulated robots are inspired by nature in its design and one can easily see the similarities to a human arm. However, the delta robot is not bound by the constraints of biomimicry but instead its theoretical base lies purely in mathematics and geometry. The motors are placed in the base which allows for the design of the delta robot's moving parts to be very light in comparison to other types of robots. The motors are usually high torque and may be driving the arms directly or through a gearbox. Thanks to the combination of light weight of the moving parts and high torque motors the delta robot can produce acceleration of up to 15 g. Dean Elkins, Senior General Manager at Yaskawa Motoman said

> *In the mechatronic design of delta robots, the motion is being translated down through, in most cases, carbon fiber arms, where there's far less mass being moved. They've become a very, very efficient way of x, y, and limited z translation.*

which describes both the advantage and drawback of delta robots. They are fast in certain application but limited in its workspace. [17]

1.1.4 What to Develop Upon

The three types of robots described form a solid ground of already established and well tested techniques within robotics. The aim of this thesis is to combine these techniques into something superior to and more versatile than the mentioned types.

Designing the AgilePKM, elements from both serial and parallel kinematics are combined. Much like the delta robot the main concern of this new design is the light weight of the moving parts. A key component to achieve this is not carrying the motors on the arms, and instead placing them in the base. Also the parallel kinematics will come to use when designing the arms.

As an attempt to bring the positives of a light and quick arm design and avoiding the negatives of a restricted workspace of the delta robot, inspiration is also drawn from SCARA and articulated robots. Thanks to the serial kinematics, the workspace is much larger than that of a delta robot compared to the floor (or ceiling) area the robot will cover. This knowledge will be put to use and the arms will not only draw inspiration from parallel kinematics, but also have serialized joints rendering a much larger workspace compared to that of a delta robot.

1.1.5 Agile-PKM Overview

The concept for realizing these advantages is presented in Figure 1.2 and a short description of central parts is found below.

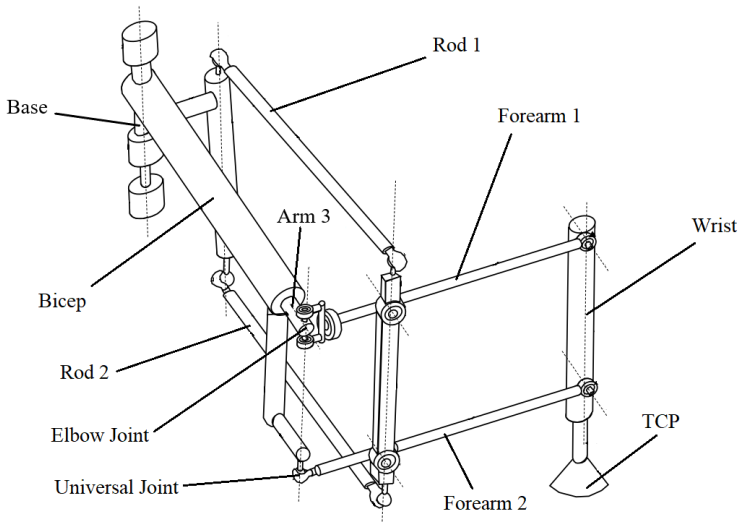

Figure 1.2: Concept 2 overview[21]

The *base* is the heart of the robot. In the first prototype, all motors will be placed here. The base is to be regarded as all motors placed within close proximity of each other and not necessarily on the same axis and orientation.

Extending from the base is the *bicep*, which carries the elbow joint. The bicep is rotated in the horizontal plane by motor 1 ($M1$). The bicep consists of a large hollow

pipe containing a thinner solid axle, which attaches directly to the *elbow joint*. This axle is driven by motor 3 ($M3$) to actuate vertical movements of the TCP.

The TCP is carried by a *wrist* mechanism which in turn is carried by two rods, $forearm\,1$ and $forearm\,2$. $Forearm\,1$ is directly connected to the *elbow joint* actuating, as previously mentioned, the vertical movements and allowing free rotationin the horizontal plane. $Forearm\,2$ is connected to a universal joint, attached to the *bicep*, which mimics the movement of the elbow. This mechanism allows the *wrist* to be aligned vertically in vertical movements. The horizontal movement is actuated by $rod\,1$ and $rod\,2$ which are connected to motor 2 ($M2$) through a short lever. They act in parallel to both each other and the *bicep* and keeps the *wrist* aligned vertically in horizontal movements. This guarantees that the TCP is always oriented vertically, independently of position in the work-space.

The target of this thesis, in terms of design, is to develop the elbow joint and choose servo motors. The remaining components and structure, such as the wrist mechanism, base, parallel rod attachments, amongst others will be developed in parallel by the company.

1.2 Issues and Aim

The thesis includes mainly the implementation of automation platform, selection of the servo motors and design of the elbow link. This should lead to the first prototype of the AgilePKM. The goal of the prototype and the overall design of the robot is to compete with modern industrial robots, mentioned in Section 1.1.

From the main tasks there are many subtasks and investigations that need to be completed and conducted. These are listed below and should be viewed as the basic outline and planning of the project.

In association with controller implementation

- Examine and select suitable servo motors
- Evaluate kinematics
- Evaluate trajectory planning
- Get acquainted with TwinCAT 3
- Implementation of controller in TwinCAT 3

In association with design of elbow link

- Force analysis
- Component examination and dimensioning
- CAD modelling
- FEM verification

1.3 Limitation of Scope

The end goal of this project is to design a functioning prototype, which is a rather large task. Therefore limitations have been set in compliance with Cognibotics and Lund University. These mainly include delimitations in what this thesis should cover and what areas are to be developed in parallel by Cognibotics to facilitate building of the prototype.

Acceleration : The TCP is assumed to experience forces equivalent 15 *gravitational forces* to achieve 200 pick-and-place cycles per minute

Range : The workspace will have a reach of 1.2 meter

Kinematics : Cognibotics will supply a basic kinematic structure

Axes : The first prototype will consist of no more than four axes

Agile-PKM : Cognibotics will in develop the base, the wrist and other parts of the arm structure in parallel.

Chapter 2

Elbow Design

This chapter covers the basic design of a proof-of-concept prototype focusing on the design of the physical structure of the elbow joint.

2.1 Introduction

The AgilePKM structure is largely based on one patented drawing, see Figure 2.1, where the elbow joint is labelled *16*.

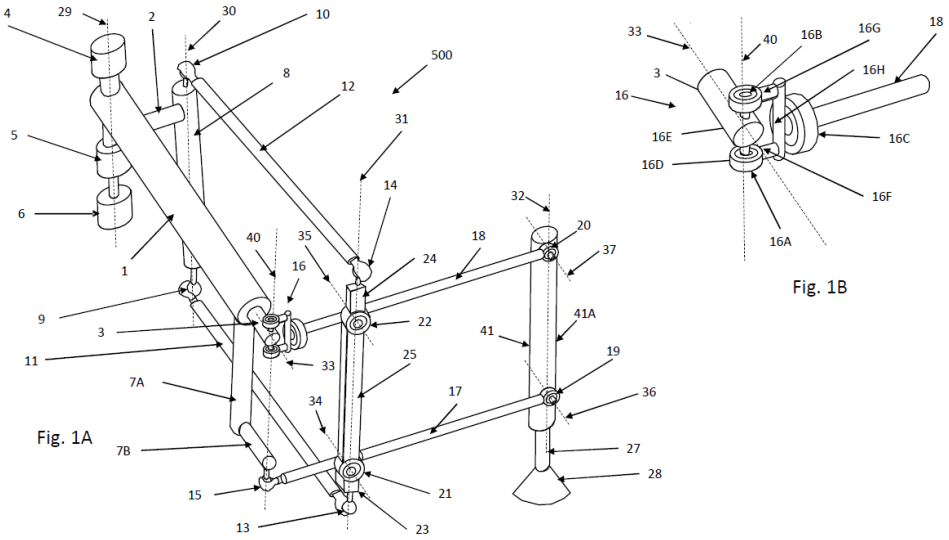

Figure 2.1: Patented Drawing[21]

The elbow is a crucial component of the AgilePKM since it attaches the load carrying forearm to the bicep. It is a 1 DoF joint which actuates vertical movements of the TCP and acts as lever to the parallel links or rods in horizontal movements, labelled *rod* 1 and *rod* 2 in Figure 1.2. It needs to withstand heavy loads and high torques generated from the ambitious specifications of the test cycle. On the robotic market single DoF joints exists but none match requirements of the AgilePKM elbow. The rotation of the joint axle, in other words lifting loads with the elbow joint, is carried by heavy motors in articulated robots and is simply avoided in delta robots because of the high torques created. Therefore the elbow needs to be designed from scratch and a thorough process is necessary in order to reach a competitive performance.

To strategically plan and execute the design process Ulrich and Eppinger's [10] "Prod-

uct Design and Development" has been consulted. That book thoroughly presents and develops the design and development process of product realization, and the design of the elbow will be based on this with some adaptations to better fit the highly technical demands on the elbow.

2.1.1 Brief Process

The design process is initialized by identifying the product needs, from which target specifications are established. After this, concepts will be generated to fulfil all or some of the target specifications. The concept generation is based on market research of single DoF joints where established designs are analysed and inspiration from existing solutions is collected. When these designs are identified and evaluated the full concept generation commences to incorporate a wide solution set. These are then scored and the highest scoring or most promising concept is then developed to determine optimal arrangement, type and size of components. Once the final concept is fully developed it is analysed with finite element method (FEM) to ensure that it fulfils the requirements.

2.2 Product Needs

The foundation of the product development and design are the product needs, from which concepts and solutions are to be formulated. This deems the process of identifying these needs as critical in order to facilitate good concept generation.

2.2.1 Identifying Needs

Ulrich and Eppinger refer to this task as identifying customer needs [10, p.73] but for the design of the elbow the task is rephrased as identifying needs. This is because the development is targeted to fulfil the technical requirements of the the test cycle rather than those of the customer. The technical requirements are derived from the patented robot structure, interviews with the company from previous prototyping experience and applicable examples from literature [10]. After these needs are mapped they will be reduced to comparable metrics in order to score and rank the different concepts.

This process is initially diverging trying to identify all possible needs of the elbow and then condensing the needs into categories. These categories will then be nested into a final list representing all identified needs. The list is then organized into a hierarchy ranging from *(5) crucial abilities* to *(1) unnecessary characteristics*. The list of categories is presented below along corresponding priority and description.

Identified Needs

5 **DURABILITY** The durability is the absolute most important property that the elbow needs to posses. If the arm does not withstand the applied loads it will fail and the robot becomes inoperable. Therefore it is of highest priority to accurately estimate loads on the elbow and ensure that the elbow is dimensioned to withstand these.

5 **MOVEMENT** Secondly and equally important as the durability is the movement or agility of the elbow. To enable the kinematics to function correctly and ensure the full reach the elbow needs to actuate sufficient movements in different directions and planes.

4 **MANUFACTURABILITY** The components that make up the elbow need to be acquired as soon as possible when the the design is verified and finalized. To enabled this they need to be easily manufactured to avoid lengthy deliveries. The same applies to components that should be available off the shelf.

4 **LOW WEIGHT** As one of the central strengths of the AgilePKM is the reduced moving mass the elbow design should be targeted towards reducing its weight. However, is this characteristic not met, the robot will still function with partially reduced performance.

3 **EASE OF ASSEMBLY** To facilitate ease of building the first prototype the elbow should be easily assembled and attached to adjacent components. From discussion with the company this is a characteristic desired for the prototype and the final product which is why it is intermediately prioritized.

2 **RIGIDITY** This refers to deformations and play affecting the TCP. The overall goal of the AgilePKM is to be fast and accurate, but as a first prototype targeted towards proof-of-concept the rigidity is not prioritized at this stage but rather implemented at later iterations when the strengths and weaknesses of the structure is mapped more accurately.

1 **SERVICEABILITY** This characteristic is also derived from interviews with the company to facilitate easy servicing of damaged components. To realize this, the design should be modularized to easily swap components without disassembling the entire elbow. At this early stage this is not prioritized.

2.2.2 Target Specifications

From the list of identified needs the characteristics should now be converted to measurable metrics. The magnitude of these metrics are derived from expectations and estimations from the company and benchmarking, although benchmarking is limited since the competitive products are scarce. In the following sections the target specifications are presented according to the corresponding category along an investigation of measurable metrics. Since the target specifications are dependent on each other the order they are presented in is diverging a bit, this is to establish limitations used in subsequent specifications.

Movement

The movement limitations of the elbow is split into two categories, where one is vertical limitations of +/- 30^o from horizontal positioning and the other is horizontal limitations, measured with α (see Figure 2.2), of 25^o - 155^o. These limitations are visualized side by side in Figure 2.2.

As one of the main objectives of the elbow is to facilitate sufficient movement, it is beneficial to define the desired movement early as a base for continued analysis, and an explanation of the movement along the limitations will now follow. The elbow is carried by the $arm\,3$ in the *bicep* and hence it will follow its movement around the base in the horizontal plane. From this attachment point, the elbow will act as a lever in horizontal movements of the TCP via the parallel rods and vertical movements from rotation of the arm 3, labelled in Figure 1.2. As the elbow is a single DoF joint it only needs to enable free rotation around a vertical axle positioned at the end of arm 3, labelled in Figure 1.2.

This rotation is actuated by the parallel rods and the required force varies with the angle-of-attack. The angle-of-attack refers to the ratio of force applied from the parallel rods to rotational movement around the elbow. When the forearm is perpendicular to the parallel rods all of the applied force will be transferred to rotational movement around the elbow, but as the forearms retract or extend the ratio will decrease and instead transfer force to the elbow. The worse the angle-of-attack is the more force is required to accelerate the forearms. It is therefore necessary to define these limitations before determining the durability requirements. From benchmarking competing robots the SCARA robot has a limiting angle in retraction which is 30^o according to ABB [2, p.31] and the improved angle of 25^o is used for the AgilePKM to ensure competitive qualities.

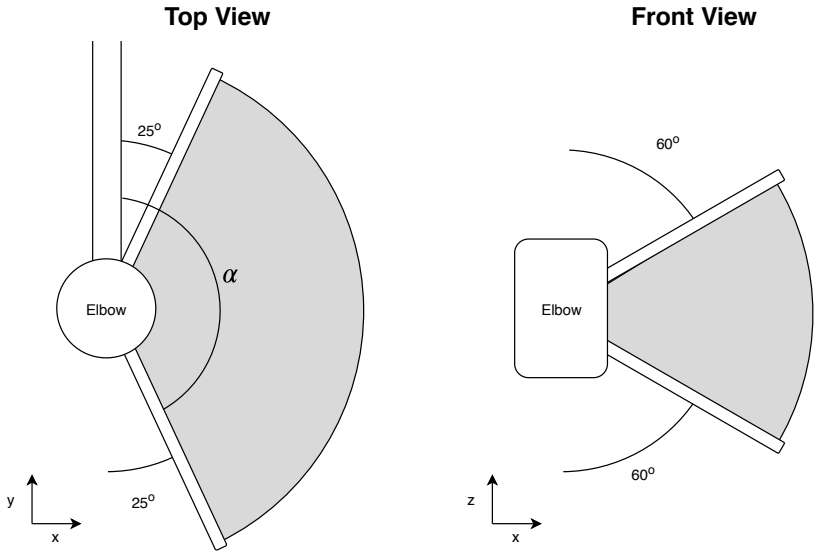

Figure 2.2: Working area limitations

Durability

The durability specifications are derived from loads at different positions of the TCP, specifically positions resulting in extreme loads. These extremities are analysed and evaluated in Appendix A and the results are presented in Table 2.1.

Weight

For the weight it is initially hard to establish target specifications since not the serial nor the parallel robots are using these kinds of joints. In serial robots these joints are

$CoG_{horizontal}$	0.348 m
CoG_{weight}	4.2 kg
F_{CoG}	337 kg
F_y	2633 N
F_x	305 N
F_z	337 N
T_y	117 Nm
T_x	106 Nm

Table 2.1: Maximum loads

replaced with motors to directly actuate movement and in parallel robots similar links are not exposed to the high torques in the AgilePKM elbow joint.

There are similarities to other mechanical joints, mainly door hinges and universal joints (only half of the universal joint is needed for 1 DoF joint). These are however not designed for the same requirements as the AgilePKM. Therefore the company has been consulted to get an estimation of a probable weight. The company recommended a maximum of 1 kg which will be used as marginally acceptable weight.

Manufacturability

The manufacturability is easily explained by the sub categories logistics and MRP (Material Requirements Planning). Commercially available products are rated based on the associated logistics where ordering and shipping is rated. If the products are widely available on the market, the process of ordering and the shipping time is simple and fast. More specialized products may require a more demanding ordering process and take longer to ship.

For fully customized products the actual manufacturing process is rated instead, based on the categories listed below. The geometry is a big factor and should be aimed at simple shapes suitable for milling or lathing. The strength requirement should also be minimized possibly by compact geometry and short force transfer design. These characteristics will be evaluated for each concept and compiled to a rating on a scale of 1 - 10, where 10 is very easy and cheap to acquire and 1 is difficult and costly.

- Cost and machineability of the raw material
- Amount of material removed
- Number of set-up operations
- Demands on machining process (lathing or milling 2-/3-/4-DoF)

Ease of Assembly

For ease of assembly, a common measurable metric is time of assembly, which unfortunately is not suitable for the AgilePKM prototype. Instead this category is targeted towards the required skills for assembly. A simple manufacturing process consists of few and simple steps. For example, if the assembly requires very accurate mounting of an axle it will attain a lower score compared to simpler steps such as tightening a screw to a predetermined preload.

Rigidity

Rigidity is very important for the final robot but since very little is known about the structure the proof-of-concept prototype will only aim for, but not prioritize, rigidity. The rigidity is measured by the risk of backlash or elastic deformation. These characteristics will only be estimated for concepts but can be estimated with FEM-analysis when concepts are considered for development.

Serviceability

Serviceability is somewhat related to ease of assembly, since the skills required to service is rated. The disassembly and reassembly should be designed such that possibility of incorrectly reassembling the elbow is minimized. To enable this, the steps should be as few and simple as possible and easily completed with simple instructions.

2.3 Concept Generation

As the specifications have been derived from the needs, the concept generation commences. The aim here is to carry out a wide search to ensure that all possible solutions are considered before deciding on and developing a final concept. The technical requirements calls for a bit narrower search in order to facilitate time for analysis and optimization of the chosen concept.

To initialize the concept generation the target of the elbow design should be revisited. The goal of this thesis is not to design a ready-for-market robot but rather a proof-of-concept prototype of the robot, which can be then analysed, improved and adapted to specific customer applications. This suggests that the components should be suitable for small scale manufacturing in contrast to large scale production. The target specifications are ambitious which implies that high quality components are required which may increases the cost and possibly the shipping time. To keep these to a minimum the concepts will be validated with FEM-and CAD analysis before ordering, in contrast to physical tests which are both time consuming and expensive.

The singe DoF rotational joint is a very common joint used in many industries today. As this mechanism is well established there is no need to reinvent the wheel. Instead this process is approached more efficiently by researching existing hinge designs to find suitable performance products and incorporate these components and features into a new tailored design. This part of the process also includes generating new concept solutions for each component in order to ensure that all possible solutions are considered in order to reach the optimal design.

Existing designs are benchmarked in order to identify common design solutions. The hinge mechanism is, most commonly used in door hinges and is widely available in many different sizes and shapes. The common form factor for this intention is flat attachments to surrounding components which facilitates a thin but tall profile. This is not optimal for the AgilePKM where the surrounding components are circular profile carbon fibre rods. The likeliness of finding a suitable door hinge is minimal and the research progresses to alternate hinge mechanism applications. These incorporates a very wide spectra of usage, from robotic to structural applications, and they are highly adapted to their intended usage and very limited availability on the market for single component orders. The conclusion is insufficient market availability for complete solutions and process continues to focus on designing a custom AgilePKM hinge.

2.3.1 Hinge Mechanism

To produce a complete concept for a custom hinge each fundamental component in the hinge needs to be investigated. In general a basic hinge consists of a mirrored pair of leaf and knuckle joined together by a central pin according to Figure 2.3. The back leaf (1) will in the AgilePKM attach to arm 3 and the front leaf (5) will attach to the forearm.

The dimensions of arm 3 and the forearm are preliminarily set and thus defines what the leafs will attach to. The remaining components in between are then required match the connection to the leafs and withstand loads and facilitate the specified movement. The concept generation starts at the base, the back leaf, and sectionally progress to the end of the elbow, the front leaf.

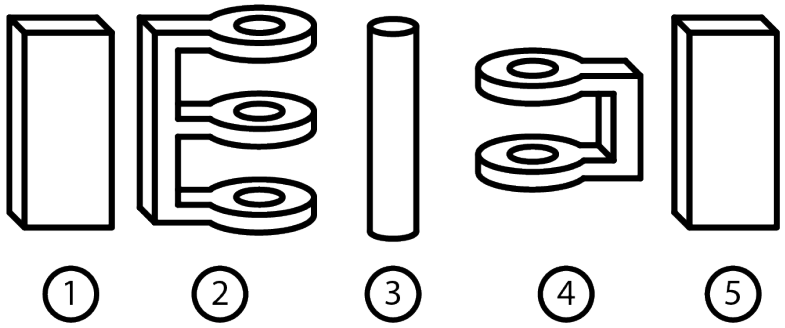

Figure 2.3: Hinge Overview

The benchmarking and concept generation for each component is described in Appendix B and composed into full hinge concepts presented below. These full concepts are rated based on the target specifications in Section 2.2.

Assembled Elbow

The first concept is based on the idea of assembling the elbow from existing components. The characteristics that is sought after with this approach is short delivery times and low costs at the expense of a bulkier and heavier design. If the advantages outweighs the disadvantages this concept is well suitable for a proof-of-concept prototype enabling cheaper tests and design alterations compared to a full custom build where each part needs to be manufactured again.

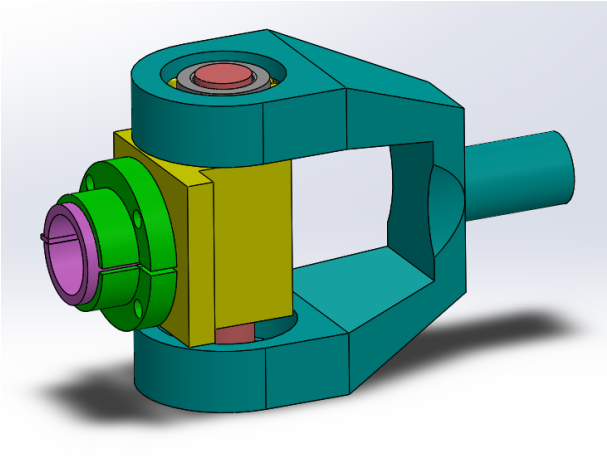

Figure 2.4: Assembled Elbow

The Assembled Elbow is assembled by benchmarked and custom made parts found in Appendix B and Figure 2.4 gives an overview of the concept. Starting at the connection to arm 3 which consists of the base leaf. In this concept the base leaf consists of a sure

grip bushing (green) paired with a key adapter (pink) followed by a industrial shaft holder (yellow), bearings (grey), custom pin (red) and custom front (blue). The conclusion is drawn that the concept is rather bulky and heavy. The interface between components has not been fully defined nor explored which leaves some uncertainty if the concept can be realized or further developed with additional parts and/or adaptors. This further increases the already high part count, making the ordering and shipping logistics more difficult. The interface of the components relies on screws enabling possible play and possibly lowering the durability. The front is custom made since assembling existing components quickly becomes bulky and does not meet the requirement. To simplify the logistics the front leaf, consisting of a peg (a simple short pin of metal), is integrated into the front knuckle since manufacturing an attachment interface for a peg is equally demanding as manufacturing an actual peg into the front knuckle.

Weight	**Characteristic**	**Score**	**Weighted Score**
5	Durability	7	35
5	Movement	2	10
4	Manufacturability	5	20
4	Weight	2	8
3	Ease of Assembly	4	12
2	Rigidity	3	6
1	Serviceability	6	6
	Total		**125**

Table 2.2: Assembled Elbow Rating

The rating of the Assembled Elbow is presented in Table 2.2. The score of 125 makes the concept viable but the uncertainties may outweigh the advantages compared to other concepts.

Pipe Elbow

For this concept the aim is to integrate basic structural elements into an efficient design to reach an efficient and cheap design which may cater for larger scale manufacturing at the same time. The structural elements are processed to incorporate multiple features and to keep the part count and size low. The rigidity and durability is aided by a few market components.

Figure 2.5 gives an overview of the concept where the back leaf and knuckle are combined into one part consisting of a pipe (blue) with a processed inner diameter to enable a snug fit around arm 3 enabling large surface contacts for good adhesion properties. The back of the pipe is processed with a piercing hole to hold the pin and a slit to enable clamping. The custom pin (orange) holds two bearings (grey) sitting in a similar custom front (green) with an integrated peg as front leaf. Not shown in the overview is the integrated support of the pin by the carbon fibre pipe, which is instead shown in Figure 2.6.

This concept becomes much sleeker in comparison to the previous but it is questionable if the pipe supports the fixation of the pin enough. It is problematic that the ends of the pipe are subjected to the largest stresses and at the same time spires. The front needs to be able to swivel around base while being attached to the pin. The clamp increases the dimensions of the front knuckle since the front not only needs to reach around the base but also the pipe clamp. Other solutions for pin fixation are discussed in Appendix

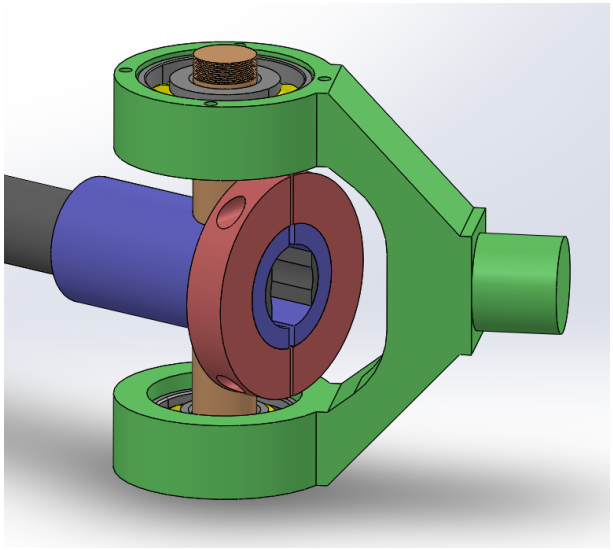

Figure 2.5: Pipe Elbow

B including processed holes for screws and shrink clamping but the pipe clamp is considered the most viable. In terms of manufacturing the front has similar demands as the previous concept while the pipe requires as mentioned post processing and will most likely be ordered in larger dimension lengthwise than needed. This will drive the cost up while enabling backup components to be manufactured cheaply.

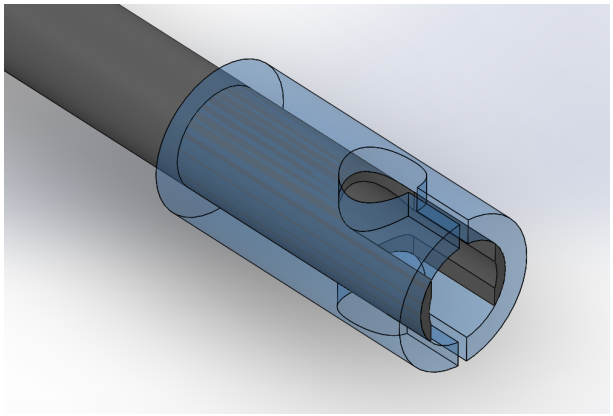

Figure 2.6: Reinforcement

The rating for the Pipe Elbow concept is found in Table 2.3. The concept is sleeker than previous and has a low part count. The durability for the pin grip is the largest uncertainty and if this is found insufficient back-up base components will be unnecessary.

Weight	**Characteristic**	**Score**	**Weighted Score**
5	Durability	6	30
5	Movement	8	40
4	Manufacturability	6	24
4	Weight	6	24
3	Ease of Assembly	7	21
2	Rigidity	8	16
1	Serviceability	8	8
	Total		**163**

Table 2.3: Pipe Elbow Rating

Turned Elbow

The last concept approaches the elbow with custom design components. This enables the design to incorporate efficient features for an optimal design. The drawback is that the manufacturing can become expensive but if features are designed with manufacturability in mind these costs can be minimized.

The Turned Elbow consists of a base (blue) turned from a metal cube attaching to arm 3 (left rod). The pin (orange) is fitted in a hole running through the base similarly to the Pipe Elbow concept and clamped with a pair of screws in processed holes at the back. The front (green), incorporating the front leaf, is fitted onto the bearings (grey) is a bit more compact since there are no bulky components clamping the base. The base is reinforced compared to the Pipe Elbow concept in order to, with higher certainty, withstand the stresses from the pin. Arm 3 is glued to the base.

The rating for the Turned Elbow is found in Table 2.4. The manufacturing is a bit more demanding here but can be manufactured from a singe piece of metal making it suitable for single component manufacturing.

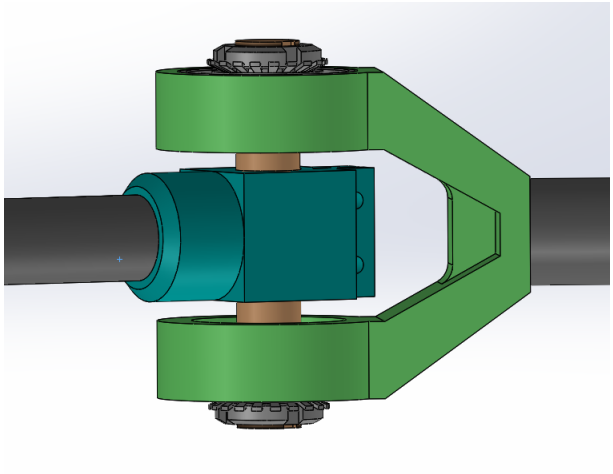

Figure 2.7: Turned Elbow

Weight	**Characteristic**	**Score**	**Weighted Score**
5	Durability	9	45
5	Movement	8	40
4	Manufacturability	8	32
4	Weight	6	24
3	Ease of Assembly	8	24
2	Rigidity	8	16
1	Serviceability	7	7
	Total		**188**

Table 2.4: Turned Elbow Rating

2.4 Concept Evaluation and Selection

A compiled rating list is presented in Table 2.5. The concepts are fairly similar in the layout but contain different characteristics. These will now be compared and discussed to determine the most promising concept for further development.

All full concepts share the same front which concludes that it advances to be developed in the final concept and used in the final prototype. In Appendix B alternate solutions are discussed and concluded to be implausible and thus not included in full scale concepts.

The same goes for the pin arrangement where multiple solutions are evaluated Appendix B to finally arrive at the implemented solution in the concepts.

The two last concepts, Pipe Elbow and Turned Elbow, scored very highly while the Assembled Elbow scored a bit lower. This corresponds with the feasibility of the concept since there are many parameters that need to align in order to realize the Assembled Elbow concept. The other concepts are more probable to be successfully developed to meet the requirements.

The Pipe Elbow has the disadvantage of being more catered for the large scale manufacturing. This is because the base pipe is manufactured at longer lengths than requires which makes it ineffective cost wise to produce a single elbow from this. Additionally a simple FEM-analysis questionable results was completed.

The Turned Elbow is better fitted to single manufacturing since there is no need purchase excessive material and together with enhanced development possibilities seems like a probable option to advance to further development.

Weight	**Assembled Elbow**	**Pipe Elbow**	**Turned Elbow**
Durability	35	30	45
Movement	10	40	40
Manufacturability	20	24	32
Weight	8	24	24
Ease of Assembly	12	21	24
Rigidity	6	16	16
Serviceability	6	8	7
Total	**125**	**163**	**188**

Table 2.5: Concept Selection Rating

2.5 Concept Development

As the Turned Elbow concept is selected, further development to specify components and dimensions is to commence. A central component that influences surrounding component dimensions is the pin. In order to efficiently determine sufficient and efficient dimensions the pin will be dimensioned and from there the rest of the elbow.

During the concept generation the company has in parallel developed the structure and components surrounding the elbow. These design advancements renders new anticipated weights and dimensions for components used to calculate loads on the elbow. They are presented in Table 2.6.

2.5.1 Pin

In Appendix B the pin stresses are discussed, and with the updated component properties the required pin dimensions will now be calculated along with associated properties. Determining the max torque stress in the pin is done by slicing the pin at different sections and calculating the torque required for equilibrium. The forces are displayed in Figure 2.8 and the maximum torque of 49 Nm is found at the inner force pair.

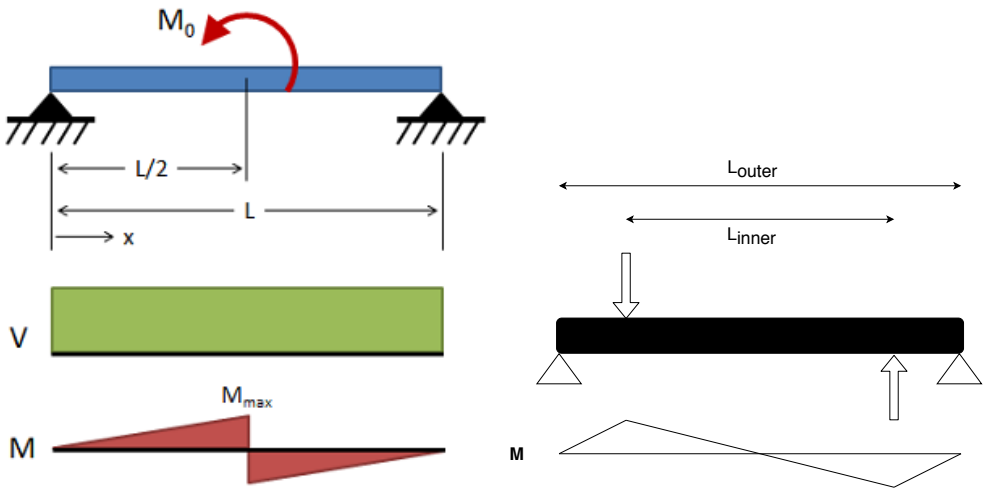

Figure 2.8: Initial pin stress [12](left) and developed pin stress case (right)

To determine the required force, the strength of the pin needs to be researched. Heavy duty hinges in the industry use high-strength low-alloy steel (HSLA) which has a yield strength of 290 MPa [20, p.421]. The stress in in Equation 2.1 generated by the torque and the section modulus of a circular profile, presented in Equation 2.2 is aimed at 193 MPa for a safety factor of 1.5. This renders a radius of 6.86 mm which is reasonable for the elbow and to match dimensions of common bearings the diameter is set to 15 mm.

$$\sigma_{max} = \frac{M}{W_b} = 193 \quad [\text{MPa}] \quad (2.1)$$

$$W_b = \frac{\pi \cdot r^3}{4} \quad [\text{m}^4] \quad (2.2)$$

The pin is also subjected to shear stress which is calculated similarly to torque in a beam, slicing the pin and calculating the resulting forces. Equation 2.3 shows that this stress is much lower than the bending stress at the set dimension.

$$\sigma_{max} = \frac{F}{A} = 27 \quad [\text{MPa}] \quad (2.3)$$

$CoG_{horizontal}$	0.348 m
CoG_{weight}	4.2 kg
F_x	305 N
F_z	337 N
T_y	117 Nm
T_x	106 Nm

Table 2.6: Updated loads

Initially the pin is set to be custom made with threads at each end to allow lock nuts and washers to fixate the bearings. After consultation with the company an alternate solution was developed where the custom pin is replaced with a standardized pivot pin. There is a wide market for this consisting mostly of designs not allowing preload (which will be further discussed in Section 2.5.2). However, there exists shouldered pivot pins, shown in Figure 2.9, threaded at one end allowing a locknut to be fixated, thus enabling preload. This is a much more efficient design as the preload, which is distributed equally between the bearings automatically, would then only need to be applied at one end. This also reduces the part count and standardises the parts, which is an overall improvement.

Figure 2.9: Pivot pin threaded with locknut[18]

2.5.2 Bearings

The dimensions of the pin are now established and the concept generation can continue to research adjacent components. Bearings will enable low friction rotation around the arm and will now be researched to find suitable models with a matching bore diameter. There are many different variants of bearings that are suitable for different arrangements and applications. To determine suitable bearings SKF offers a thorough guide [29]. To initially narrow down the selection robot industry standards are deep groove ball bearings and thin section bearings for light and space limited applications, for heavier applications tapered roller bearings are used, according to AST [4].

Loads

To determine the loads exerted on the bearings the test cycle needs to be defined in more detail. The cycle will be explained in Section 3.1 and the cycle time is aimed at 0.3 sec. The horizontal movements are estimated to take a total of 0.2 sec, which is 66.7% of the cycle leaving 0.025 sec for each vertical movement, totalling 33.3% of the cycle. Assuming a triangular speed pattern the top speed will be twice the average speed. The horizontal movement of 0.3 m has to average 3 m/s and thus a top speed of 6 m/s at 0.05 sec constantly accelerating for the first half and deceleration the second half at120 m/s^2. The vertical movements of 0.025 m is similarly derived to an acceleration 160 m/s^2.

The location of the test cycle needs to be established as this greatly influences the forces involved. For the vertical movement load is constant, however for the horizontal movement the loads vary greatly depending on location of the arm. This makes calculations of the load during a cycle complicated since the load will not only vary between different movements but also within each movement. The aim for the AgilePKM is to enable the test cycle to be carried out independently of location within the defined workspace

and thus for the cycle will be placed in an exposed location to ensure durability in the entire workingspace.

In the horizontal movement, which is actuated the parallel rods, it is clear that the worst case is present when at the worst angle of attack for the parallel rods at 25^o or 155^o. Resulting in radial forces of 3507 N split between the two bearings according to Equation 2.4 derived from equations A.11 and A.12. Here a simplified acceleration of 150 m/s^2 is used since the test cycle and its accelerations are not fully specified at this stage and can be adapted for more even accelerations. The horizontal movements do not contribute to any vertical forces and only the weight of components should be considered for the axial load on the bearings, generating 31 N which is relatively small in terms of radial loads for bearings.

$$F_{radial} = \sqrt{\left(F_{CoG} \cdot \left(\frac{CoG_{horizontal}}{sin(\alpha) \cdot a} - sin\left(\alpha\right)\right)\right)^2 + \left(F_{CoG} \cdot cos\left(\alpha\right)\right)^2} \quad \text{[N]} \quad (2.4)$$
$$= 3507$$

The vertical movement is following a spherical trajectory centred at the elbow with $TCP_{horizontal}$ as the radius. This deems the load to be a constant 256 N regardless of position, calculated in Equation 2.5, for each bearing. The vertical movements also generate vertical forces which contributes an axial load of 480 N.

$$F_{radial} = \frac{\sqrt{\left(F_{CoG} \cdot CoG_{horizontal} \cdot sin\left(\alpha\right)\right)^2 + \left(F_{CoG} \cdot CoG_{horizontal} \cdot cos\left(\alpha\right)\right)^2}}{0.06} = 2561 \quad \text{[N]} \quad (2.5)$$

The loads on the bearings have been determined and next in the selection process is the defining the application they are going to be used in. The AgilePKM will generate no full rotations for the bearings but an average of 79 RPM according to Equation 2.7 with the weighted average speed in Equation 2.6 in horizontal movements. In the vertical movement there is no rotation of the bearings.

$$V_{avg} = \frac{V_{low} + 2 \cdot V_{high}}{3} = 5 \quad \text{[m/s}^2\text{]} \quad (2.6)$$

$$V_{rpm} = 1 \Big/ \frac{r \cdot 2 \cdot \pi}{V_{m/s} \cdot 60} = 79 \quad \text{[RPM]} \quad (2.7)$$

This deems the application for the bearings to be mainly static since the RPM is slow for 2/3 of the cycle and at standstill for the remainder. The overall slow speeds and pivotal movements make dimensioning based on rating life unsuitable. Instead the sizing will be based static load solely.

Bearing Arrangement

The arrangements of bearing pairs should be considered when deciding bearings types. There are three main types of bearings, locating/non-locating, adjusted and floating which are suitable for different applications. The AgilePKM demands a rigid design which eliminates the floating arrangement since this would introduce play. The remaining arrangements are both suitable for the elbow depending on what feature is valued.

In the locating/non-locating arrangement only one bearing is exposed to axial load which is suitable as the axial load is as previously stated low. This design would enable the bearing exposed to only radial loads to be dimensioned a bit smaller. The adjusted arrangements are as described by SKF[27] suitable for applications where the arrangement is exposed to low axial displacement, caused by temperature differences and length of mounting shaft, which is the case for the elbow. This arrangement allows for pre-load during mounting which eliminates back-lash and is suitable for tapered roller bearings and angular contact ball bearings. This also allows the possibility of pre-load which increases the proportion between axial and radial forces, which imposes better favourable conditions for angular contact bearings. Viewing the figures 2.10 and 2.11 it is clear that the adjusted arrangement is the optimal.

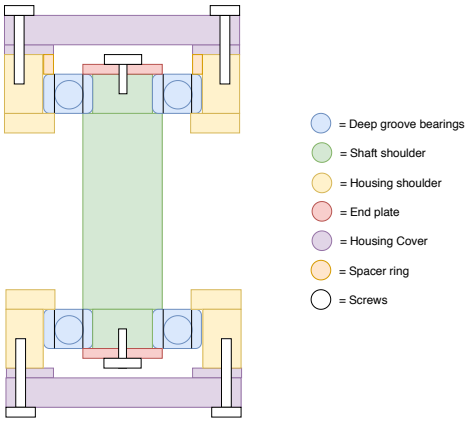

Figure 2.10: Locating/ non locating arrangement

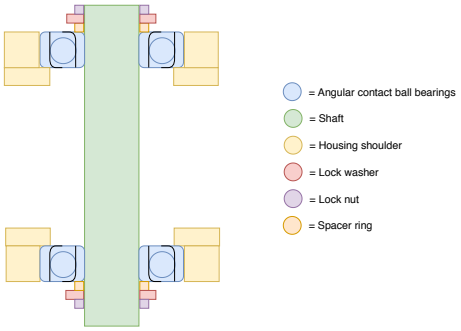

Figure 2.11: Adjusted Arrangement

The loads of the test cycle are already evaluated and the missing component in the force analysis is the pre load. There are no standard guidelines to set the preload according to SKF[28]. Instead it is recommended to follow established implementations of preload applications, and if such does not exist it is recommended to perform tests to determine sufficient preload. The lack of hardware at this stage makes this impossible. To eliminate loss of preload for unloaded bearing the preload should exceed the maximum load applied to the bearing pair, with a safety factor. This ensures that the displacement form deformations on the shaft of outer fixations from the load does not exceed the displacements from the preload. Since the maximum axial load on the contact angular ball bearings is fairly low already there is room for a safety factor of 1.5 without applying unnecessary loads to the front and pin, resulting in a preload of 720 N.

Bearing Fixation

To enable a rigid mounting of the bearings the fitting needs to be snug both radially and axially depending on the arrangement of the bearings. To accomplish the axial fit there are various solutions including shaft/housing shoulders, lock nuts/threaded rings, end plates/housing covers, distance rings and snap rings. These are combined with each other depending on the application. It seems suitable for the pin to be fitted with a shoulder centrally to secure the bearings from sliding to the middle, and at the same time increasing the section modulus (the geometrical strength of a profile for bending and shearing) for the inner section. For the outer section a shoulder is not suitable since the bearing would be unable to slide on to the shaft. There are multiple other options for mounting the bearing at the end of the shaft.

Solutions for radial fixation are not as elaborated and only solutions for tapered shafts and bearings exist. This is because the bearings are fitted tightly to the shaft based on just tolerances, which imposes tolerance demands on the shaft. If the shaft diameter is smaller than the bearings it can be radially fixated with a adaptor or withdrawal sleeve, the small diameter of the shaft makes suitable adaptors available on the market scarce leaving rendering the solution unsuitable.

Outer axial fixation of the bearings to the front piece of the hinge have many possibilities for fixation. Here it also seems suitable to fit the inner fixation with a shoulder because limited reachability when mounting, making it unsuitable since for example lock nuts would be hard to tighten. The outer fixation has many other options including threaded ring, housing cover and snap ring.

The arrangement of the bearings also influences the fixation. If an adjusted arrangement is chosen it is sufficient to have just one fixation on the shaft and one on the housing. On the other hand if a locating/non-locating arrangement is chosen double sided fixations on both the shaft and the housing is required, one bearing fixated tightly and the other with a bit of play. If the bearings are sized differently weight can be saved if the design is unsymmetrical.

Tapered roller bearings are excessive for the elbow as the smallest available bore diameter is 15 and the smallest bearing (30202) has a safety factor of 5.3 according to Equation 2.8 where $Y_0 = 0.9$ according to SKF [31] setting the radial force as P_0 in Equation 2.9.

$$P_0 = \quad 0.5 \cdot F_r + Y_0 \cdot F_a < F_r \qquad \text{[RPM]} \quad (2.8)$$

$$S_0 = \quad \frac{C_0}{P_0} = 5.3 \qquad (2.9)$$

The proportion of axial and radial forces in the vertical movement is 0.187 deeming the load to be mainly radial which makes angular contact bearings unnecessary. From this the conclusion was drawn that ball bearings should be used instead because of the relatively low load, thus the tapered roller and thin section bearings are excluded.

Bearing Selection

The actual bearing model is now to be chosen. SKF is a world wide distributor and their products are available at numerous different retailers. It is therefore suitable to choose bearings from their assortment. Their online catalogue is well presented making comparisons between different bearings easy.

A suitable bearing matching the pin diameter is single row, angular contact ball bearing *7302 BEP*. The rating of the bearing[26] needs to be evaluated against the loads. In Equation 2.10 the equivalent static load is calculated to be 1655 N when $F_r = 2561$, $F_a = 720$ and $Y_0 = 0.52$.

$$P_0 = \quad 0.5 \cdot F_r + Y_0 \cdot F_a = 1655 \qquad [\text{N}] \quad (2.10)$$

$$S_0 = \quad \frac{C_0}{P_0} = 2.6 \qquad (2.11)$$

The safety factor becomes 2.6 for *7302 BEP*[26] with $C_0 = 6.7$ KN when using the larger radial load instead of the equivalent static load. The axial/radial load ratio is recommended to be above 1 which will not be fulfilled for the test cycle, but can be adapted if found necessary. The low speeds should lower the effect of a possible defect bearing and the unfulfilled recommendation is thus considered to be neglected for the prototype.

If the safety factor is considered to be high the next size available for the same type of bearing is the *7202 BEP* decreases the diameter from 42 mm to 35 mm and the weight from 80 g to 45 g. This also decreases the safety factor to 1.7 and would imply some design changes to the front leaf and knuckle.

2.5.3 Front

The front knuckle, attaching the bearings to the forearm via the front leaf, needs to be designed as well. The fitting with the base of the hinge will determine the movement range of the hinge. The preliminary design of surrounding components, specifically the parallel rod attachments, is shown to be a tight fit at the extremities of the horizontal angle shown in Figure 2.12. Here the parallel rods have been mounted 110 mm from the pivot center (labelled L_3 in Figure 4.5) in order to allow the inner most angle to be accessed. The rod then reaches a distance of 70 mm from the pivot center leaving this as the maximum usable distance for the elbow.

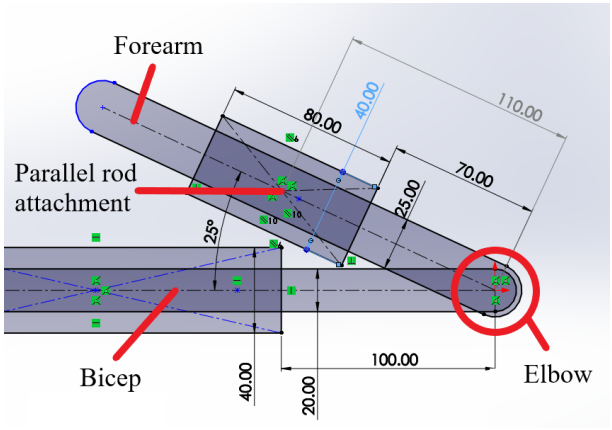

Figure 2.12: Top view of inner position of arm with parallel rod attachments developed by the company

To ensure comparability the elbow should be mounted at least 10 mm from the parallel rod attachment. As will be mentioned in the following section the forearm attachment should be mounted internally to liberate space which means that at the attachment the width of the elbow should be the same as the inner diameter of the forearm, 210 mm.

This allows the thickness at the mount of the forearm attachment to be 13.8 mm, calculated in Equation 2.12 derived from Figure 2.13. The allowed thickness is the distance x which is determined by the perpendicular distance ($c = 60 \cdot sin(25) - 10$) to arm 3 derived from the parallel rod attachment distance ($a = 60$), half of the thickness of the forearm ($b = 10.5$), all parameters are given in mm and marked in Figure 2.13.

$$x = \frac{\frac{200}{2} - a \cdot sin(25) - b \cdot cos(25)}{sin(25)} \quad \text{[mm]} \quad (2.12)$$

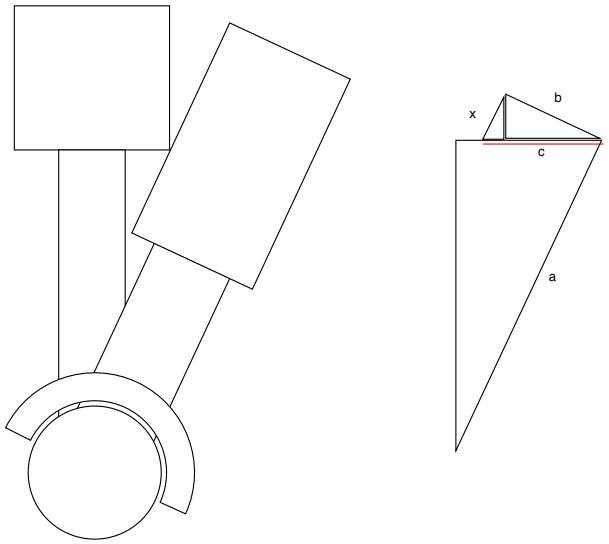

Figure 2.13: Top view of arm with marked parameters

2.5.4 Base

The design of the base is mainly derived from the dimensions of arm 3 but also the stress in the pin. The overall design goal is to keep the dimensions to a minimum while still facilitating enough strength transfer the torque. This is to keep the weight as low as possible. Calculations were made to ensure that the profile interface between the back leaf and the knuckle is sufficient, determining the outer diameter of the back leaf. The back knuckle is derived from the dimensions of the back leaf in order to keep the design minimal. The profile is expanded to a full square in order to support the pin better. The length of the back slits are derived from similar designs used in the industry today.

2.5.5 Material

The materials that front and base pieces are going to be made of have not been discussed yet. This is one area that should be briefly researched to establish suitable candidates. The first is heavy duty hinges, here S & D [32] lists the following materials to be common in industrial heavy duty hinges.

- Aluminium (various grades)
- Mild Steel

- High Strength (HSLA) Steel
- Cold Rolled Steel
- Hot Rolled Pickled & Oiled Steel (HRP&O)
- Galvanized Steel
- Brass
- Copper
- Stainless Steel
- Titanium

These materials are now compared to sought after characteristics such as high tensile strength, low density, low elongation and good milling characteristics. Aluminium match many of these characteristics. After interviews with the company the alloy 6061-T6 is recommended with improved tensile strength from double heat treatment. It is common in bike frames and model aircraft where weight and strength are prioritised. Aluminium is commonly milled and the T6 treatment may increase demands on the milling process. The yield strength is at least 240 MPa but more commonly reaches up to 270 MPa according to Material Properties Database[16].

2.5.6 Epoxy Adhesion

The attachment to both arm 3 and the forearm is relying on the strength of epoxy and therefore this is calculated in equations 2.13 and 2.14. The adhesion area is interpreted as the surface area of the carbon fibre rod and x is the length of the adhesive. The force (20 500 N) is derived from necessary shear force applied to the outer surface of the carbon fibre rod. A safety factor of 1.5 is used and the epoxy strength of 31 MPa according the data sheet[24] supplied by Rock West Composites.

$$\tau = \frac{F}{A} = 31 \quad \text{[MPa]} \quad (2.13)$$

$$x = \frac{1.5 \cdot 20500}{\tau \cdot \pi \cdot 0.02} = 0.0158 \quad \text{[m]} \quad (2.14)$$

2.5.7 Final Concept

The many design aspects of the elbow are now researched and are now combined to a final concept presented in Figure 2.14. This concept should withstand the vertical and horizontal loads of the test cycle while facilitating enough rotation to reach the extremities of the work space, fulfilling the crucial target specifications. The incorporated components are few and consists of two custom pieces attaching to arm 3 and the forearm, two bearings, one pivot pin and nut and lastly two M4 screw and nut pair. The standard components are easily acquired and the custom parts are manufacturable. The weight is estimated to be under 0.5 kg which is considered acceptable compared to the estimated component weights on the forearm. The front and base are joined by standard bearings and a pivot hinge. The in is clamped by two M4 screws (which will be fitted in the empty holes in the left model in Figure 2.14). The assembly is simple and straight forward. The bearings are easily fitted into the front by sliding them into their cavities, assisted by the chamfered edges. The pin is the fitted through the upper bearing, base and lower bearing and tightened with the set preload. This is also easy as the base is also equipped with guiding chamfers. The base is then aligned centrally to the front by clamping the pin with the M4 screws and nut pair. The large allowable rotation of the front makes these screws easily accessible. The last steps are glueing the base and the front to their respective rods.

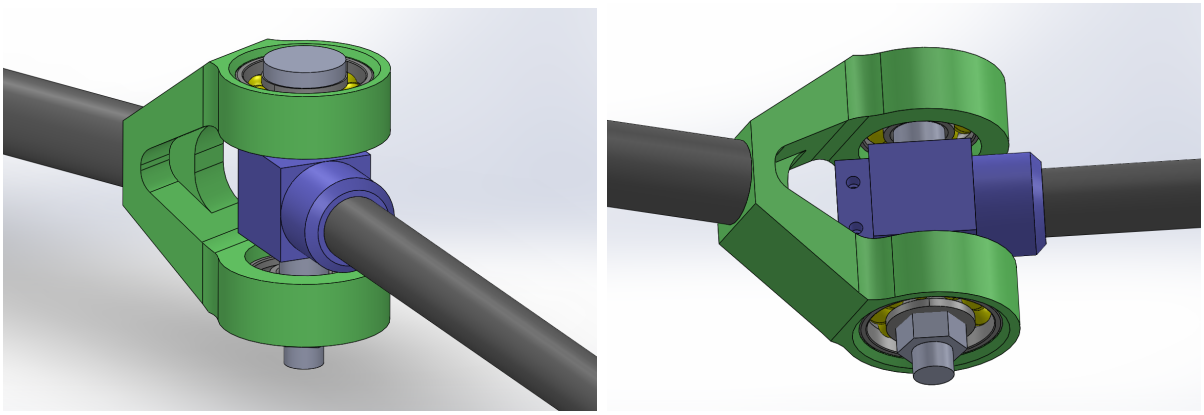

Figure 2.14: Final Concept

The bill of materials is presented in Table 2.7 and the drawings of the custom parts can be found in Appendix D. In Figure 2.15 an exploded view is presented to give a better overview of the components.

Count	Title
1x	Custom Base
1x	Custom Front
1x	Precision Pivot Pin & Lock Nut
2x	SKF Bearing 7302

Table 2.7: Bill of materials

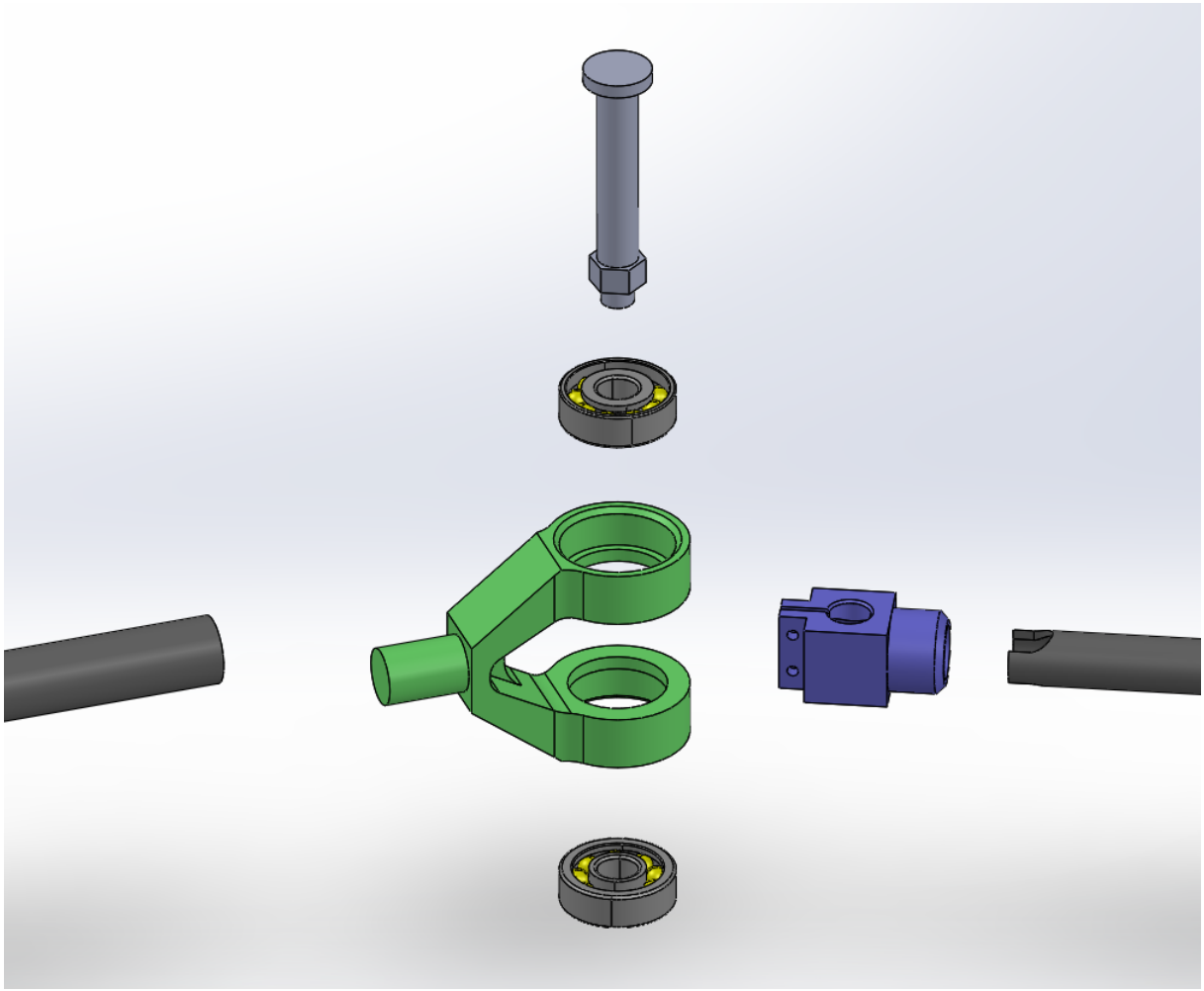

Figure 2.15: Exploded view of final concept

2.6 Concept Evaluation

As the concept has been fully developed it is now to be verified in Ansys Workbench with a FEM-analysis. The full set-up of the analysis is presented in Appendix C. All the analyses are run with a successful convergence setting, meaning the mesh is iteratively refined in high stress areas until the stress converges within 10% of the previous analysis, verifying realistic results as the stresses stagnate.

2.6.1 Front Evaluation

The results of the full front FEM analysis is presented in Figure 2.16. Since the the front is the target of this analysis the shaft component is hidden in Figure 2.17 for a clearer overview. On the left is the legend for the stress indicated by corresponding colors in the model. The max stress in the legend is at 381 MPa which is considerably higher that the yield strength for Aluminium 6061-T6. However, there is no color present for indicating this level of stress in the model. This is because the high stress is experienced in the carbon fibre forearm which is hidden in Figure 2.17 for a better overview of the results for the front. The stress in the forearm is not alarming since the carbon fibre rod has a yield strength of 2.8 GPa[19]. The full setup of the front analysis can be seen in Figure C.7.

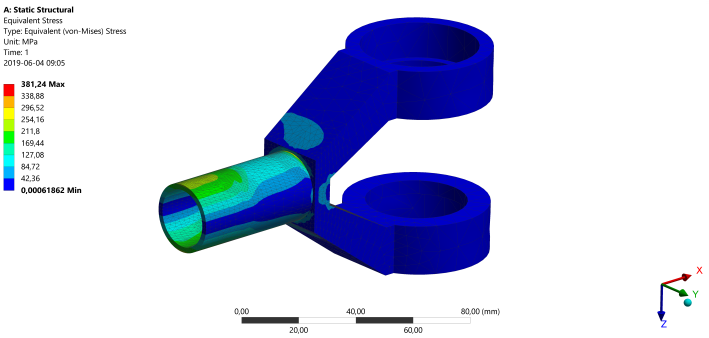

Figure 2.16: Stress overview vertical movement full front setup

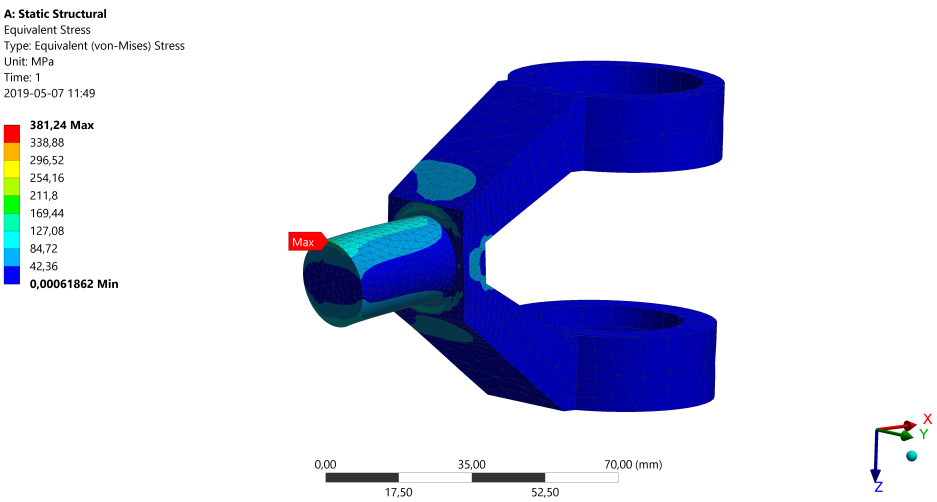

Figure 2.17: Stress overview vertical movement front

In Figure 2.18 the model is displayed with clapped (hidden) ISO surfaces, meaning the volumes containing stresses higher than the set stress are hidden. The stress is here set to 160 MPa which is a sufficient safety factor for 6061-T6. There are barley any volumes hidden except the very tip of the peg where the max stress indicator is located. To get an understanding of how the stress is spread internally throughout the front Figure 2.19 shows a cut section of the front for the vertical movement. The internal stresses are relatively low which deems a very good result for the FEM-analysis and the front should thus handle the loads applied by the vertical movements of the test cycle.

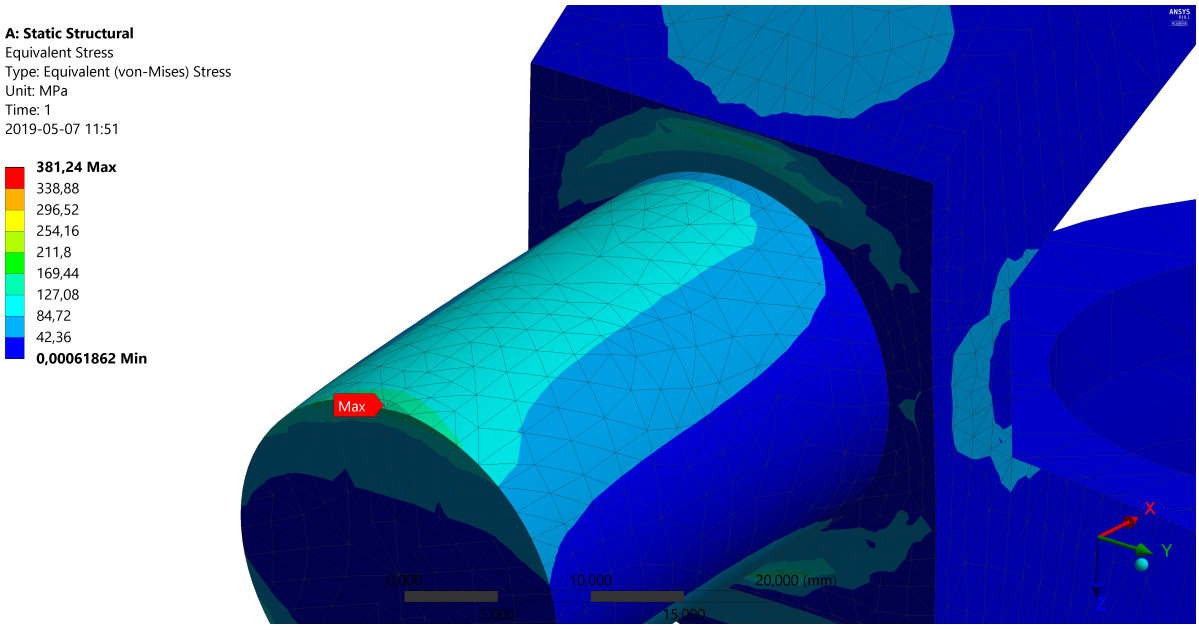

Figure 2.18: Clapped ISO surfaces

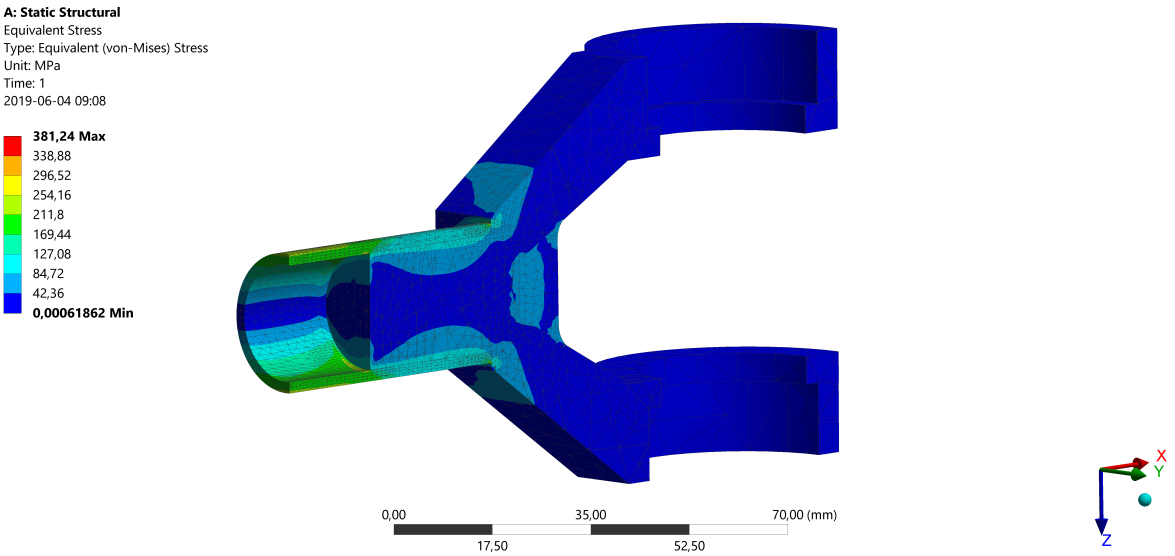

Figure 2.19: Cross section of vertical front analysis

Figure 2.20 shows the analysis for the horizontal movement, set-up is described in Appendix C. The stresses are very low in the whole structure as seen in the legend.

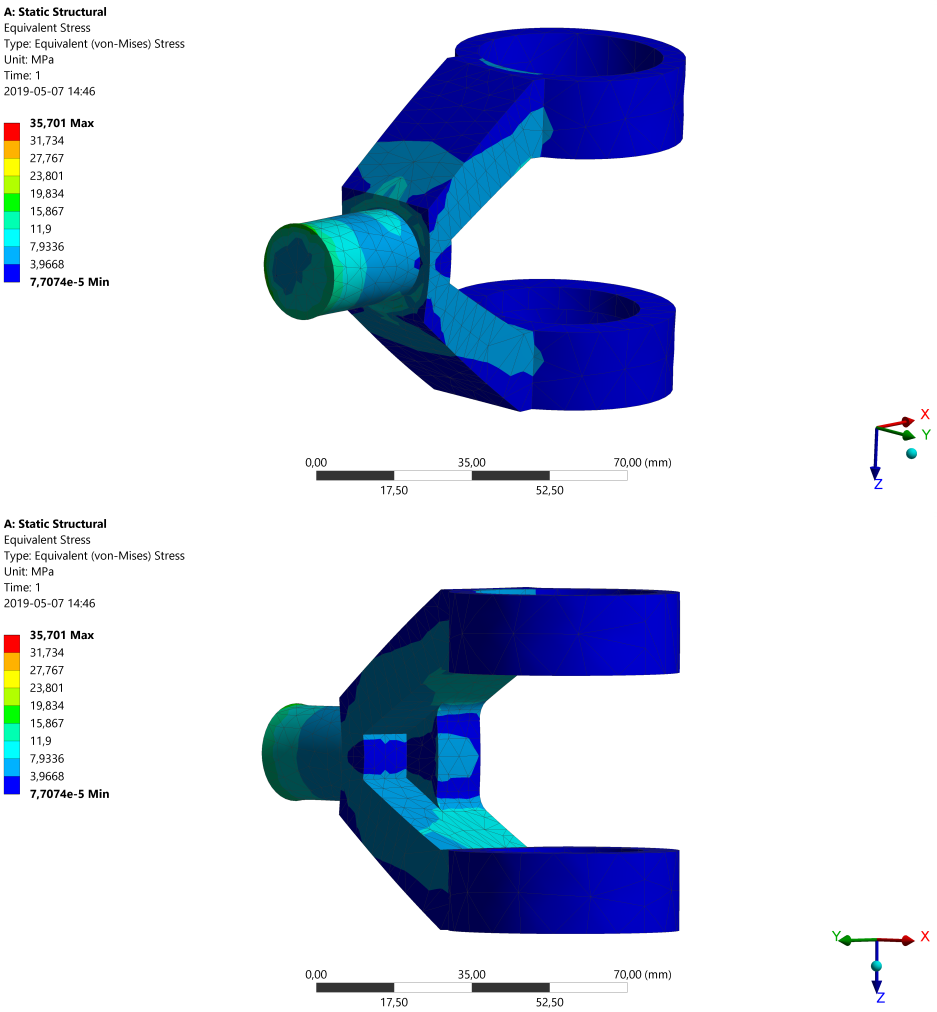

Figure 2.20: Stress overview horizontal movement of front, front and back view

2.6.2 Base and Pin Evaluation

The analysis of the vertical movement is presented in Figure and show a good result as well. The max stress is found at the bottom of the base, more clearly shown in Figure 2.22. The model is displayed with clapped volumes above 160 MPa. Since the whole model is shown, the stress does not exceed the accepted stress levels.

The final FEM-analysis is the loads from the horizontal movement. The results are set up in such that the force of 3505 N is applied at a 25 degree angle, corresponding to the innermost position of the TCP. These results are promising as well as the maximum stress does not appear in the elbow components and thus assuring that the design will withstand these loads.

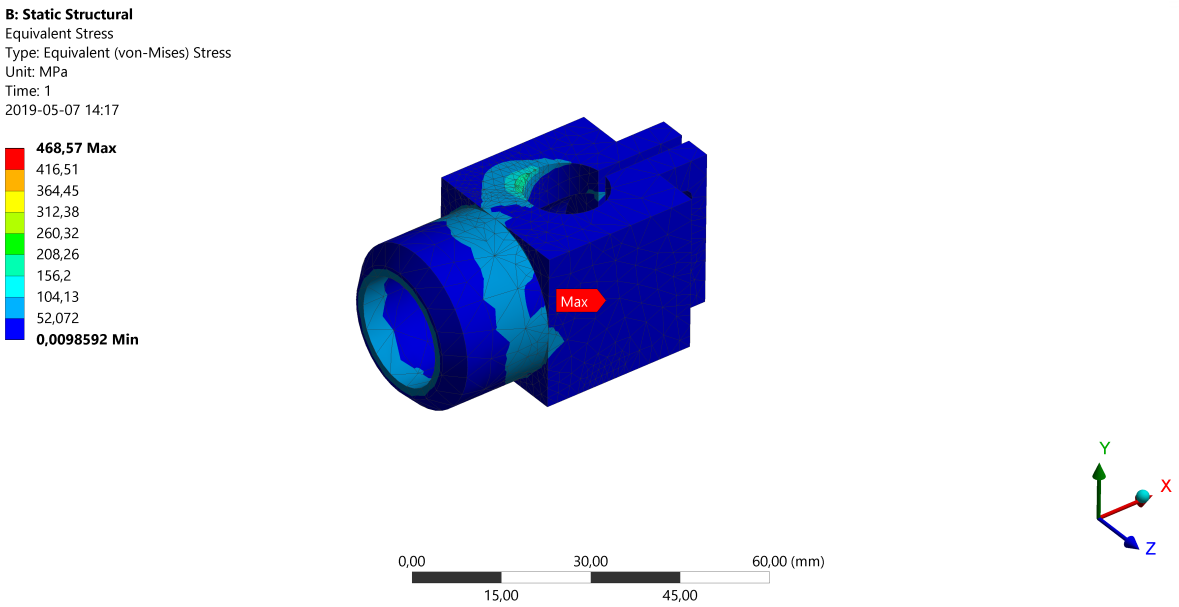

Figure 2.21: Stress overview vertical movement of the base

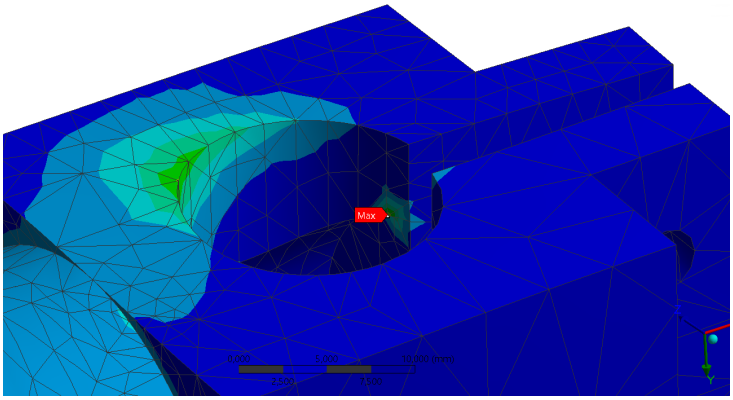

Figure 2.22: Stress overview vertical movement of the base

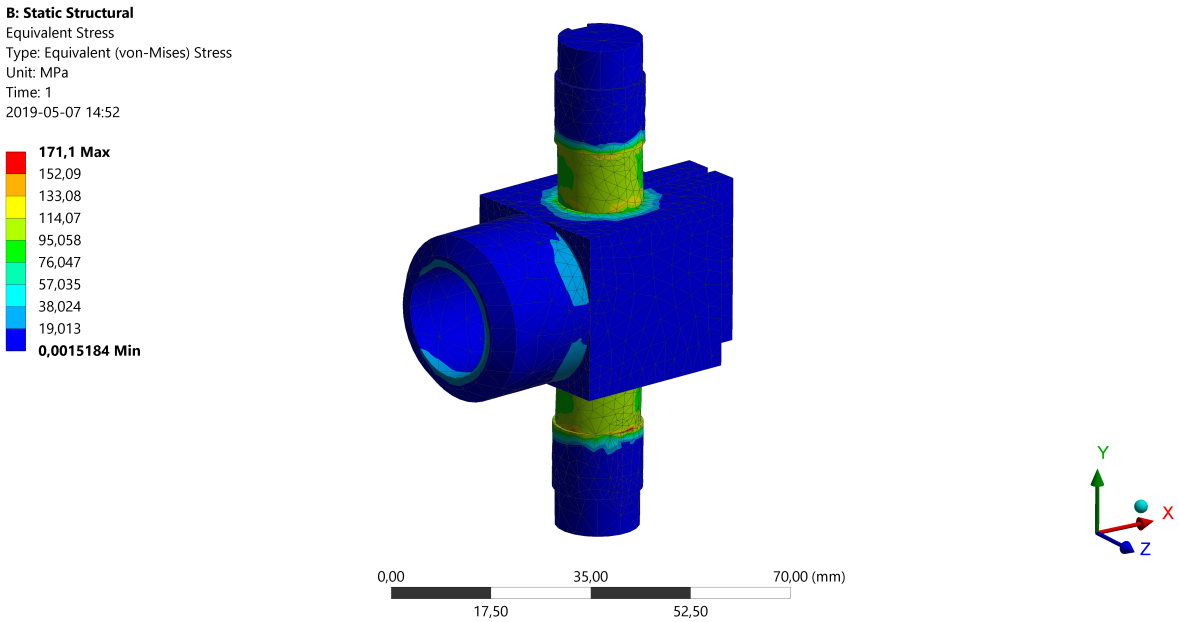

Figure 2.23: Stress overview horizontal movement of the base

2.7 Discussion

The design and development of the elbow has been thorough and elaborate and the final design reached is considered suitable for the prototype. The continued development includes a redesign based on new, and more accurate, loads on the elbow from a simulated tests cycle. The included components will be re-evaluated and if changed the custom parts will be redesigned to match the new dimensions, and further optimized in terms of weight.

The process, as previously stated, has been thorough which has laid a great base for considered solutions. The focus of the process was initially to calculate and develop an optimal solution but has, as the process progressed, shifted towards a "good-enough" solution which is more adapted to how the industry functions. The elaborate start was a great introduction to designing robotic joints, but with the experience gained throughout the development the "good-enough" approach renders faster results and leaves more time for further development and optimization.

The elbow joint has reached an ultimate design and cannot be improved much without hardware tests. The custom parts, mainly the front, can be somewhat further optimized in terms of weight due to the low stresses in the FEM analysis. However, since the loads will be updated from the previously mentioned test cycle simulations and because of a lack of time it has not been done at this time. The remaining components will most likely not be affected by the new loads, apart from increasing or decreasing in dimension, and the current design will most likely be implemented in the physical prototype of the AgilePKM.

Chapter 3

Servomotor Selection

3.1 Introduction

As mentioned in Section 1.1.4 the servo motors will be placed in the base of the robot. Servomotors are the choice of motors since they facilitate precise control of position, velocity and acceleration. Performance and speed outweighs efficiency in choosing motors for the prototype. The motors may control the arms either directly or through gearboxes or ball screws. There are many suppliers of servo motors which is why one company is used as a starting point and comparing a few other suppliers to this one. The main concerns are the torque and RPM of the motor and what automation platform it is compatible with. Since this is a choice of motor for a prototype the energy efficiency is not of much importance and oversizing is preferred to undersizing. Should the prototype be commercialised, the energy efficiency should be looked into more carefully due to the energy cost making up around 96 % of the motors cost during its life cycle[36]. Due to former experience with Beckhoff's products within the company and well compiled data sheets this will be the starting point. Other suppliers will be taken into consideration.

Most of the suppliers have compiled their motors specifications on their web pages and/or convenient brochures which makes the selection process quite straight forward when the specifications are set. Gathering information from the parties involved in the project and making the required assumptions and calculations to set the specification for the motors will be central in choosing motors.

3.2 Specifications

3.2.1 Test cycle

The path used as a benchmark is a standard test cycle used by ABB to test their SCARA robots. The cycle consists of two main movements, one in the X/Y-plane and one in Z-direction. The movement in the X/Y-plane and variables referencing this path will be called or indexed top path. Same applies to movement in Z-direction but it will instead be referenced to as vertical movement.

The coordinate used to describe the path will be Cartesian (x, y, z) with some arbitrarily fixed origin, measured in millimeter. The path of the TCP starts in origin and the orientation of the TCP will be aligned with the Z-axis throughout the full path. With

Model	1kg picking cycle ISO 9283 [s]
IRB 910INV-3	0.35
IRB 910INV-6	0.4
IRB 910SC-3/0.45	0.38
IRB 910SC-3/0.55	0.37
IRB 910SC-3/0.65	0.385
IRB360-1/1130	0.36
IRB360-3/1130	0.4
IRB360-8/1130	0.38
IRB360-1/1600	0.4
IRB360-6/1600	0.43

Table 3.1: Data of ABB's SCARA robots' cycle time[3]

these conditions in mind the path will be

$$(0,0,0) \rightarrow (0,0,25) \rightarrow (300,0,25) \rightarrow (300,0,0) \rightarrow (300,0,25) \rightarrow (0,0,25) \rightarrow (0,0,0) \tag{3.1}$$

As can be seen in the path, the top movement will be 300 mm (d_{top}) and the vertical movement will be 25 mm ($d_{vertical}$). The path can be seen in Figure F.1.

3.2.2 Initial specifications

The AgilePKM is aimed to compete with the best SCARA robots in regards to speed and at the same time have a significantly increased working area. These robots will hence be used as a benchmark and the initial specifications will match the best SCALA robot's cycle time. Since the specifications are set ambitiously they may be subject to change as the analysis progresses. A lot of simplifications and assumptions are also made in this early stage of specifying the robot.

As can be seen in Table 3.1 the fastest cycle time of ABB's SCARA robots is 0.35 s. As a starting point the AgilePKM is assumed to be able to beat this cycle time and a cycle time of 0.3 s is set as the initial goal.

As described in Section 3.2.1 the test cycle consists of two main movements, one in Z-direction and one in the X/Y-plane. There are several motors running to complete the sequence but intuitively M1 or M2 will be the motors which will perform the greatest work. Hence, one of these motors will be chosen first. Ideally M1, M2 and M3 will be of the same model. The reasoning behind this is that the motors should be able to be mounted on the same bracket to keep manufacturing costs down and to be able to keep only one spare motor and replace any damaged motor indifferent of its position.

The speed pattern is assumed to be triangular in the test cycle and the duty cycle is calculated accordingly. The reasoning behind the choice of the speed pattern is that performance is measured by the test cycle. Here the robot is supposed to show itself at its peak performance, which is why it should have servo motors dimensioned not to reach their maximum RPM in this cycle. It should only max out in other cycles with longer paths.

Keeping the ambitious mindset the movement in the X/Y-plane is assumed to take a total of 0.2 s rendering a one way time of 0.1 s (t_{top}) and giving a duty cycle of M1 of 66 %. This leaves a total of 0.1 s to all vertical movement. The robot needs to move the distance of 25 mm in the Z-direction four times to complete one cycle which means the

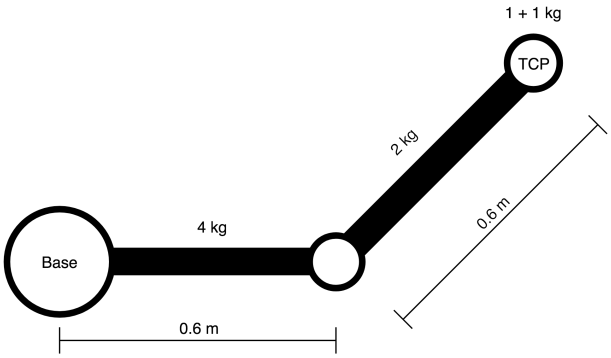

Figure 3.1: Simple figure of the biceps, forearm TCP and its assumed weights and lengths in X/Y-plane

vertical movement may take up to 0.025 s at this point.

$$v_{topAvg} = d_{top}/t_{top} = 3 \qquad [\mathrm{m\,s^{-1}}] \quad (3.2)$$

As seen in Equation 3.2 the average speed of the top path is 3 m/s. Assuming a triangular speed pattern and constant torque where it switches sign half way to decrease the speed instead of increasing it, the maximum speed will reach 6 m/s (v_{topMax}). As mentioned, the time for completing the top path once is 0.1 s. The acceleration will be

$$a_{top} = \frac{v_{topMax}}{t_{top}/2} = 120 \qquad [\mathrm{m\,s^{-2}}] \quad (3.3)$$

In Figure 3.1 the components' mass (m) based on data from the ongoing mechanical design within the company can be seen and its sum is 8 kg . Also the arms' lengths are specified. Using this image the center of mass (l_m) is assumed to be 0.675 m from the base in the worst case scenario. Since the acceleration scales linearly thanks to the constant angular acceleration and the lever (l), the acceleration of the center of mass will be

$$a_{top,m} = a_{top} \cdot \frac{l_m}{l} = 67.5 \qquad [\mathrm{m\,s^{-2}}] \quad (3.4)$$

This gives the desired torque acting on the arm

$$\tau = a_{top,m} \cdot m \cdot l_m = 364.5 \qquad [\mathrm{N\,m}] \quad (3.5)$$

The maximum torque will be required at the highest RPM which is

$$\dot{\omega}_{revMax} = \frac{60}{2\pi} \cdot \frac{v_{topMax}}{l} = 47.75 \qquad [\mathrm{RPM}] \quad (3.6)$$

This gives the highest required power[13]

$$W_{topMax} = \frac{\tau \cdot \dot{\omega}_{revMax}}{9.5488} = 1823 \qquad [\mathrm{W}] \quad (3.7)$$

The moment of inertia of the external load will in the worst case be

$$J_E = m \cdot l_m^2 = 3.38 \qquad [\mathrm{kg\,m^2}] \quad (3.8)$$

These specifications form a solid ground in what torque and RPM is needed from the actuator.

3.3 Selection Criteria

There are several criteria to consider when choosing a motor. The specification of the task is an important base and starting point to weed out some of the motors, but other factors are also important to consider. There seems to be a general consensus in the work flow of choosing a servo motor correctly since many companies and third parties presents very similar flow charts. Wilfried Voss' flow chart presented in the book *"A comprehensible guide to servo motor sizing"* is easy to read with a good balance of clarity and comprehensiveness so this will act as guidelines during the selection process[36, p.12]. The flow chart and its stages will be explained in this section. The following sections assumes M1 is driving the entire load, keeping M2 out of the analysis for now. M2 may in reality aid M1 in the rotational movement which may ease the torque needed in M1.

3.3.1 Rotor speed

When choosing a motor the first thing to consider is the rotor speed, commonly measured in RPM. The motors will drive the load through a gearbox. The gearbox is gearing down (i) the rotational speed of the motor shaft, which means distance is traded for torque. The motor shaft will spin fast with a low torque and through the transmission the load will instead experience slow rotational speed and high torque.

The needed RPM is calculated starting from the desired movement of the robot arm and handling all transmissions until the motor is encountered. The desired maximum speed of the TCP is stated by the company as well as the length of the TCP's distance from the base rendering the calculation in Equation 3.6.

$$\dot{\omega}_{motor} \geq i \cdot \dot{\omega}_{revMax} \qquad [\mathrm{rad\,s^{-1}}] \quad (3.9)$$

3.3.2 Torque

After the speed of the motor has been specified the torque will be considered. The maximum torque is of great importance in this high performance application due to the desired accelerations of the TCP. Using direct drive of the arms is nearly impossible because of the desired torque on the load calculated in Equation 3.5, which is why the gearboxes mentioned in Section 3.3.1 will be used. When selecting a motor the gearbox is assumed to be able to handle the specified torque.

The maximum desired torque (τ_{max}) should be specified and matched to the maximum torque of the motor considering the gear ratio such that

$$\tau_{motor} \geq \frac{\tau_{max}}{i} \qquad [\mathrm{N\,m}] \quad (3.10)$$

Figure 3.2 shows a typical torque graph for servo motors. As can be seen the maximum torque decreases with a higher RPM. In high performance usage one may usually reach more than three times higher torques than the motor is rated according to a salesman at Bosch Rexroth. This is confirmed by Cognibotics who in another project reached multiple times the maximum rated torque for a period of a few milliseconds with no problems.

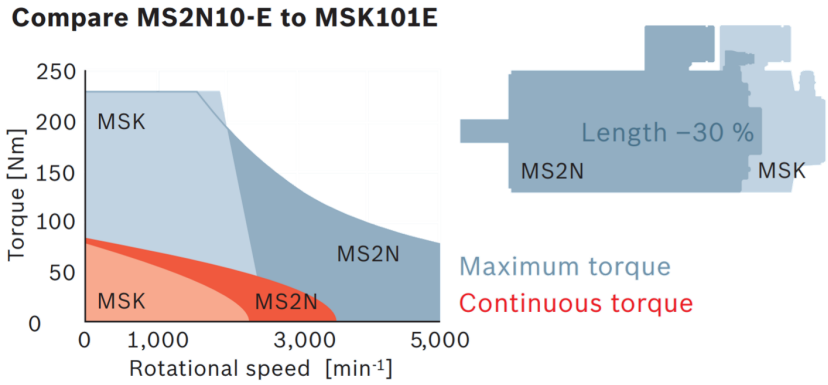

Figure 3.2: Typical torque rating graph comparing two of Bosch Rexroth's motors[23, p.6]

3.3.3 Torque Root Mean Square

Since the amount of test cycles per minute is not defined it is as of now not possible to calculate a general torque RMS (Root Mean Square). The reasoning to why RMS is used is that the direction of the current does not matter, the heat generation will be the same indifferent of direction of the current and the torque which follows. The torque RMS will have to be calculated separately for each application. An example of how one would calculate the torque RMS of a motor follows.

Through Newton's second law it is found that the torque (τ) depends on the moment of inertia (J) and the angular acceleration (α).

$$\tau = J \cdot \alpha \qquad [\mathrm{N\,m}] \quad (3.11)$$

Assuming constant moment of inertia the torque is directly proportional to the acceleration. In order to find the torque RMS for a trajectory the angular acceleration for each time period (t_k) is translated to torque and its RMS is calculated according to

$$\tau_{RMS} = \sqrt{\frac{\tau_1^2 t_1 + ... + \tau_n^2 t_n}{t_1 + ... + t_n}} \qquad [\mathrm{N\,m}] \quad (3.12)$$

In the case of a conveyor or something similar, the trajectory and moment of inertia is very predictable. This is not the case for a robot as the trajectory and moment of inertia is decided by the application and programmer. As the selection is for a prototype and not an application with well defined loads and trajectories, apart from the test cycle, the torque RMS will not be of great weight to the selection. Instead the maximum torque will be focused on as the robot only needs to complete one test cycle with maximum performance. When selecting motors for production the torque RMS will be of greater importance.

3.3.4 Inertia Ratio

The inertia ratio is the ratio between the total inertia of the load (J_L) and the inertia of the motor (J_M). Generally, a lower inertia ratio gives a more responsive system. The inertia ratio is often a central part in choosing servo motors which is why it will be handled in this section. However, it is not of great significance when choosing servo motors for robotics since sensors are located in the motor and not further out in the system. In other

cases, such as for CNC-machines, it is possible to take into consideration to simplify the dynamics. The ratio is described as

$$J_{ratio} = J_L / J_M \qquad [\mathrm{kg\,m^2}] \quad (3.13)$$

where J_L consists of several components such as the inertia of the actuator (L_A), the gearbox (L_G) and the actual external load (L_E) mentioned in Section 3.2.2 as described in Equation 3.14.

$$J_L = J_A + J_G + J_E \qquad [\mathrm{kg\,m^2}] \quad (3.14)$$

The inertia ratio in itself is a complex subject, but here it will be boiled down to two main concerns: acceleration and stability. In conclusion a lower inertia motor allows for higher acceleration of the motor, but may compromise responsiveness in the system should it be too low. On the other hand a higher inertia motor will increase the responsiveness and thereby the stability of the system, but will not accelerate as quickly.[15]

The motor inertia is generally much lower than the inertia calculated in Equation 3.8. Using direct drive these numbers would generate a very high inertia ratio which in turn would give a very unresponsive system. One method to alter the inertia ratio without changing the motor or the external load would be to add some sort of gearing. The inertia ratio is divided by the gear ratio (G) squared as

$$J_{ratio} = \frac{J_L}{J_M \cdot G^2} \qquad [\mathrm{kg\,m^2}] \quad (3.15)$$

In this application a transmission with a gear ratio from 45:1 to 60:1 is being discussed by other parties involved in the project. Taking this into consideration, combined with the data for the AM8061wNyz motor (11.1 $\mathrm{kgcm^2}$) which has the lowest inertia of the motors supplied from Beckhoff (in range 5000-10000 W), one can specify the desired inertia ratio and calculate the external load needed or vice versa. As an example the desired maximum inertia ratio is set to 1:1, which gives good responsiveness in most systems, gives the maximum external load

$$J_{LMax} = J_{MLowest} \cdot G_{60}^2 = 3.996 \qquad [\mathrm{kg\,m^2}] \quad (3.16)$$

for the worst case scenario. Compare this to only the external load of 3.38 $kg\,m^2$ in Equation 3.8 and notice the small headroom of the motor. As of now there is not much room for inertia in the gearbox or the actuator to sustain this ratio, but this example assumes worst case scenario using the AM8061wNyz with lowest inertia of Beckhoffs motors in range 5000-10000 W.

3.4 Selecting Motors

The actual selection of the servo motors will use the method and selection criteria discussed previously in Section 3.3. In this section the selection will be made based on the final parameters and presented in its finality. The reasoning to not handle this in the same chapter as the criterias is that the process of choosing a motor is similar independent of the parameters and use, but the outcome is wildly different.

During the pre studies in Chapter 3.3 the motors looked into were from Beckhoff. As most servo motor suppliers provide similar specifications and functionality, the suppliers are somewhat interchangeable. Due to the company having previous experience and a good relationship with Bosch Rexroth, in combination with their ability to supply not

only motors, but also drivers, industrial PC and transmissions with a supposedly wider range of compatibility than Beckhoff, they will now be the main candidate.

In order to find a suitable fit a motor is preliminarily selected and calculations are made to control whether the specifications are met or not. Should the motor fail to meet the required specifications of the system, a new motor size, one or several sizes above or below, will be chosen as the new preliminary selection. This is iterated until the most suitable motor is found. This is a tedious process and only the calculations of the chosen model are shown here.

The selected motor is Bosch Rexroth MS2N04-D0BQ[23]. It has a maximum torque 19.7 Nm ($\tau_{M,Max}$) and a continuous torque of 4.65 Nm ($\tau_{M,Cont}$). Its top speed is 6000 RPM (n_{Max}) with a moment of inertia of 0.0002 kg m^2 (J_M). The maximum torque needed on the load to reach the specified top speed of 10 rad/s ($\dot{\omega}_{load}$) is 815 Nm (τ_{load}). The gear ratio between the motor and the load is calculated as

$$i \geqslant \frac{\tau_{load}}{\tau_{M,Max}} \tag{3.17}$$

The ratio will be matched to a real gearbox satisfying the gear ratio above. After the gear ratio is specified the maximum motor speed of 6000 RPM ($\dot{\omega}_{M,Max}$) is checked.

$$\dot{\omega}_{M,Max} \geqslant i \cdot \dot{\omega}_{load} \tag{3.18}$$

An upper limit of the gear ratio can be found using the motor speed giving a range of what gear ratio can be used with the motor.

$$i \leqslant \frac{\dot{\omega}_{M,Max}}{\dot{\omega}_{load} \cdot \frac{60}{2\pi}} \tag{3.19}$$

This motor is suitable for the task assuming a gear ratio of $41.3 \geqslant i \geqslant 62.8$ which is a reasonable range considering what is supplied by Bosch Rexroth. RMS analysis and inertia will not be taken into consideration due to reasons discussed in Section 3.3.3 and 3.3.4 respectively.

3.5 Discussion

The servo motor selection has established a good recipe for selecting suitable motors for the AgilePKM. In this recipe, key factors in the robotic structure and test cycle have been identified and mapped to desired characteristics in the motors in order to facilitate an optimal choice.

As the motor selection has progressed, the structure and components of the AgilePKM have continually changed making it impossible to determine the ultimate motor. As the they will continue to change in the development of the prototype and further in adaptations for customer applications, the focus has changed from choosing the optimal motor to formulating a recipe that can easily be followed once final specifications of the structure and components have been set.

To demonstrate the process of the recipe and indicate what range of motors that will be suitable, a preliminary proposal has been presented based on the current specifications of the AgilePKM. The criteria for selecting the motor is well balanced between theoretical principles and practical selections, including the many theoretical aspects that need to be matched with existing motors on the market. This expertise is imperative when designing a prototype and initializing larger scale production.

For the prototype, the same motor is chosen for the axes 1, 2 and 3. This is most likely not the most optimal selection but in terms of building a prototype it has many advantages. These include the ability of quickly replacing the motor on any axis in case of failure, without requiring having expensive replacement motors for different models in stock. The loads for the 3 axes have been estimated to be very similar which implies that the same motor model will not be exceedingly incorrectly dimensioned. For the large scale production the motor selection will certainly differ between the axis as the loads have been accurately identified.

Chapter 4

Control Software

The automation platform will form a connection point for all the modules needed in controlling the robot. The kinematic code was supplied by the company in Python. The code prototype has been implemented by the company in Python to simplify rapid prototyping and implement restrictions and other functionality before optimizing the code. The Python prototype was debugged and further developed and translated using Visual Studio Code on Ubuntu. This is explained further in 4.4.4. The final code was brought into an automation platform called TwinCAT, which will be explained in detail below.

4.1 Introduction

An automation platform will in this case allude to the base on which the controller will be built. The platform is supposed to supply an environment where most, if not all, of the different subsystems can be controlled. Thanks to prior knowledge of TwinCAT within the company, this is the automation platform of choice for implementing the controller. The way the different subsystems are handled are with submodules implemented or imported mostly independent from each other and each dependency is to be manually configured by the programmer.

Within the TwinCAT automation platform many modules are ready to use, such as the CNC kernel provided by ISG Stuttgart and most of the common kinematics for robots such as SCARA and delta. Using the existing libraries is a quite straight forward process, however, power users may be disappointed with the limited support and obscure workarounds when implementing new functionalities within in connection to the platform.

The modules written in C++ primarily handle the kinematics. Here both forward and inverse kinematic transformations are described and fed into TwinCAT. Integrating custom kinematics is not trivial since most common kinematics are built into TwinCAT. The desire to do so is rare, but it can be implemented and imported as a C++ module to be called from the ISG kernel. The kinematics are explained in detail in Section 4.4.

The kinematics was supplied as Python code by the company. The prototype has been implemented by the company in Python to simplify rapid prototyping and implement restrictions and other functionality before optimizing the code. The Python prototyped was debugged and further developed using Visual Studio Code on Ubuntu.

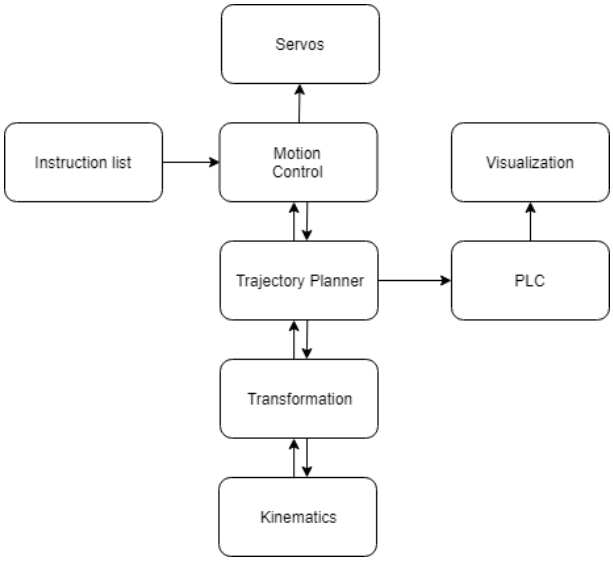

Figure 4.1: Structure of the TwinCAT project and the communication between modules and subprojects.

4.2 Automation Platform

TwinCAT is an abbreviation for The Windows Control and Automation Technology, created by Beckhoff, which can turn any compatible computer into a real-time controller with a multi-PLC (Programmable Logic Controller), NC (Numerical Control) axis control, programming environment and operating station. TwinCAT supports all IEC 61131-3 language standards[22]. It also offers connection to all common field buses, which makes the controller flexible in its connection to other hardware.[6]

Within TwinCAT processor cores may be reserved for a specific task rendering great control over the timing and planning of each subtask. Due to the real time components this is desired in order to have a reliable system with high performance and accuracy. TwinCAT offers a huge variety of tools and frameworks for implementing real time controllers, logging, I/O and much more. One particularly important tool used in this implementation is the integrated ISG kernel which forms the base of the ISG Motion Control Platform (ISG-MCP). The ISG-MCP contains functionality for motion generation such as position control, interpolation and operator control of the drive interfaces[5]. This simplifies the control task significantly for the programmer as the focus can be directed to implementing and integrating the kinematics into TwinCAT instead of trajectory planning.

The TwinCAT project is the main software project for controlling the robot containing several subprojects and modules. A figure demonstrating the structure of the TwinCAT project can be seen in Figure 4.1. Each module and subproject will be explained further in this section.

4.2.1 Windows

When implementing the controller for the AgilePKM, Windows 7 will be the operating system of choice. According to Beckhoff they are currently using Windows 10 and are planning on not supporting Windows 7 within a few years. Beckhoff has only tested Windows 10 on their own hardware and not on other suppliers components such as industrial PCs and drivers. ISG runs Windows 7 with unclear support on Windows 10. Because of how crucial the ISG kernel is to the controller it will act as a limiting factor making the

choice of Windows 7 trivial. The build which is used when implementing the solution will be 7601.

4.2.2 Motion

The motion block is regarded as the core since this is where the CNC is initialized which contains all communication to axes and a channel to the G-code. The CNC contains three different tasks. The two tasks, COM and SDA, handle communication and pass parameter values. The third task, GEO, has the highest priority of the tasks and handles geometrical interpolation with help of the ISG-MCP.

The channel takes G-code from a pre written *.nc file which specifies the parameters needed for a trajectory between two points to be planned. This code is sent to the ISG-MCP block which in turn returns motor angles to the motion block. A real time view of the target angles, current angles, angular velocity etc. can be seen in the channel as a result of the input from the ISG-MCP. These plots are compiled in Appendix F.

4.2.3 Trajectory Planner

The ISG kernel is a software solution incorporated in TwinCat which claims to be suitable to handle almost all CNC, robotics and motion control applications with the incorporation of PLCopen. The kernel claims to have outstanding path and velocity planning which is desirable when controlling a robot with high speed and accuracy, which is why this tool is chosen for the trajectory planning. [14, p.2]

The kernel is used in such a manner that one can specify parameters for different properties of each axis. These properties can be the maximum acceleration and speed, how to act when transitioning from one movement to another and so on. The kernel gets instructions from the instruction list further explained in 4.2.4. It then calls the kinematics, both forward and inverse, in order to plan the movement of each axis in such a way that the robot will carry out the instructions defined in Cartesian space. All while staying within the properties defined by the user.

The kernel lacks some functionalities which are desired when implementing a robot and one can tell it is more geared towards traditional CNC-machines than implementing new kinematics and dynamics. One of the most important features it lacks is the ability to dynamically constrain the axes. Different angles of particularly the parallel kinematic part of the AgilePKM causes drastically different strain on the mechanical construction. This may be worked around with fake drives and scaling of the angle between the fake and the real drive.

As it is not mentioned by Beckhoff as anything other than the ISG Motion Control Platform and they do not link to any web page or company specifically, ISG-stuttgart is the ISG in question. ISG's documentation is scattered across many documents with variable names mostly in German, which makes it unnecessarily difficult to work with. However, it seems to be the best tool to work with in TwinCAT. Trajectory planning will be discussed further in Section 4.3.

4.2.4 Instruction List (G)

The G-code describes movement of the TCP, so this module is what an end user might input to execute a specific task with the robot. G-code in itself is quite simple since it

is merely a question of specifying the desired movement. It is rather the path planning which poses a problem for the end user, where the programmer needs to take obstacles and efficient movement patterns into consideration. Restrictions of reach and more detailed instructions on how to reach the points specified in this module is implemented in the actual controller in the kinematics module.

As an example of how this code might look a snippet demonstrating the programming of a test cycle can be seen in the code presented below. The first step is to activate the correct kinematics and make sure it is turned off. Thereafter the feedrate (F) is set and a linear movement (G01) is conducted to the specified coordinates. The servos are firstly controlled directly and moved to a position which is known to be valid. The transformation is then to be turned on (#TRAFO ON) and the program is temporarily stopped (M00). To control the blend (corner cutting), the contour mode is turned on and the allowed deviation is specified. The lines containing G61 signifies a blended corner, which means it is not required to reach the point exactly but can cut the corner. G60 tells the robot to come to a complete stop at the specified coordinates. M30 tells the program that it has reached the end.

```
#KIN ID[65]
#TRAFO OFF
F100000
G01 X90 Y90 Z0 A0
#TRAFO ON
M00

F360000
G01 X150 Y1000 Z0 A0
M00

#CONTOUR MODE [DEV PATH_DEV=150]
F360000
G60 X150 Y1000 Z0 A0
G01 X150 Y1000 Z25 A0 G61
G01 X-150 Y1000 Z25 A0 G61
G60 X-150 Y1000 Z0 A0
G01 X-150 Y1000 Z25 A0 G61
G01 X150 Y1000 Z25 A0 G61
G60 X150 Y1000 Z0 A0
M00

#TRAFO OFF
G01 X90 Y90 Z0 A0
M30
```

4.2.5 Transformation

The transformation of signals, concerning units and scaling, are carried out by a module implemented in C++. This layer handles all input and output regarding kinematic transformation to and from the ISG kernel. It also contains a large portion of auto generated code which handles transitions over object states and control of whether the transformation is supported or not. As mentioned in Section 4.2.3 the kernel does not use SI units

so the programmer has to account for the conversion. All conversions are handled in the transformation block before the actual kinematic calculations are carried out, which are explained more closely in Section 4.4. Not only conversion and I/O is handled by the transformation block, but error messages are also cast should the point passed be out of range or some mechanical restriction come in play. If the kinematic transformation for the point supplied by the ISG-MCP is valid, the functions return an OK flag, otherwise it will return an ERROR flag.

4.2.6 Kinematics

The modules written in C++ primarily handle the kinematics. Here both forward and inverse kinematic transformations are described and fed into TwinCAT. Integrating custom kinematics is not trivial since most common kinematics are built into TwinCAT. The desire to do so is rare, but it can be implemented and imported as a C++ module to be called from the ISG kernel. The kinematics, its mathematical definition and code implementation are explained in detail in Section 4.4.

4.2.7 PLC

The PLC is used for handling low level communication and execution such as starting and stopping the servo motors safely. Handling the system on such a low level is outside the scope of the thesis but will need to be taken care of once the first prototype is built. It also has direct access to the ISG kernel which makes it able to send data to a scope project, explained further in Section 4.2.8, for the data to be displayed and saved. The data available from the ISG kernel is the Cartesian position of the end effector, each joint's position, velocity, acceleration etcetera.

4.2.8 Visualization

When debugging and evaluating the programming of the robot, visualization of the data is a great tool. In order to plot values of each joint as well as the Cartesian position of the end effector data is passed to a TwinCAT Scope subproject through the PLC. The data is then plotted in graphs and CSV-files may be exported and input to a simulation using for instance Modelica in order to simulate mechanical strain to simplify the mechanical design process. The insight gained in these simulations may also affect the programming of the robot as some working areas may be better mechanically than others.

4.3 Trajectory Planning

In order to execute a command sent from the G-code a trajectory has to be planned. This section will describe the practice of how it is done, but it will be handled in the ISG kernel, thus hidden from the programmer. This kernel is already integrated in TwinCAT as mentioned in Section 4.2 and further explained in Section 4.2.3. However, the concepts are important to grasp when setting parameters for the kernel. There is no need for the programmer to truly go to the depth of trajectory planning, hence the explanations of the trajectory planner will be held quite brief.

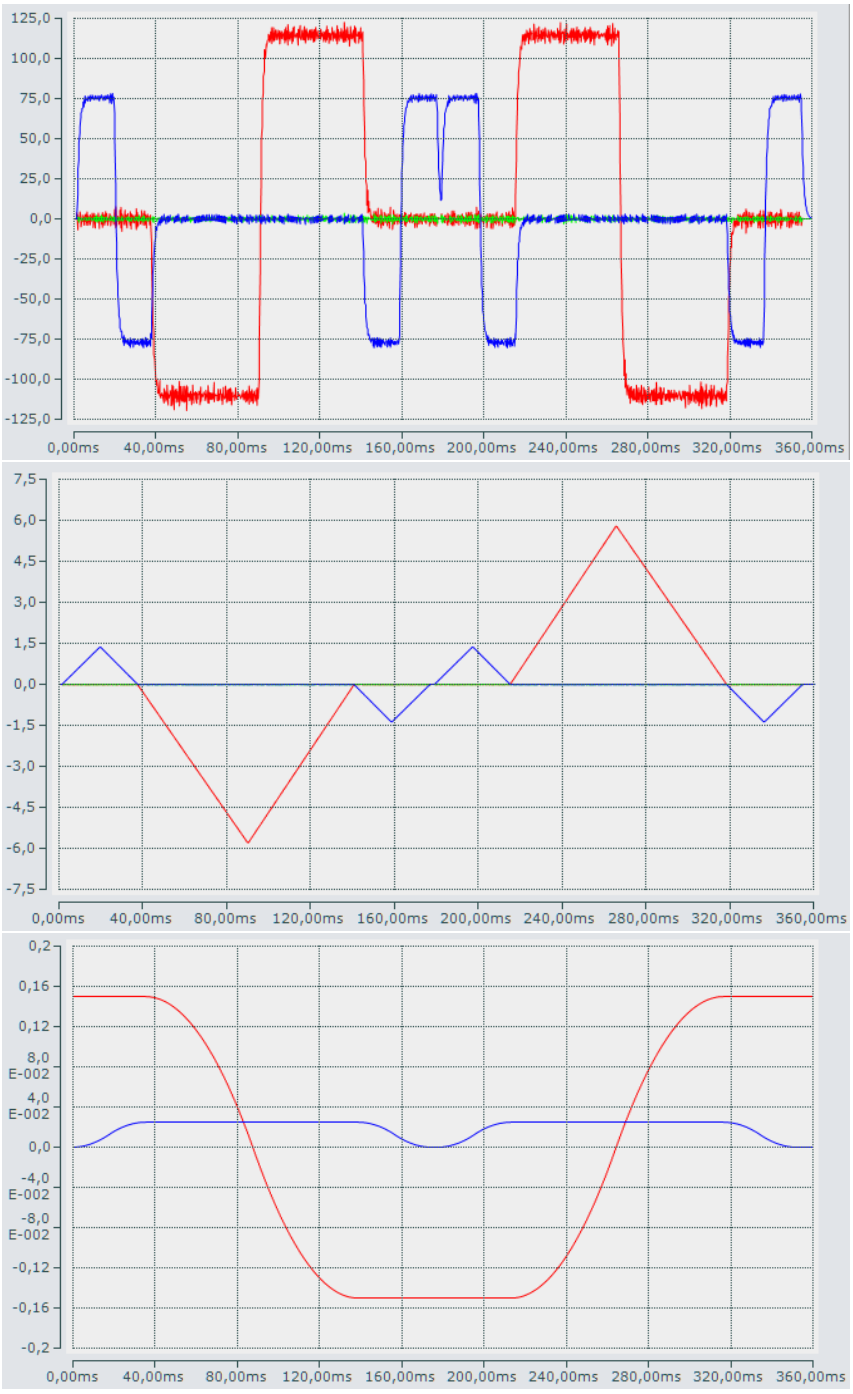

Figure 4.2: Graphs showing the Cartesian acceleration, velocity and position of the test cycle in millimetres. X: red, Y: green, Z: blue.

4.3.1 Path

The trajectory planner takes some instructions from e.g. the G-code and interpolates a path from the starting point to the finish, taking constraints into consideration. This is usually done in joint or Cartesian space. In this application Cartesian space is used unless stated otherwise.[8, p.155]

The algorithm for generating the joint trajectory set points is not very complicated and can be explained as:

> $t = t_0$
> *loop: next control interval ?*
> $\boldsymbol{h}(t)$ = *where the manipulator joint position should be at time* t*;*
> *If* $t = t_f$*, then exit;*
> *go to loop;*
>
> *where* Δt *is the control sampling period for the manipulator.* [8, p.156]

As can be seen in the algorithm, the computation consists of a trajectory function $\mathbf{h}(t)$, which is updated every cycle of the control loop. The function must follow four constraints imposed on the planned trajectory. These four rules has been described well as:

> *First, the trajectory set points must be readily calculable noniteratively. Second, intermediate positions must be determined and specified deterministically. Third, so that the planned joint trajectory is smooth, the continuity of the joint position and its first two time derivatives must be guaranteed. Finally, extraneous motions, such as "wandering", must be minimized.*[8, p.156]

4.3.2 Velocity, Acceleration and Jerk

When discussing velocity one may think of setting a specific acceleration in order to reach the goal. Just setting an acceleration instantly would result in a jerky motion pattern, which is not desired. In order to get a smooth movement of the robot a term ironically named "jerk" is introduced. Jerk is defined as the derivative of acceleration and is an important term when discussing motion profiles. In Figure 4.3, should the acceleration be defined as the top left graph, the velocity will have very distinct breaking points as can be seen in the top right graph. Should instead the derivative of the acceleration, the jerk, be defined as the top left graph, the velocity will be much smoother as can be seen in the bottom left graph. This is desirable as it will be less harmful to the mechanical components and will give a better impression of the robot to observers.

For a specific position to be reached within a specific time limit, the integral of velocity during the time limit has to equal the length of the movement. Same applies for all further derivatives. Limits can hence be set separately on the amplitude of the position, velocity, acceleration and jerk in order to get a desired behaviour as long as it is still able to fulfil the requirements of the task and stay within the restrictions of the mechanics. Starting from the "bottom" with the jerk, should its maximum amplitude be lowered the slope of the acceleration would become gentler rendering smoother movements. If the amplitude of the acceleration were to be lowered the same thing would happen to the velocity and so on.

An example trajectory can be seen in Figure 4.4 where the motor is to be moved from a position of -6 to 6. The jerk is set as a constant for some time and then changed to other constants until the desired position is reached.

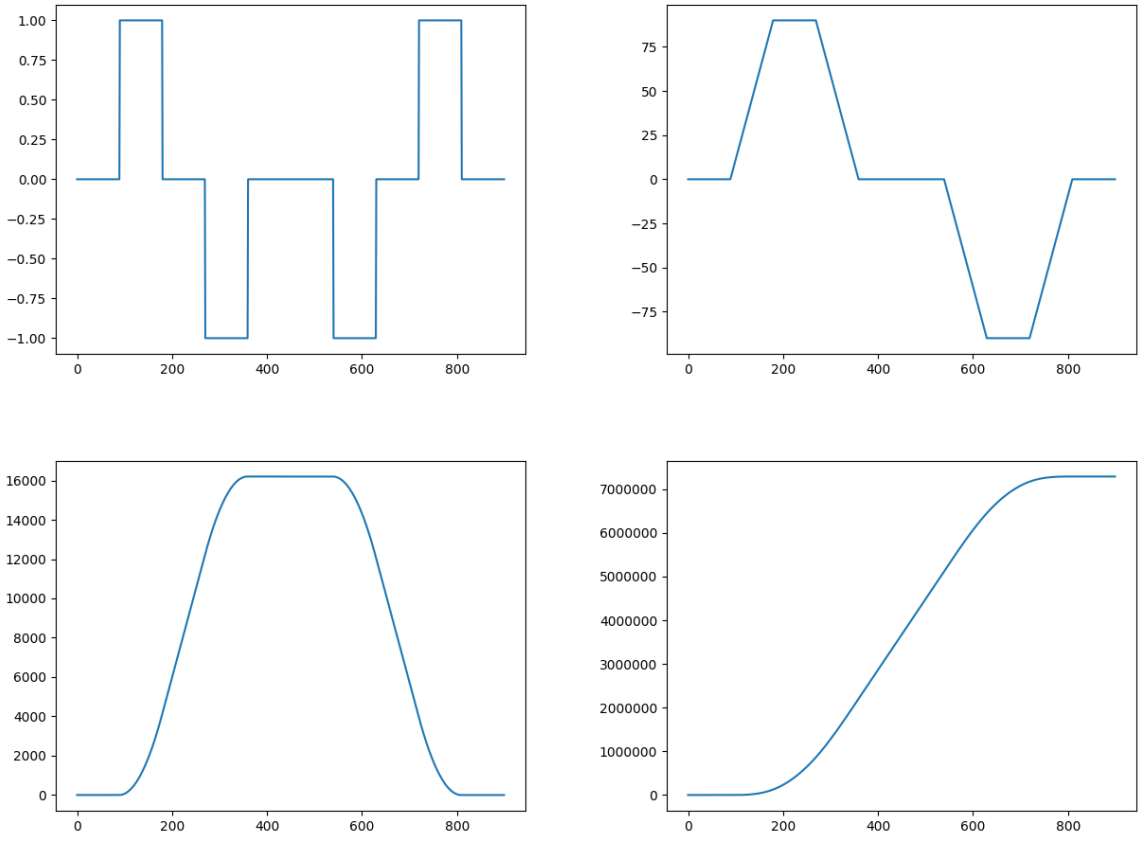

Figure 4.3: Graphing of an arbitrary function and its integrals.

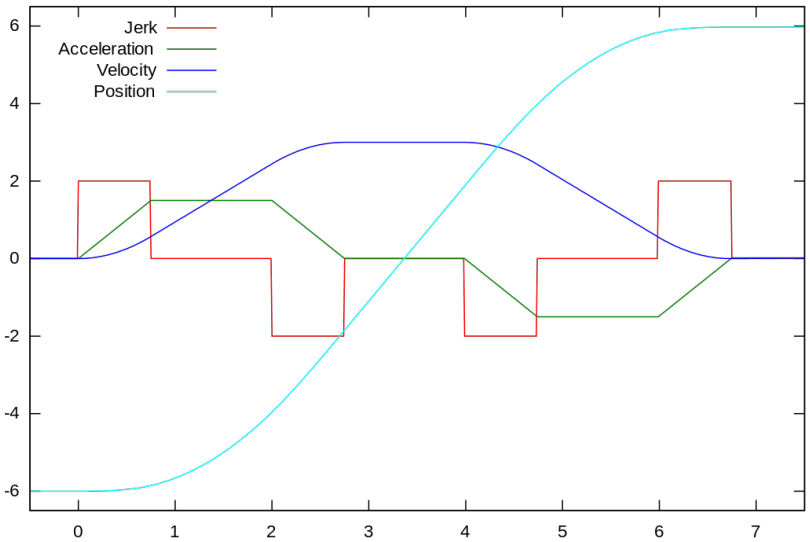

Figure 4.4: Plot describing control of servo motor over time with jerk[37]

4.3.3 Constraints

When the path is well defined some other parameters must also be taken into consideration. The constraint of the path is that it needs to stay within the robots reachable working space. The constraints of the velocity has to do with the maximum speed of the driving shaft, which in turn is constricted by the transmission and driving motor. The acceleration is what demands torque from the motors and will put strain on the mechanical components. In a worst case scenario, failing to set these constrictions properly may have catastrophic consequences and may harm the mechanical design or the motors severely. However, the specification of the limits will be supplied by the company as it is outside the scope of this thesis.

4.4 Kinematics

The kinematic transformations were supplied by the company as Python code. Specifically, that code implemented the prototype version of the formulas for the inverse kinematics and for the forward kinematics, see Section 4.4.1 and Section 4.4.2 respectively. These sections are written to document and further explain the involved computations, which then are to be rewritten in a real-time capable manner, as reported in Section 4.4.4. In order to derive the kinematics the mechanical design of the robot needs to be defined to some extent. One can keep the program quite flexible in terms of lengths of the arms or placements of connection points.

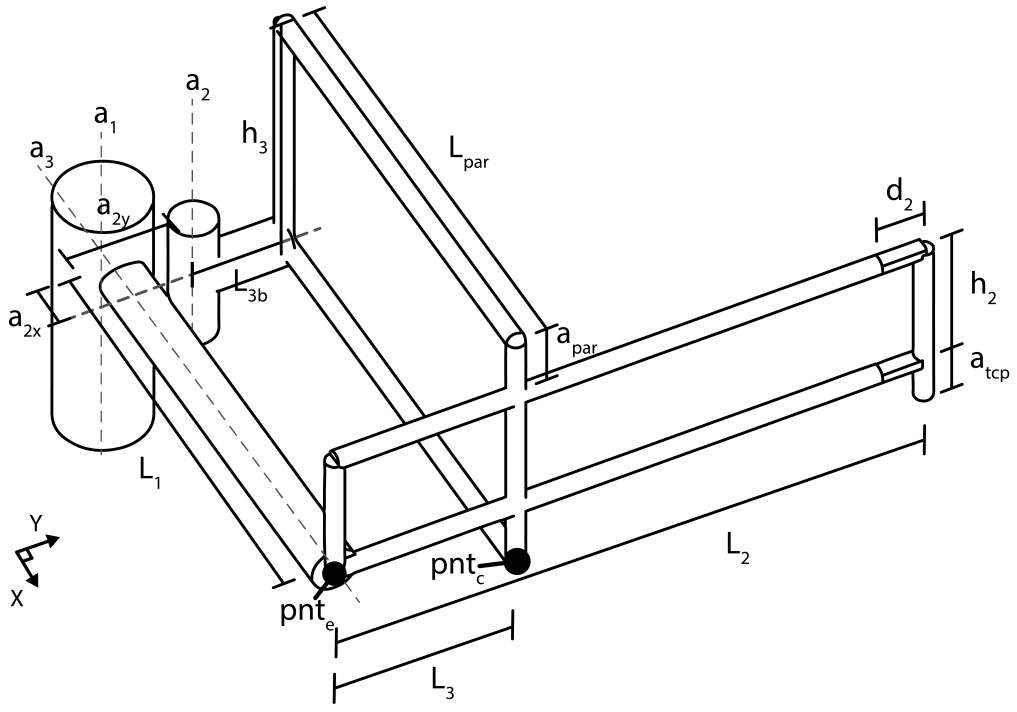

Figure 4.5: Drawing showing a conceptual version of the robot with measurement notations

4.4.1 Inverse kinematics

Inverse kinematic refers to calculating what angles on the axes are needed in order to reach a certain position of the TCP. Since the desired TCP position is the only data available, this is used as a starting point. Calculations are made step by step until the base is reached and all angles have been calculated. All dimensions not introduced in this section can be seen in Figure 4.5. Given a position of the TCP (or in this case the flange where the tool will be mounted) as $[x, y, z - a_2, \phi]$ the angles for each joint, $[q_1, q_2, q_3, q_4]$, will be calculated. The arms L_1 and L_2 are also called biceps and forearm respectively.

An important part of the kinematics are the restrictions. Most restrictions have their base in the mechanical design of the robot. If not enforced properly the physical structure may break, which is why it is of utter importance to have the restrictions well defined and enforced, including a safety factor. Should any of the restrictions not be fulfilled, the input position will be deemed invalid. The restrictions will be briefly explained when the corresponding dimensions are handled.

Forearm tilt

By design the "wrist", marked as d_2 will always be parallel to the x/y-plane. The length d_2 will hence never cause a movement in z direction. To find the tilt of the forearm, d_2 is removed from the total arm length making the equation for the tilt

$$L_{2,tilt} = \arcsin\left(\frac{z}{L_2 - d_2}\right) \quad [rad] \tag{4.1}$$

This is where the first mechanical constraint comes into play. A restriction on $L_{2,tilt}$ of $\pm 30^o$ around axis 3 is set. One thing to keep in mind when implementing this is that it is not a restriction of the TCP but specifically on $L_{2,tilt}$, which is the reason why the TCP's position is not used. As can be seen in the coordinates describing the position of the TCP it is offset by a_2, which is not included when calculating $L_{2,tilt}$.

Forearm projection

This tilt is then used to calculate forearm's projection on the x/y-plane. d_2 is once again subtracted in the calculations regarding only the tilt, but needs to be added when calculating the entirety of the projection as

$$L_{2,proj} = \cos(L_{2,tilt}) \cdot (L_2 - d_2) + d_2 \quad [m] \tag{4.2}$$

Forearm direction and finding q_1

After calculating L_2's projection on the x/y-plane the direction of L_2 needs to be determined. At first it seems like quite a daunting task, but can be simplified using some geometry. Looking at the robot from the top and placing a coordinate system with x_r-axis starting from the base reaching out to the flange will form a base for the calculations. The biceps and forearm may now move in circles around the well defined points (base and flange) in the newly formed coordinate system illustrated in Figure 4.6.

$$radius : r = \sqrt{x_r^2 + y_r^2} \quad [m] \tag{4.3}$$

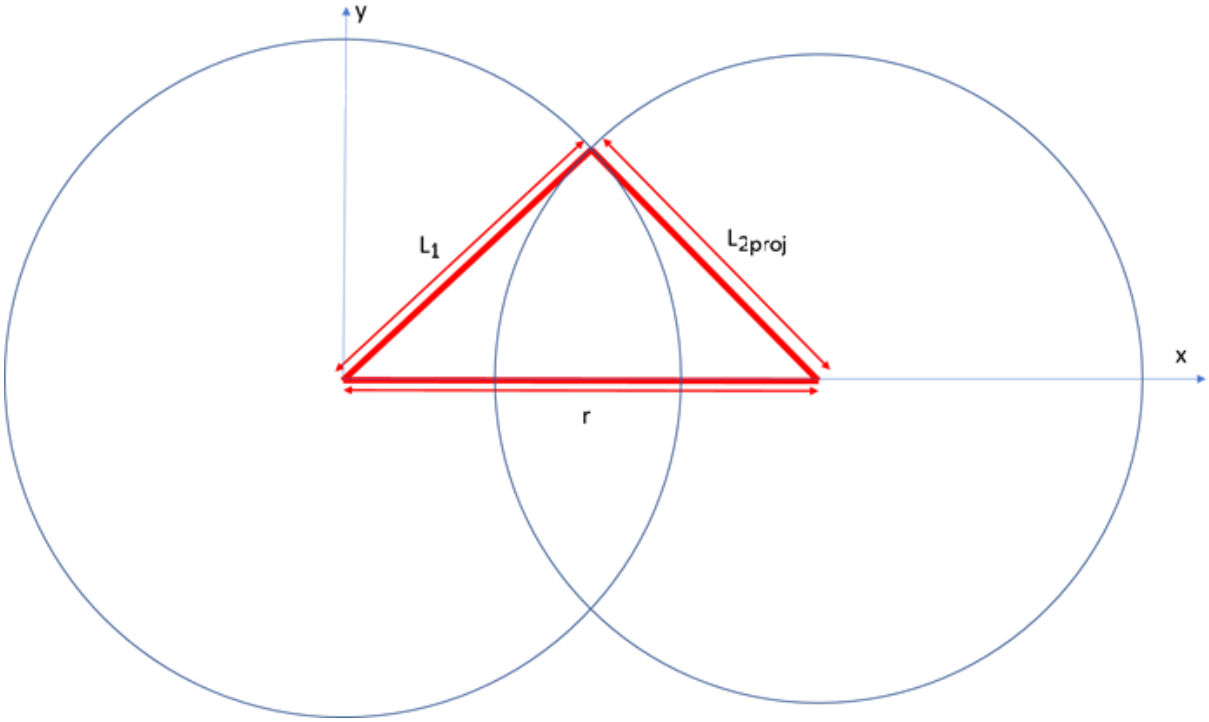

Figure 4.6: Description of a coordinate system where the x-axis in coincident with the line from the base to the flange. The figure was provided by the company.

$$biceps : x_r^2 + y_r^2 = L_1^2 \quad [m^2] \tag{4.4}$$

$$forearm : (x_r - r)^2 + y_r^2 = L_{2,proj}^2 \quad [m^2] \tag{4.5}$$

A control is conducted to check whether the desired point is within reach as $L_1 - L_{2,proj} \leqslant r \leqslant L_1 + L_{2,proj}$. To find the interception's x-position using this system of equations in the newly introduced coordinate system, Equation 4.5 may be subtracted from Equation 4.4 and simplified giving

$$x_e = \frac{L_1^2 - L_{2,proj}^2 + r^2}{2r} \quad [m] \tag{4.6}$$

As can be seen in Equations 4.7 and 4.8, x_e is involved in trigonometrical calculations hence restrictions of $x_e \leqslant L_1$ and $r - x_e \leqslant L_{2,proj}$ are introduced. The last step is to convert this into the angles sought after. To get the angle of L_1 and L_2 in the original coordinate system the angles needs to be offset as

$$q_1 = L_{1,ang} = \arctan(y/x) - \arccos(x_{int}/L_1) \quad [rad] \tag{4.7}$$

$$L_{2,ang} = -\pi/2 + \arccos(x_{int}/L_1) + \arccos((r - x_e)/L_{2,proj}) \quad [rad] \tag{4.8}$$

$L_{1,ang}$ is defined with zero parallel with the x-axis and $L_{2,ang}$ with the normal of the plane created by L_1 and Z-axis as zero, both with counter clockwise as positive rotation. The concept explained is a particularly useful one and will be used in similar cases and referred to when used. A restriction of the kinematics is introduced in order not to put unnecessarily large strain on the mechanical components. $L_{2,ang}$ is restricted to $-65^o \leqslant L_{2,ang} \leqslant 65^o$.

Finding elbow and q_2

Next up is the elbow point, which is defined as an array of three coordinates ($[x, y, z]$), as all points will be from here on since the rotational orientation of points is not relevant apart from the TCP. The elbow point (pnt_e) will always be in level with the x/y-plane and depends only on the biceps. It is described as

$$pnt_e = [L_1 \cdot \cos(L_{1,ang}), L_1 \cdot \sin(L_{1,ang}), 0] \quad [m] \tag{4.9}$$

All coordinates of the connection point (pnt_c) depend on the tilt of the forearm. The connection point is described as

$$pnt_c = [L_1 - L_3 \cdot \cos(L_{2,tilt}) \cdot \sin(L_{2,ang}), L_3 \cdot \cos(L_{2,tilt} \cdot \cos(L_{2,ang}), L_3 \cdot \sin(L_{2,tilt})] \quad [m] \tag{4.10}$$

The distance and the angle from the base rotation point of a_2 to the connection point in the local coordinates are calculated as

$$c_{dist} = \sqrt{(pnt_c[1] - a_{2,x})^2 + (pnt_c[2] - a_{2,y})^2} \quad [m] \tag{4.11}$$

$$c_{ang} = \arctan\left(\frac{pnt_c[2] - a_{2,y}}{pnt_c[1] - a_{2,x}}\right) \quad [rad] \tag{4.12}$$

To calculate the projection of L_{par} on the x/y-plane Pythagoras' theorem is used leading to

$$L_{par,proj} = \sqrt{L_{par}^2 - pnt_c[3]^2} \quad [m] \tag{4.13}$$

Another mechanical restriction needs to be controlled and its condition is $c_{dist} \leqslant L_{3b} + L_{par,proj}$. Using the same methodology as when finding the interception in Equation 4.6, the position of the connection point is calculated

$$x_c = \frac{L_{3b}^2 - L_{par,proj}^2 + c_{dist}^2}{2c_{dist}} \quad [m] \tag{4.14}$$

One important note is that x_c is the distance from a_2 to the connection point of L_{3b} and $L_{par,proj}$ and a temporary coordinate system is introduced according to Figure 4.6. Hence c_{ang} needs to be added in order to account for the skewed angle of x_c. Assuming the restriction of $x_c \leqslant L_{3b}$ is fulfilled, the second angle is calculated as

$$q_2 = \arccos\left(\frac{x_c}{L_{3b}}\right) + c_{ang} \quad [rad] \tag{4.15}$$

Finding q_3

When finding the third axis the forearm is projected on a plane with the third axis as a normal as

$$L_{2,orth} = \cos(L_{2,ang})(L_{2,proj} - d_2) \quad [m] \tag{4.16}$$

$$q_3 = \arctan\left(\frac{z}{L_{2,orth}}\right) \quad [rad] \tag{4.17}$$

Finding q_4

Calculating the angle of the fourth axis is a function of the arms leading down to the base and the desired angle as

$$q_4 = \phi - L_{1,ang} - L_{2,ang} \tag{4.18}$$

In the end the calculations shows one possible solution for the angle of each joint to reach the desired position. These values are then what is sent to the trajectory planner which in turn sends control signals to the servos.

4.4.2 Forward kinematics

Forward kinematics means calculating the final position, $[x, y, z, \phi]$, of the TCP given a certain set of angles of each axis, $[q_1, q_2, q_3, q_4]$. Note that these are angles of the driving mechanisms. In the case of q_1 the angle of the driver and the driven will be the same, i.e. q_1 will be the same as $L_{1,ang}$. This is not the case of q_2 thanks to mechanisms between the driver and the final axis to be driven. Calculating the forward kinematics for an articulated robot is a quite straight forward process since each joint is in series with its previous joint. When mixing this with parallel kinematics it becomes slightly more complicated.

While the inverse kinematics starts from the TCP, the forward kinematics starts at the base traversing until the TCP is reached. The first step is to define where the parallel rods attach on the base side in comparison to the base. In order to do this, the angle of the first joint is used together with the offset of the second axis and then projected on the plane through axis 3 and the forearm.

$$pnt_{a,2} = [a_{2,x} + L_{3b}\cos(q_1), a_{2,y} + L_{3b}\sin(q_2), 0] \quad [m] \tag{4.19}$$

$$pnt_{a,2,proj} = [pnt_{a,2}[1], pnt_{a,2}[2]\cos(q_3), 0] \quad [m] \tag{4.20}$$

In preparation to be able to use the same methodology as when finding the intersection in Equation 4.6 a vector from $pnt_{a,2,proj}$ to the elbow is calculated. The length and angle relative to the bicep is then extracted.

$$r_{par,proj} = [L_1, 0, 0] - pnt_{a,2,proj} \tag{4.21}$$

$$r_{len} = \sqrt{r_{par,proj}^2 + r_{par,proj}[2]^2} \tag{4.22}$$

$$r_{ang} = \arctan(r_{par,proj}[2], r_{par,proj}[1]) \tag{4.23}$$

The parallel rods are then projected onto the same plane

$$L_{par,proj} = \sqrt{L_{par}^2 - (pnt_{a,2}[2]\sin(q_3))^2} \quad [m] \tag{4.24}$$

The preparation for finding the intersections of the circles with centres at a_2 and $r_{par,proj}$ are done and the result is as follows

$$x_{par,b} = \frac{L_3^2 - L_{par,proj}^2 + r_{len}^2}{2r_{len}} \tag{4.25}$$

The angle of the forearm around a_3 in the plane through axis three and the forearm assumes that $x_{par,b} \leqslant L_3$. When this is satisfied $q_{2,3}$ can be calculated as

$$q_{2,3} = \pi/2 + r_{ang} - \arccos(x_{par,b}/L_3) \tag{4.26}$$

Transformation matrices will be used in order to rotate and translate the position. These are explained in detail in Section 4.4.3. In order to find the position and direction of pnt_e, q_1 is fed into the rotation matrix in Equation 4.36 and multiplied by the translation matrix.

$$pose_e = T_x(q_1)T_{trans}(L_1, 0, 0) \tag{4.27}$$

To find the position of the hinge axis by the flange both rotation around X- and Z-axis as well as translation need to be considered. To calculate this the serial part is kept in mind and all changes are multiplied together as

$$pose_{a,h} = T_x(q_3)T_z(q_{2,3})T_{trans}(0, L_2 - d_2, 0) \tag{4.28}$$

In order to get the direction of L_2 in the X/Y-plane relative to a_1 the perspective transformation of $pose_e$ is used.

$$q_{2,1} = \arctan(\frac{pose_{axh}[2,4] - pose_e[2,4]}{pose_{axh}[1,4] - pose_e[1,4]}) \tag{4.29}$$

The distance from the hinge to the wrist and from the wrist to the flange are calculated and added to the perspective transformation of $pose_{a,h}$ in order to find the final translation.

$$d_{h,w} = [d_2 \cos(q_{2,1}), d_2 \sin(q_{2,1}), 0] \tag{4.30}$$

$$d_{w,f} = [0, 0, -a_2] \tag{4.31}$$

$$T_{final} = pose_{a,h} + d_{h,w} + d_{w,f} \tag{4.32}$$

The final orientation of the flange in Z-axis is determined by

$$\theta_{tool,z} = q_{2,1} + q_3 - \pi/2 \tag{4.33}$$

This gives the final position and orientation of the flange where the tool will be mounted. When attaching the tool an offset is needed to consider its positional offset compared to the flange. The values which are returned are the three rightmost values in the transformation matrix, replacing the scaling factor with $\theta_{tool,z}$.

4.4.3 Homogenous Transformation Matrix

In order to describe the TCP's position fully in Euclidean space it is not sufficient to specify its position. Information about its direction in said space would be omitted, which is why the approach of using a homogenous transformation matrix (HTM) is preferable. The HTM has the dimension $(n+1) \times (n+1)$ which gives representation of 3D Euclidean space the dimension of 4×4. One might say that HTM consists of four submatrixes. The top left 3×3 matrix is the rotational matrix, the vector to its right with the dimension of 3×1 is the positional vector, the vector with the dimension of 1×3 below the rotational vector represents the perspective transformation, and the element in the lower right corner is the global scaling factor.[8, p.65]

There are three specific versions of the HTM called basic homogenous rotation matrices which are central to rotating the TCP when calculating the forward kinematics. There is also a basic homogenous translation matrix which is used to translate the TCP with no rotation. The matrices in question are[8, p.66]

$$T_x(\phi) = \begin{bmatrix} 1 & 0 & 0 & 0 \\ 0 & \cos(\phi) & -\sin(\phi) & 0 \\ 0 & \sin(\phi) & \cos(\phi) & 0 \\ 0 & 0 & 0 & 1 \end{bmatrix} \tag{4.34}$$

$$T_y(\phi) = \begin{bmatrix} \cos(\phi) & 0 & \sin(\phi) & 0 \\ 0 & 1 & 0 & 0 \\ -\sin(\phi) & 0 & \cos(\phi) & 0 \\ 0 & 0 & 0 & 1 \end{bmatrix} \tag{4.35}$$

$$T_z(\phi) = \begin{bmatrix} \cos(\phi) & -\sin(\phi) & 0 & 0 \\ \sin(\phi) & \cos(\phi) & 0 & 0 \\ 0 & 0 & 1 & 0 \\ 0 & 0 & 0 & 1 \end{bmatrix} \tag{4.36}$$

$$T_{trans}(dx, dy, dz) = \begin{bmatrix} 1 & 1 & 0 & dx \\ 0 & 1 & 0 & dy \\ 0 & 0 & 1 & dz \\ 0 & 0 & 0 & 1 \end{bmatrix} \tag{4.37}$$

4.4.4 Implementation

As mentioned in Section 4.4 a prototype implemented in Python was supplied by the company. Once all functionality is implemented and tested in Python the kinematic code is translated to C giving a significant performance boost making the calculations more than one hundred times faster. The code was first translated automatically, which rendered an even slower execution time. In order to facilitate the high demands of the system, the code was translated by hand, giving a well commented and easily read source code. The C code was also implemented and debugged in Visual Studio Code and a flag can be sent to the program defining the environment, Linux or TwinCAT. There are some slight differences to the versions, such as available libraries and global variable names.

After translating to C the final execution time became two to five microseconds for the forward and inverse kinematics. The final implementation of the kinematics can be seen in Appendix E. To verify that the transformation results' resolution are up to par the forward kinematics are run and the result is fed into the reverse kinematics where the angles returned should be identical to the angles entered in the forward kinematics and vice verse. One example of a function used to test the kinematics can be seen below. The positions are provided by the ISG kernel in 0.1 μm and the transformation results need to be available to the ISG kernel in this resolution.[1, p.10]

```
int test_fwd_inv(bool print){
        double pos[][4] = {     {1, 0, 0, 0},
                                {0, 1, 0, 0},
                                {0.6, 0.6, 0.1, PI},
                                {0.3, 0.8, -0.1, 0}};
        double errPos[][4] = {{},{},{},{}};
        double errQ[][4] = {{},{},{},{}};
```

```
        double q[4] = {0, PI/2, 0, 0};
        double qNom[4] = {};
        double posNom[4] = {};

        cout << "Error codes for fwd_inv (b f):\n";
        for (int j = 0; j < 4; ++j){
                for (int i = 0; i < 4; ++i){
                        posNom[i] = pos[j][i];
                }
                int b = APKM_backward(pos[j], q);

                for (int i = 0; i < 4; ++i){
                        qNom[i] = q[i];
                }
                int f = APKM_forward(q, pos[j]);
                double qTemp[4] = {};
                int q2 = APKM_backward(pos[j], qTemp);
                for (int k = 0; k < 4; ++k){
                        errPos[j][k] = posNom[k] - pos[j][k];
                        errQ[j][k] = qNom[k] - qTemp[k];
                }

                cout << b << '\t' << f << '\n';
        }
        for (int i = 0; i < 4; ++i){
                for (int j = 0; j < 4; ++j){
                        if(errPos[i][j] > 1e-14 || errQ[i][j] > 1e-14)
                                return -1;
                }
        }

        if (print){
                show_errors(errQ, errPos);
        }
        return 0;
}
```

Chapter 5

Conclusion

The result for each of the three tasks is viewed as successful. The development of the elbow has been elaborate as a wide scope of possible solutions have been considered while still leaving time for the development of the final prototype. A lot of knowledge has been gained in both the design of technical components and considerations in designing a robot structure.

The design of the elbow joint has fulfilled the identified requirements. The design, interplay between and dimensioning of the components ensure that the elbow joint will withstand the loads of the test cycle. This has further been verified with a FEM analysis, indicating stresses lower than the yield stress (including a safety factor) of the chosen material Aluminium 6061-T6. The required movement is mainly enabled by the design of the custom front, and the entire elbow joint, along adjacent features of the AgilePKM, has been modelled in CAD in order to validate that the extremities of the workspace can be reached. The chosen bearing pair consisting of angular contact ball bearings in adjusted arrangement is minimalistic and retain a low weight and a compact design. The included components are either standardized, and can easily be ordered, or designed with manufacturing in mind, ensuring high manufacturability of the elbow joint as a whole. Features that ease assembly has been implemented and the low part count ensures that few assembly steps are required. The rigidity and serviceability have not been prioritized but are predicted to have good characteristics due to durable design and ease of assembly. The design can be somewhat further optimized, but this work is mainly dependent on new load estimations.

The selected motor Bosch Rexroth MS2N04-D0BQ[23] meets the preliminary specifications from the current structure of the AgilePKM and the test cycle well. The proposed gearing, the maximum and continuous torque rating of 19.7 Nm and 4.65 Nm along the top speed of 6000 RPM facilitates the the requirements of the test cycle. For further developments of the AgilePKM a motor selection recipe has been developed to adapt to adapt to the continually alternating structure and components, until the final specifications are set.

The implementation of the automation platform has reached the initial goal but throughout the process limitations in the platform have been found. All servo motors are being controlled virtually with good positional accuracy. TwinCAT and its submodules are not easily understood by a new user and a lot of experience is needed before one can work around problems such as no support for four axis CNC control (where one will have to add a fifth unused axis), variable names in German and random lock-ups.

The test cycle has been successfully simulated and the restrictions have been integrated for the workspace as well as acceleration, which is the foundation for future

development. Lack of functionality in implementing dynamic limitations of the acceleration of each axis poses a great challenge in the design of the controller. This is needed for high acceleration movement and is crucial for the final implementation. TwinCAT may not actually be the correct platform for the task and other platform should be considered before developing this project any further.

Process wise, it has been pleasant to prototype in Python and manually translating to C. It will give a much smoother developing process as the readability and simplicity of Python minimizes mistakes and makes testing and debugging simple. Making the C-code runnable on both TwinCAT and Linux using compile flags has been convenient when new functionality were to be built.

5.1 Future Work

A lot of knowledge has been gained from the development of the elbow, servo selection, implementation of the automation platform and from the process of establishing an overall structure by the company. The continued work from this point consists of redesigning the robot based on new load cases generated from simulations of the test cycle. These simulations are based on trajectory data generated in the test cycle simulation and allows the loads to be accurately mapped before doing tests on hardware, saving time and costs. From this new intelligence the components, where it is found necessary, will be redesigned and ordered to facilitate the build the first proof-of-concept prototype.

This prototype is hoped to spark interest from customers and from there determine specific applications to niche adaptations of the AgilePKM towards. If this stage is successful the AgilePKM will be produced at large scale and adopted in many industries to compete with existing robots.

As for the specific future work for the subtasks of this thesis, the work for the elbow is fairly straight forward. The new simulations are not expected to change the extreme loads the elbow is designed for since the vertical movement loads are dominant and easily derived from the vertical trajectory. There is however always room for improving the elbow in different aspects such as manufacturability, weight reduction and cheaper or higher quality components. The components of the elbow also need to be manufactured and ordered in time for assembly of the prototype. This work has partially been initialized as the standard components are available for ordering from many retailers. The custom parts have been confirmed with a local workshop that they can be manufactured.

The servo selection for the initial prototype is finished and the recipe has been determined. Should the specifications change one only needs to follow the recipe to find motors which are suitable for its tasks. The most urgent control development that needs to be addressed are the dynamic restrictions. Once this issue is resolved the development continues with calibration, vibration dampening and user interface.

Appendix A

Force Analysis

The durability is measured by probability to withstand applied loads of forces and torques along different axis. The elbow is aimed at withstanding the worst case loads in the workspace. To determine whether the elbow design is sufficient the loads and torques are, for measurability, derived into combinations forces and torques along different axis. The following calculations present the methodology, discussion and first iteration of force and torque loads on the elbow. These results are continually updated throughout the process as the surrounding components are designed. These results can be easily deduced from the same methodology and equations.

To investigate and estimate the magnitude of forces the structure of the robot needs to be described and mapped to determine at what positions the maximal forces are experienced. This is done in Section 1.1.5 and Figure 1.2 shows an overview of the structure of the Agile PKM (Concept 2) and the components surrounding the elbow joint are marked out. Only direct adjacent components will be taken into account for the analysis of the elbow with the exception of the *bicep*, which is considered, for sake of analysis, to be static and thus excluded. Also rod_1 is included since it determines the forces on $forearm_1$.

At this stage the Agile PKM is only conceptually designed and very little is known about how the design is going to be realized. This requires rough assumptions to be made in order to get an estimate of the magnitude of forces. These initial estimates are based on recommendations from the company which has both experience in mechanical design and has done background research to establish initial specifications for the Agile PKM. The prominent specification is an acceleration of 150 m/s^2 which is slightly higher than the calculated 120 m/s^2 in Section 3.2.2 but can simply be achieved with more rigours assumptions in the calculations and will be used in the initial analysis for a more rigid analysis.

When the peak acceleration is established free body equations can be set up to

Length [m]	$forearm_1$	0.7
	$forearm_2$	0.7
Weight [kg]	$forearm_1$	1
	$forearm_2$	1
	$wrist$	1
	$payload$	1
	$extra$	1

Table A.1: Inital Estimations

determine forces in single components. A simplified model of the elbow and the connected components is used here where only the elbow link, $forearm_1$ and the wrist mechanism are included. The properties of these components are presented in Table A.1 and are approximated based on research from the company and the following reasoning. The total reach is aimed at 1.2 m to be able to compete and even prevail against the SCARA robot which has a reach of 1 m accordning to Denso Robotics [9, p.1]. For the workspace of the Agile PKM to reach from 1.2 m to the base of the robot the bicep and forearm should be about the same length, 0.6 m. The forearm will however have angular limitations which redeems an increased length of 0.7 to fulfil requirements. The payload is set to 1 kg for the test cycle and the company estimates the wrist and arms to be 1 kg each along an extra weight of 1 kg to anticipate for additional components and weight.

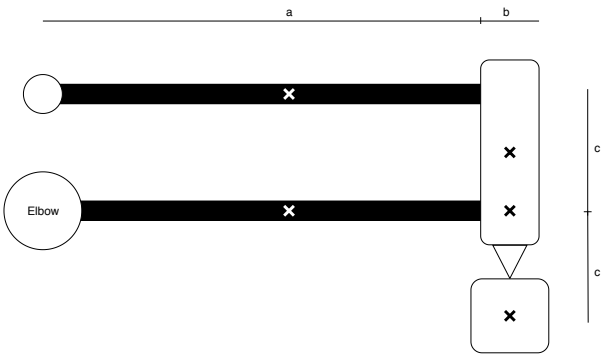

Figure A.1: Center of Gravity

Preliminary weights of the components are now set and the analysis can continue to evaluate the CoG of the arm in reference to the elbow. Figure A.1 displays a simplified model viewed from the front consisting of the elbow, arm and wrist mechanism where the "X" marks CoG of the different components. The horizontal CoG is calculated in Equation A.1 and vertical CoG in Equation A.2 where a = 0.6 m, b = 0.1 m, c = 0.2 m and d = 0.1 m, the depth CoG is located in the same lane as all the components and hence does not need to be calculated. As the mass is collected at the CoG for the force analysis the relative acceleration needs to be taken into account, Equation A.3 calculates this (where $TCP_{horizontal}$ is the horizontal length to the TCP) and Equation A.4 calculates the equivalent force generated by the acceleration accordning to Newton's second law.

$$CoG_{horizontal} : \frac{a}{2} \cdot (W_{arm} + W_{arm}) + \left(a + \frac{b}{2}\right) \cdot (W_{arm} + W_{extra} + W_{payload}) = 0.348 \quad [m] \quad \text{(A.1)}$$

$$CoG_{vertical} : \quad 0 \cdot (W_{arm} + W_{extra}) + (c \cdot W_{arm}) + \left(\frac{c}{2} \cdot W_{wrist}\right) - (d \cdot W_{payload}) = 0.04 \quad [m] \quad \text{(A.2)}$$

$$CoG_{acceleration} : \quad \frac{CoG_{horizontal}}{TCP_{horizontal}} \cdot 150 = 117.7 \quad [ms^{-2}] \quad \text{(A.3)}$$

$$F_{CoG} : \quad CoG_{mass} \cdot CoG_{acceleration} = 337 \quad [N] \quad \text{(A.4)}$$

The acceleration and the CoG determines the magnitude of forces the elbow joint and the forearms will experience. Since these are established the loads on the individual components can now be mapped. The first case is the arm seen from the side, presented

in Figure A.2, where a simplified model is seen to the left and the corresponding beam case to the right. Equation A.5 determines the force load on the lower rod. As previously mentioned the lower rod is carrying the TCP and surrounding components in vertical movements, and now as described by Equation A.5 a large portion of the horizontal loads.

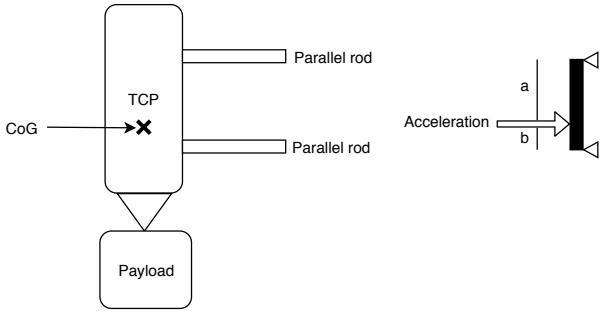

Figure A.2: Side Case

$$F_{LowerRod}: \quad F_{CoG} \cdot \frac{a}{a+b} = 470 \quad [N] \tag{A.5}$$

Continuing to the view the arm from the front, presented in Figure A.3, the torque load on the elbow can be determined Equation A.6, since the vertical movement is only actuated by the elbow acting on the lower arm. The equation encompasses the angular range of 25^o-155^o and shows a constant load on the elbow, however for arm_1 and speed and load varies from the highest load and the lowest speed at $\alpha = 90^o$ and the lowest torque and highest speed at $\alpha = 25^o$ and 155^o, for this analysis only the load for the elbow is considered.

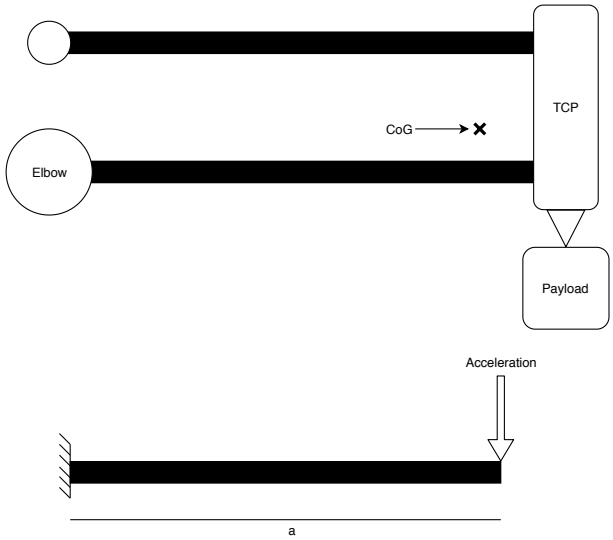

Figure A.3: Front Case

$$T_y = \frac{\sqrt{\left(F_{CoG} \cdot CoG_{horizontal} \cdot sin\left(\alpha\right)\right)^2 + \left(F_{CoG} \cdot CoG_{horizontal} \cdot cos\left(\alpha\right)\right)^2}}{0.06} = 2561 \quad [N] \tag{A.6}$$

The last case, the configuration viewed from the top in Figure A.4 is a bit more complicated. The distance the parallel rods attaches to the forearms is not yet defined,

Attachment Distance [m]	$F_{parallel}$ [kN]	$T_{forearms}[Nm]$
0.01	30	294
0.05	6	270
0.1	3	241
0.15	2	211
0.2	1.5	182

Table A.2: Attachment distance

and since this will greatly affect the force loads on the elbow the relation between force from the rods and the attachment distance should be analysed. As in previous figures a simple model is presented above and below is the corresponding beam case. The force required from the parallel rods is greatly affected by the attachment distance as seen in Equation A.7, which in turn impacts the stress in the forearms. The torque from the parallel rods on the forearms is calculated in Equation A.8.

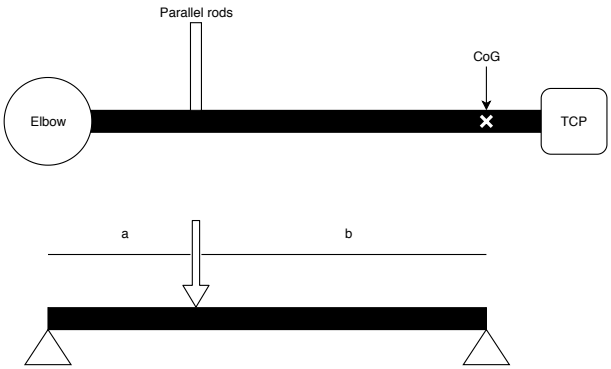

Figure A.4: Top Case

$$F_{parallel}: \quad F_{CoG} \cdot \frac{CoG_{horizontal}}{a} \quad [N] \tag{A.7}$$

$$T_{forearms}: \quad \frac{F_{parallel} \cdot a \cdot b}{a+b} \quad [Nm] \tag{A.8}$$

Combining Equations A.7 and A.8 we get a simplified expression for the torque loads on the forearms, Equation A.9. To map $F_{parallel}$, the attachment distance and $T_{forearms}$ the attachment distance was varied from 0.01m - 0.2 m and the result presented in Table A.2. A reasonable length seems to be 0.1 m in terms of force and torque.

$$T_{forearms}: \quad F_{CoG} \cdot (CoG_{horizontal} - a) \quad [Nm] \tag{A.9}$$

From $F_{parallel}$ the force loads on the elbow can now be determined. Figure A.5 shows the angular limitations set for the forearms, where the working space is defined between 25^o from from full extension and full retraction as explained in Section 2.2.2. $F_{parallel}$ will vary with the angle according to Equation A.10 and the maximum forces occur when alpha is at its extremities. Equations A.11 and A.12 calculates the reactionary forces in the elbow at the extremities and Equation A.13 the maximum vertical load.

$$F_{parallel}: \quad \frac{F_{CoG} \cdot CoG_{horizontal}}{sin(\alpha) \cdot a} = 7102 \quad [N] \tag{A.10}$$

$$F_y: \quad F_{parallel} - F_{CoG} \cdot sin(\alpha) = 6853 \quad [N] \tag{A.11}$$

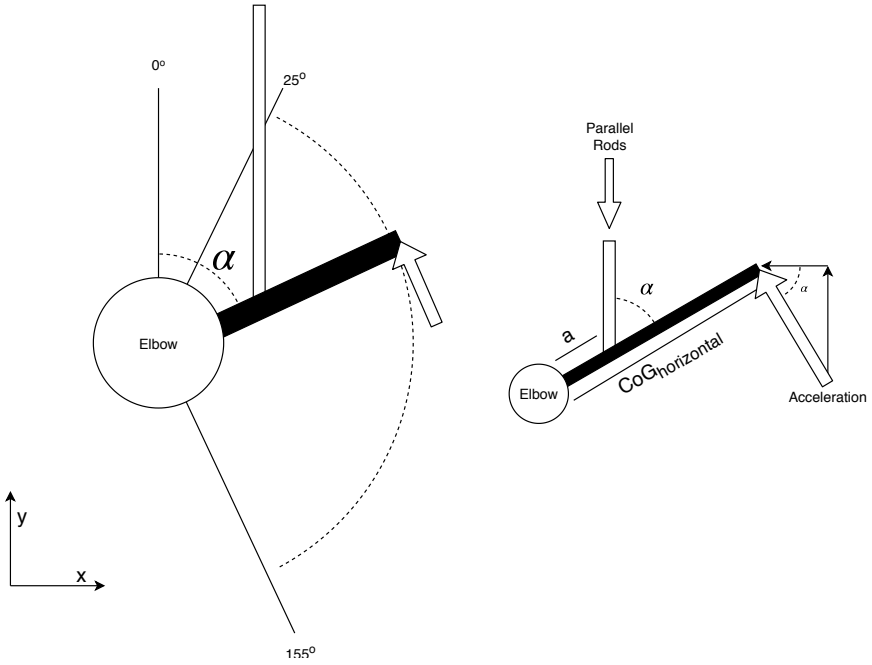

Figure A.5: Horizontal angle limitations

$$F_x: \quad F_{CoG} \cdot cos(\alpha)) = 533 \quad [N] \tag{A.12}$$

$$F_z: \quad F_{CoG} = 589 \quad [Nm] \tag{A.13}$$

$$T_y: \quad F_{CoG} \cdot CoG_{horizontal} \cdot sin(\alpha) = 300 \quad [Nm] \tag{A.14}$$

$$T_x: \quad F_{CoG} \cdot CoG_{horizontal} \cdot cos(\alpha) = 272 \quad [Nm] \tag{A.15}$$

As the properties of the surrounding components are updated throughout with process with the same methodology the final values used in the development are presented in Table A.3 according to the properties in Table A.4.

$CoG_{horizontal}$	0.348 m
CoG_{weight}	4.2 kg
F_{CoG}	337 kg
F_y	2633 N
F_x	305 N
F_z	337 N
T_y	117 Nm
T_x	106 Nm

Table A.3: Maximum loads

Attachment Distance [m]	Weight [kg]	Distance to elbow [m]
Parallel Attachment	0.5	0.1
Forearms	0.1	0.3
Wrist	1	0.65
Payload	1	0.65
Extra,(Elbow)	1	0

Table A.4: Updated component properties

Appendix B

Hinge Components

Here the very basics of the concept generation for the hinge components is presented. The hinge mechanism is, as described in Section 2.3.1 divided into five sub components (*back leaf, back knuckle, pin, front knuckle and front leaf*). These will be analysed and researched.

B.1 Back Leaf

The back leaf is the link between the base of the Agile-PKM, and the elbow joint. It attaches to arm_3 with the preliminary dimensions according to the list below. The circular profile diverges from the existing flat leaf designs which more commonly attaches to flat surfaces on doors and walls. For the leaf to be durable whilst achieving a low weight the leaf profile should match the same profile and allow for efficient attachment to the back knuckle. The actual fixation to arm_3 can be accomplished by mechanical fastening or adhesion. New Concepts and existing components that aim to fulfil all or part of the specifications listed below will now be presented.

1. **Attachment to** arm_3 The elbow needs to be attached to the carbon fibre rod with a diameter of 20 mm and thickness of 2 mm.
2. **Endure horizontal loads** The attachment needs to withstand loads generated from the parallel rods and the elbow. This load is derived from a combined axial and radial force.
3. **Endure radial torque loads** Needs to transfer the torque from the rod to the elbow, requiring high demands on both fastening to the rod and the elbow itself.

Sure Grip Bushing

Torque transfer components are common in the automotive industry where torque is transferred to or from drive shafts. For this intended purpose different types of bushings are used. These components are often over-sized in comparison to the specifications of the Agile-PKM, but in go-kart applications the bushings are reasonably dimensioned. In Figure B.1 such a bushing with its pertaining data in Table B.1 seems a good match. The bushing is fitted with a slit along the entire length allowing the bushing to clamp the shaft upon mounting. On the opposite side a key way is located. This allows for efficient

torque transfer between the shaft and the bushing, if the shaft is fitted with a key. At the back of the bushing there are four holes to attach to the back knuckle.

Figure B.1: Sure grip bushing[38] (left)

Torque Rating [Nm]	198
Weight [g]	300
Inner Diameter [mm]	25.4
Outer Diameter [mm]	41.3

Table B.1: Sure Grip Bushing Data

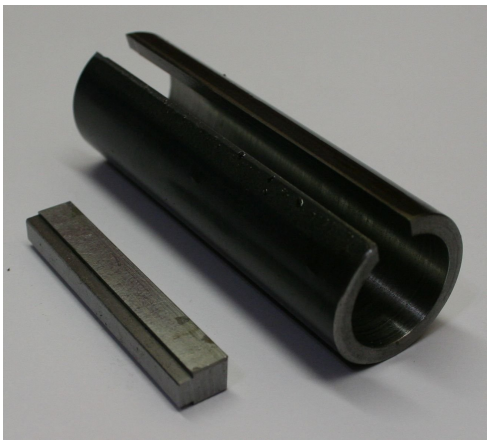

Figure B.2: Market Key Adapter

Sure Grip Bushing With Market Key Adapter

The dimensions are not perfectly matching the preliminary dimensions of arm_3 which is why arm_3 can be fitted with an adapter. These are available in a variety of sizes, enough to be able to match the final dimensions of arm_3. The adapter is fitted by sliding on the adapter base on arm_3 with some kind of adhesive and then fitting the key to the adapter. The assembly is then mounted into the sure grip bushing which clamps the assembly for a snug fit eliminating play. The bushing is very durable and forms, together with the clamp, a snug fit. The adapter is split which allows a very tight fit by clamping around the carbon fibre pipe. It is however not optimal to clamp carbon fibre rods since this impacts the durability. The bushing is rather large and not optimal size wise which affects the weight and size of adjacent components.

Sure Grip Bushing With Custom Key Adapter

This concept is very similar to *Sure Grip Bushing with Market Key Adapter* and is based on the same bushing but replacing the market key adapter with a custom adapter.

This eliminates the clamping around arm_3 and enables a very snug fit since the dimensions of the adapter can be specified to match arm_3. This further enables a promising fit since the outer diameter can be made to match the bushings. The adaptor has to be custom made which increases the cost and further affects the manufacturing score if implemented in a full concept.

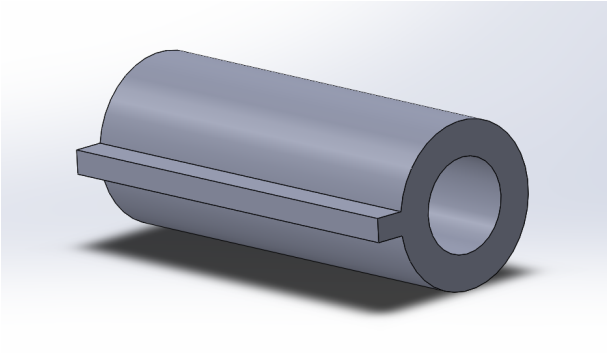

Figure B.3: Custom Adapter

Double Processed Aluminium Rod

Since finding existing products that fit the specifications is scarce more suitable components can be manufactured from existing products. This concept is based on exactly this and consists of a standard aluminium pipe with suitable dimensions, matching the outer diameter of arm_3 and a tolerable thickness to transfer the torque. The pipe would then be processed with two slits at each side to grip the pipe with a shaft clamp. Such clamps are once again available from the go-cart industry where they are used to prevent shaft splitting. This reverts back to the problem of clamping carbon fibre pipes. But to support the pipe in the clamping the inside of the carbon fibre pipe can be fitted with an expander screw. These seem to be a bit more scarce but are commonly used in bikes to fasten handlebars. When assembling this concept arm_3 would be fitted with the expander screw and then slid into the aluminium pipe. The clamping and expander screw and the clamp would simultaneously be tightened to support and secure the carbon fibre pipe. This concept is vulnerable to the attachment to the back knuckle since the tightening of the expander screw is accessed through the aluminium pipe. Further the attachment to the back knuckle needs to be developed, and this can be seen as both an advantage or disadvantage depending on if the back knuckle incorporates a tube or not. This concept is regarded as durable and with a reasonable weight, although the expander screw adds some weight that might be able to be avoided in other concepts. The assembly process is as described before complicated which also affects the serviceability. The pipe is of standard dimensions but is most likely produced in longer lengths than needed here, which drives the price up and is more suitable for large scale production. The pipe also needs to be processed to incorporate the slits.

Figure B.4: Shaft Collar[11] (left), Spacer Screw [33] (Right)

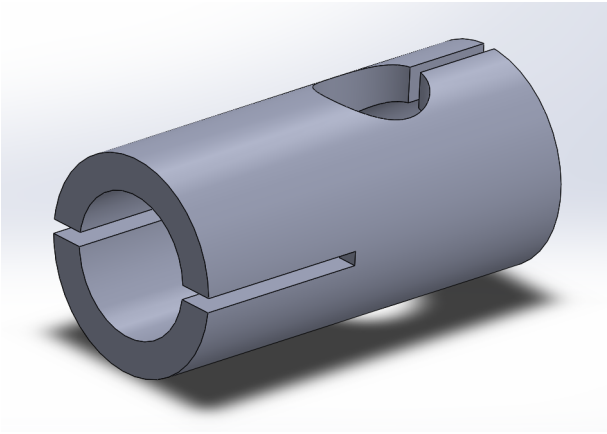

Figure B.5: Aluminium Pipe with Shaft Collar Overview

Single processed Aluminium Rod

A simple concept consists of a standard aluminium pipe processed with lathing to precisely match the outer dimensions of arm_3. This snug fit suffices adhesive fixation to transfer the torque.

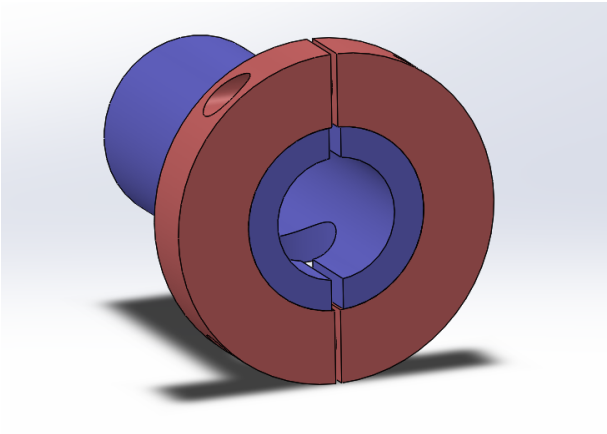

Figure B.6: Plain Aluminium Rod

This proves the fixation to be strong and does not require a large area. The durability, rigidity and weight is advantageous for this concept. The processing of the pipe makes manufacturability poor but the assembly and service ability rather good. The attachment to the back knuckle could be a problem if the pipe profile is not integrated.

Turned Pipe

At the other end of products available from market is the fully customized concept. This concept consists of lathing a hole from an aluminium cube to fit arm_3 in and secure with epoxy, much similar to previous concepts. Further features and weight optimizations can be turned or milled. This is more optimal for the single piece manufacturing for the Agile-PKM prototype. Because of the numerous possibilities of feature implementation and optimization this seem like a very feasible and optimal concept. The only withdrawal is the manufacturability and serviceability since everything is custom made.

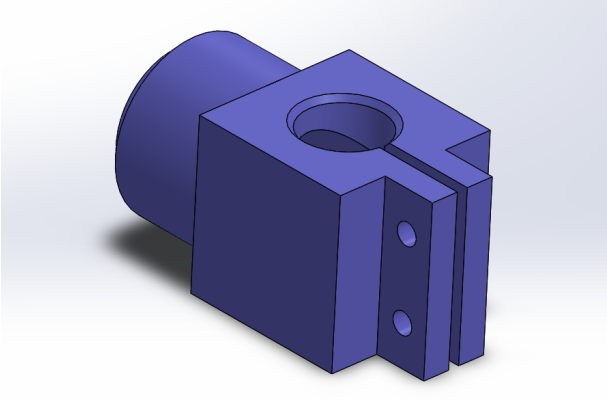

Figure B.7: Turned Pipe Concept

B.2 Pin

The next component to be evaluated and undergo concept generation is the pin. This is done before the back knuckle since the both the back and front knuckle need to be paired with each other and the pin. So to avoid spending time on generating possible unusable concept the pin is first evaluated to facilitate efficient concept generation from the results.

The pin itself is rather simple since a cylindrical shape with sufficient diameter and length is the only requirement to fulfil its primary function of withstanding shear and torque stress. Secondary requirements include fixation to back or front knuckle and fixation of bearings if such are to be used. These requirements are listed below.

1. **Endure torque loads** Needs to transfer the torque from the rod to the elbow, requiring high demands on both fastening to the rod and the elbow itself.
2. **Enable securing of rotational components** Holding rotational components (for example bearings).
3. **Endure horizontal loads** The attachment needs to withstand loads generated from the parallel rods and the elbow. This load is derived from a combined axial and radial force.
4. **Attachment to Back Leaf** Needs to incorporate an efficient and rigid attachment to back back or front leaf along fixation of rolling elements if such are to be used.

The load on the pin is derived from the number and arrangement of knuckles attaching to the pin. To investigate the effect of different arrangements the most simple arrangement of pin and knuckle should be evaluated and from there expand the arrangement. This is done in Figure B.9 where the most simple arrangement is presented to the left and from there expanded. Below each arrangement is the corresponding stress in the pin. The goal is to minimize the stress in the pin in order to also minimize the dimension requirements, but at the same time have a simple arrangement with few components. The first case is derived from a simplified case where torque is applied to the middle of a beam presented in Figure B.8.

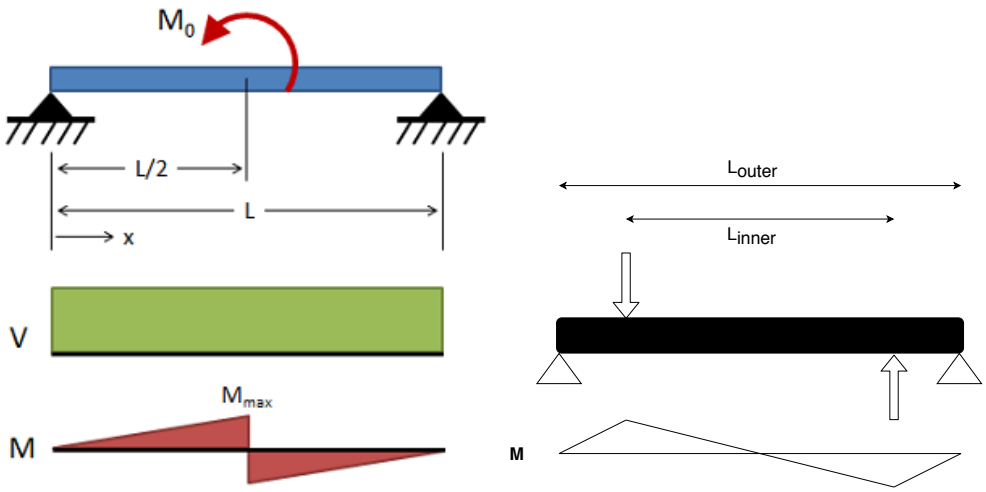

Figure B.8: Initial pin stress [12](left) and developed pin stress case (right)

The pattern is clear that the stress caused from the torque is decreasing when the number knuckles are increasing. To calculate the stress the pin is sliced at different

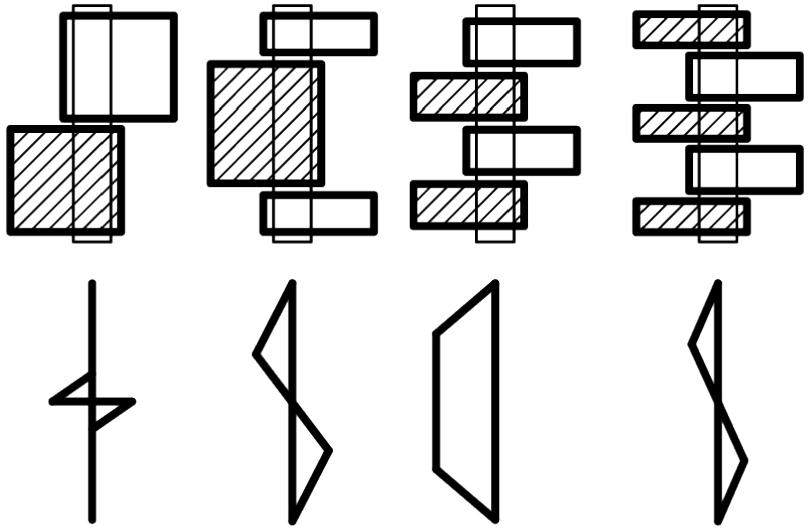

Figure B.9: Knuckle Cases

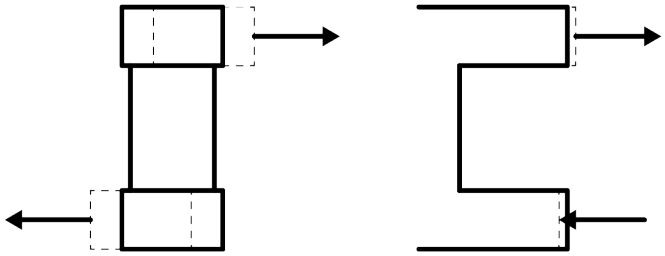

Figure B.10: Knuckle Orientation

sections and the resulting forces are calculated. It seems optimal with the case of one back knuckle and two front knuckles since the stress is reduced and the number component is still low.

As the arrangement of knuckles have been established the orientation should be determined. The outer knuckles can be attached to either the $forearm$ or arm_3. Considering the direction of the forces acting on the outer knuckles, specifically in the vertical movement, it is clear that the stresses and deformations will be limited if the outer knuckles are attached to the $forearm$. This is because the force transfer will be more direct, visualized in Figure B.10.

The elbow should consist of some rotational elements to facilitate effortless rotation. This is not required in both the base and front knuckle since only one component needs to rotate around the pin. The forces are greater in the base compared to the outer knuckles, visualised in Figure B.11, which makes it unsuitable to carry rolling elements. This is to lower the load on the rotational elements and since it is easier for a more sturdy grip without rotational element.

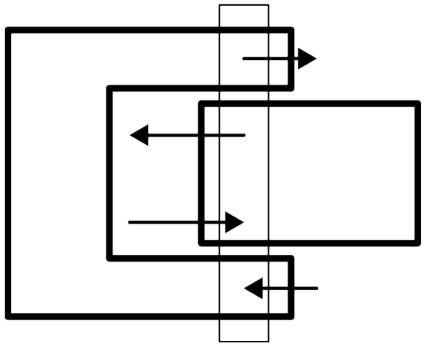

Figure B.11: Rolling Element Forces

B.3 Back Knuckle

When this fundamentals have been established the concept generation for the back leaf can commence. Here are a few requirements.

1. **Endure radial torque loads** Needs to transfer the torque from the rod to the elbow, requiring high demands on both fastening to the rod and the elbow itself.
2. **Secure Pin** Hold the pin and facilitate rotation.
3. **Attachment to Back Leaf** Needs to incorporate an efficient and rigid attachment to back back leaf

Industrial Shaft Holder

The industrial shaft holder is a standard component to secure shafts by clamping with a tightening screw. The interface to the base is also very simple with two screw holes. The adaptor is available in numerous sizes and the likeliness of finding a suitable one is high. The interface to the base may be a bit weak to suffice the torque transfer.

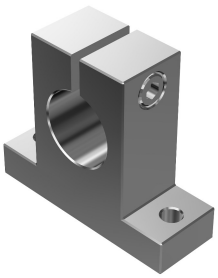

Figure B.12: Shaft Holder [35]

Pipe Holder

The pipe holder is a very standardized way to secure shafts and pipes in the industry. This is however not applicable for the Agile-PKM since it is way to weak for the forces involved.

Figure B.13: Pipe Holder [39]

Pipe Base

The pin can also be secured with a drilled pipe. This seems like a fitting solution since it can be combined with similar the back leaf concepts. There are three variants of this which are presented below.

Pin Clamping

Very similar to the pipe clamp for the front leaf but here the pipe is clamped in order to reduce the size of the drilled hole, thus clamping the pin. A very simple way to clamp the pipe since the pipe clamp is available in various sizes.

Shrink Fitting

Shrink fitting the pipe and the pin is a bit more technical clamping process where the pin is cooled to a very low temperature and the pipe is heated up. This will cause compression and expansion, letting the pin slide into the pipe and once the temperatures are restored the pipe will clamp the pin. This fixation is dependent on temperature and may be compromised if the pipe is exposed to rising temperatures.

Screw Clamping

The last of the pipe clamping concepts is the screw clamping. The pipe is, in addidtion to a pin hole and slit, simply processed with holes to fit screws through. Once the pin is in place the screws are tightened this requires a bit longer pipe and generates some stress concentrations on the pipe.

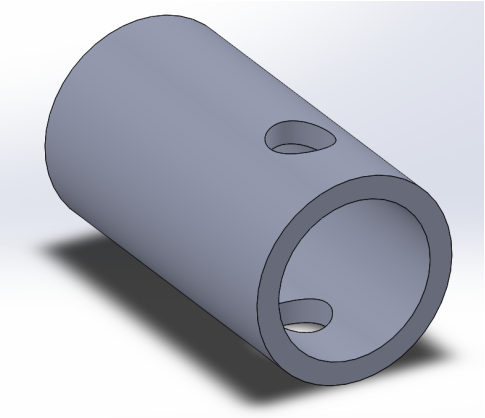

Figure B.14: Pipe Holder [39]

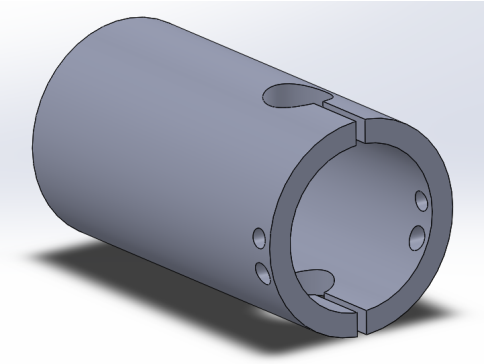

Figure B.15: Pipe Holder [39]

B.4 Front Knuckle

1. **Endure axial torque loads** Needs to transfer the torque from the rod to the elbow, requiring high demands on both fastening to the rod and the elbow itself.
2. **Secure Pin** Hold the pin and facilitate rotation.
3. **Attachment to Front Leaf** Needs to incorporate an efficient and rigid attachment to back back leaf

Bearing Housing

To hold the bearings there are plenty of bearing housings that are specifically designed for this purpose. These houses can be joined by a plate and thus create a front. It is however likely that the front needs to be custom built to meet other requirements, such as movements, impacting to the standardized qualities of the concept.

Splitting Knuckles

If the pin and base consists of a single piece the knuckles needs to be able to split in order to fit the bearing onto the pin. Two concepts were generated for this where the knuckles are split at each bearing, see Figure B.17 and upon mounting would be attached using screws, clamping around the bearing. The second concept that was generated for this was splitting the knuckles (and the front) in two and the treading on each half onto

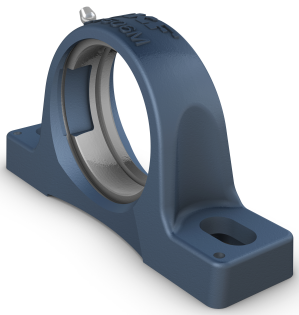

Figure B.16: Bearing Housing [30]

the bearings, see Figure B.18. Both of these concepts limits the durability of the front since it is split into sub parts and then assembled with screws making it less likely to be incorporated into a full hinge concept.

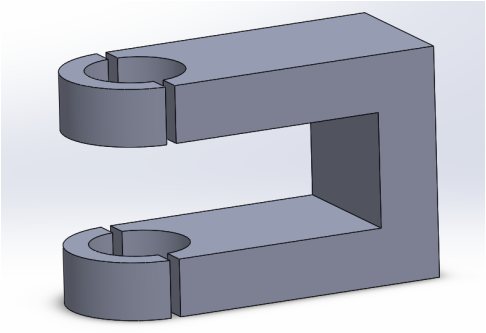

Figure B.17: Knuckle separation at bearing

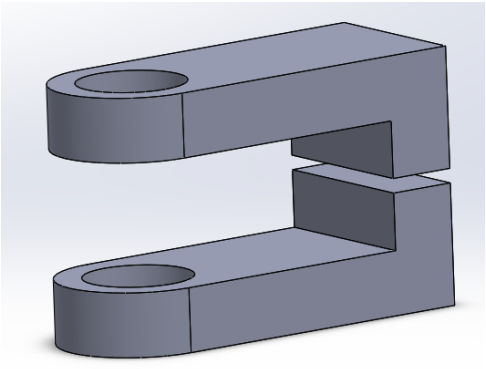

Figure B.18: Knuckle separation at midsection

B.5 Front Leaf

1. **Attachment to forearm** The elbow needs to be attached to the carbon fibre rod with the dimensions of 25 mm (diameter) and 2 mm Thickness, preferably mounted internally in the rod to make room for the parallel rod attachments.
2. **Endure horizontal loads** Similarly to the base attachment the forearm attachment needs to withstand load generated from the parallel rods and the elbow.
3. **Endure axial torque** The attachment is mounted so that vertical movement will generate axial torques.

4. **Compatibility with parallel rod attachments** The parallel rod attachment is expected to be mounted very close to the elbow. The forearm attachment will therefore have to be designed for an arranged fit with the parallel rod attachment.

The front leaf attaches just as the back leaf to a circular profile. The $forearm$ is not exposed to any torque since a bearing needs to be incorporated somewhere along the $forearm$ in order to enable the writ to be oriented vertically at all positions in the working space. This allows the peg to be attached internally or externally of the parallel rods, or even both. The attachment of the *parallelrods* may impose restrictions to the outer fixation.

Milling a peg onto the front knuckle is not optimal and an alternative is to manufacture a separate peg paired with a hole on the front knuckle. The torque and force generated by the vertical movements will most likely break the bonds on the side which are will have to be thin to enable the inner most position of the TCP. This position places the $forearm$ and peg very close to arm_3 limiting the width that supports the peg hole. The front knuckle is limited by the attachment of the *parallelrods* as described in Section 2.5.3.

Appendix C

FEM Verification

In this appendix the set-up of the FEM-Analysis will be described. The analysis is done in Ansys Workbench and the analysis is set up as a Static Structural Analysis.

The model of the elbow is created in Solidworks and exported to the neutral file format .STEP as a result of conflicting licenses on the different platforms. The CAD model consists of three different parts (base, pin and front) which are split for the analysis to simplify the analysis and in order to isolate the results and loads for the different components. The base is modelled with the pin and part of arm_3 to simulate the real world conditions and the front is modelled with part of the forearm for the same reason.

To incorporate the whole test cycle the analysis is split into two cases, the vertical movements and the horizontal movements. In the following section the connections and set-up for the FEM analysis is described.

C.1 Model Connections

For the front analysis there is only one connection between components. This connection is between the front peg and the forearm, shown in Figure C.1. This is set to bonded to match the adhesive fixation.

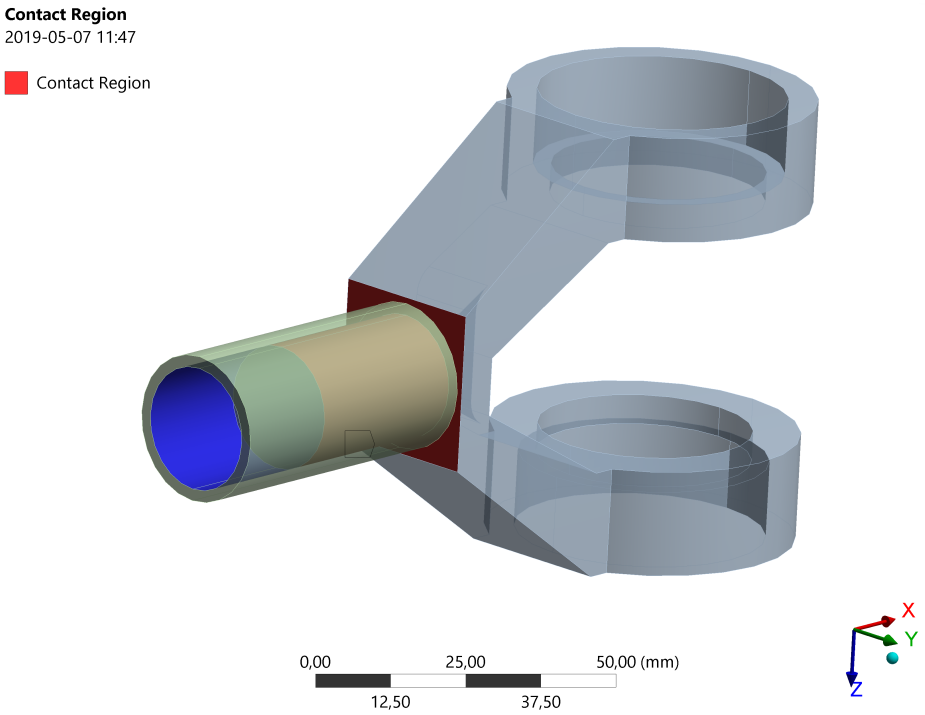

Figure C.1: Front Setup

The base model incorporates more connections, presented in Figure C.2. Arm_3 is fixated by adhesion which is why the connection to the base is set to bounded, this is also the case for the connection to the pin. The pin is mainly fixated by clamping corresponding to friction connection as the pin can only push but not pull the base.

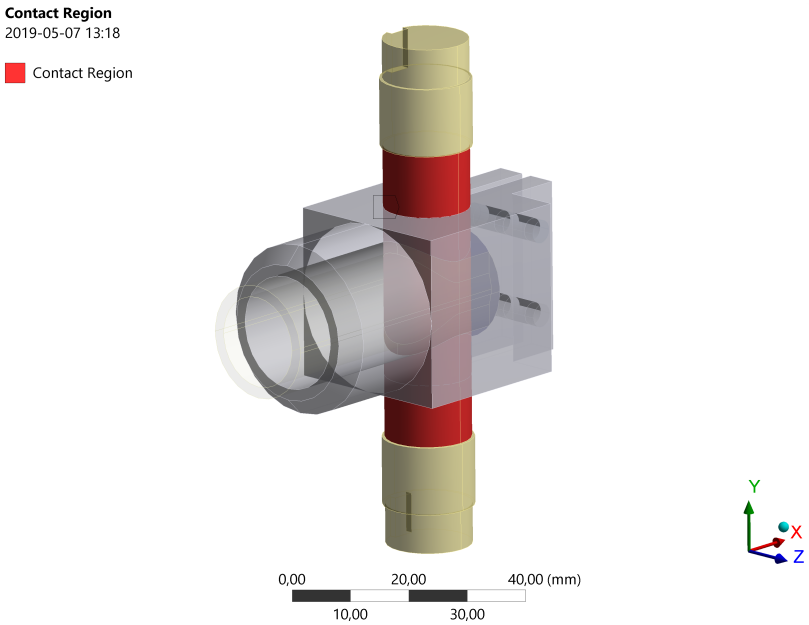

Figure C.2: Base-pin connection

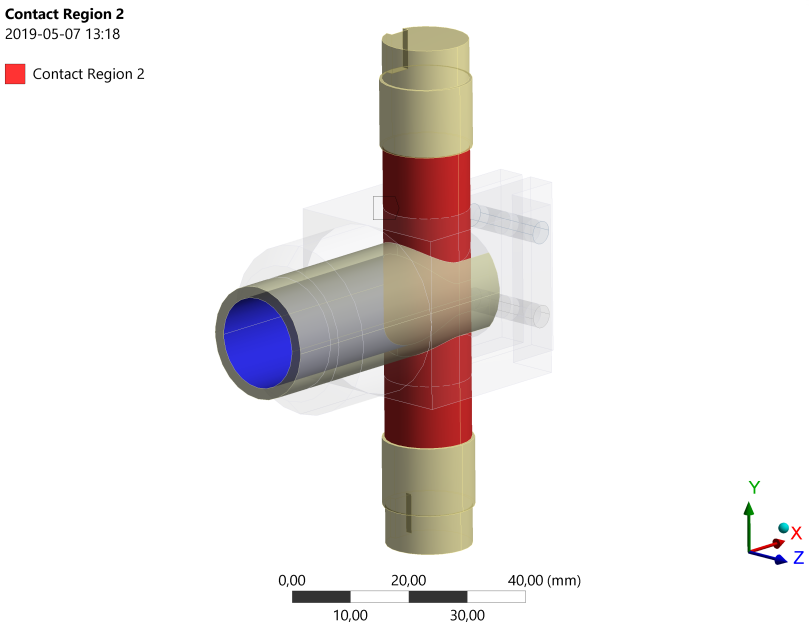

Figure C.3: Pin-pipe connection

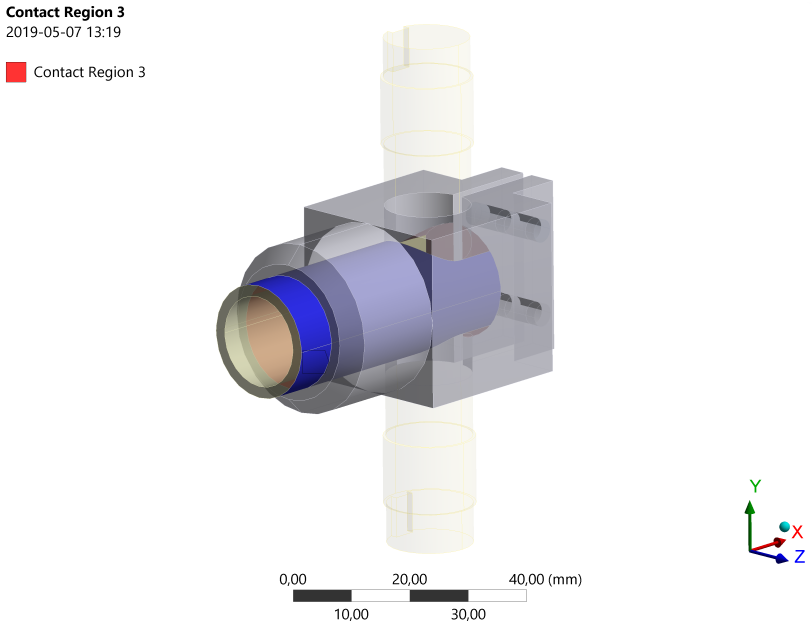

Figure C.4: Base-pipe connection

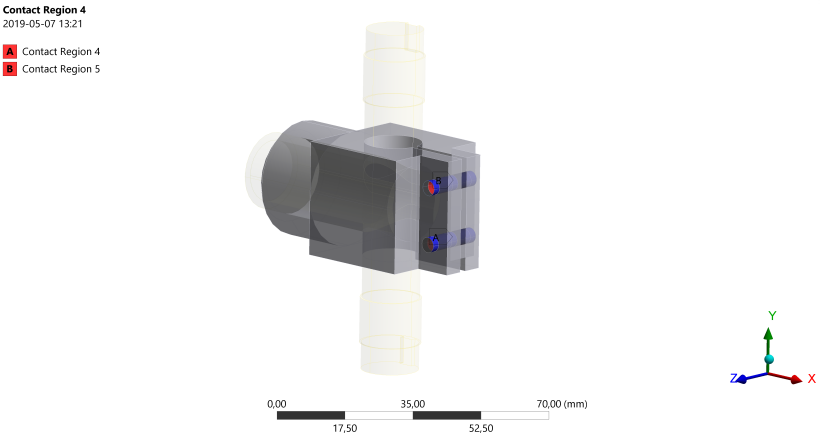

Figure C.5: Base-screw connections

C.2 Structural Setup

First up is the front and the vertical movement analysis. Figure C.7 shows the active forces and fixtures. The surfaces connecting to the bearings are set to fixed support since are carried by the bearings which connect to the base of the elbow. The torque from the accelerations at the TCP, set to 164 Nm calculated in Section 2.2 oriented around the Y-axis. The force load is set perpendicular to to the Z-axis.

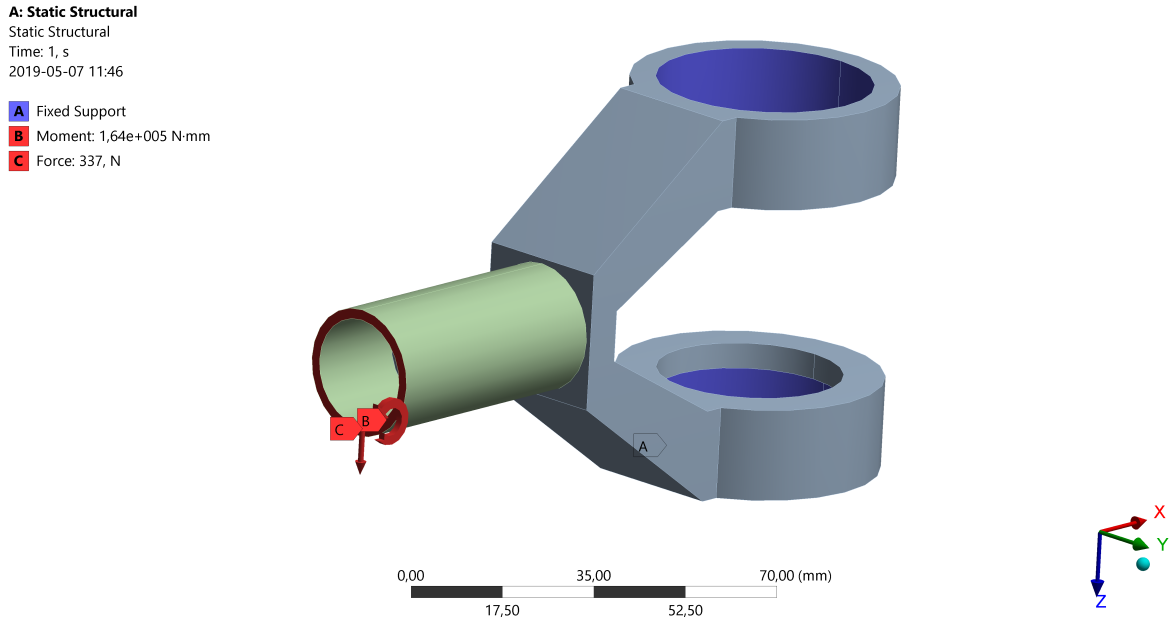

Figure C.6: Front Analysis Setup

The connection between the *forearm* and the peg is set to bounded matching the adhesive fixation.

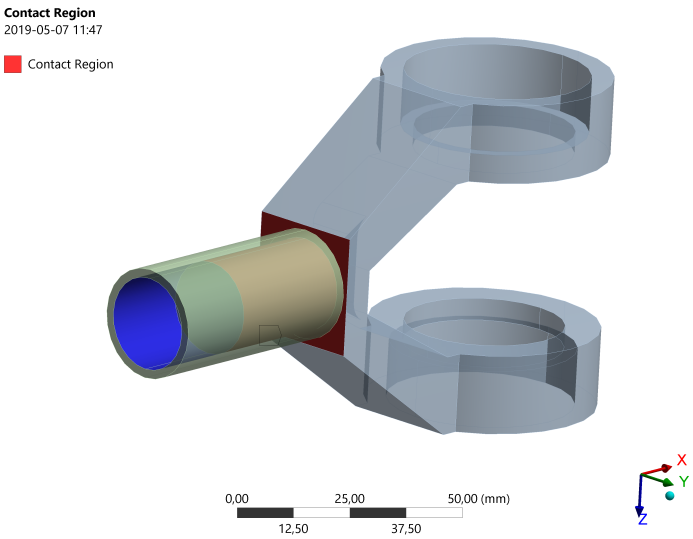

Figure C.7: Front Analysis Setup

Next is the horizontal movement analysis of the front, presented in Figure C.8. The connections are unchanged from the vertical analysis. The 3507 N calculated in Section 2.5.2 is applied along the *forearm*, simulating the horizontal movement.

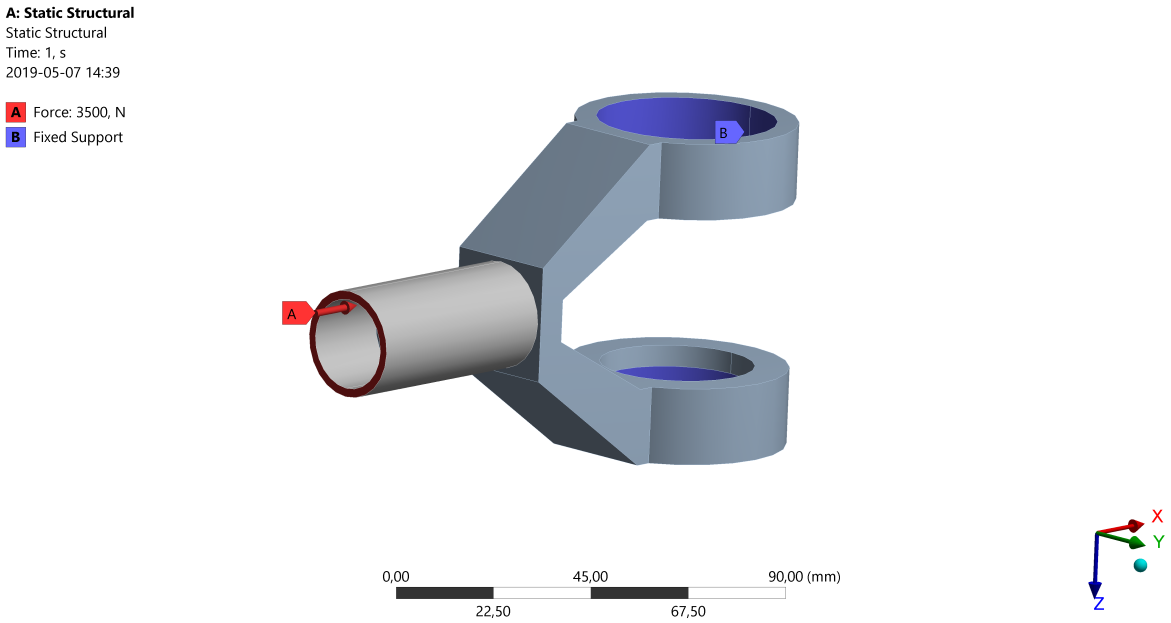

Figure C.8: Front horizontal analysis setup

The base analysis for the vertical movement is set up in Figure C.9. The set-up is very similar to the corresponding case for the front. The areas where the bearings attach to are set to Fixed Support as they carry the front of the elbow. This enables the torque to be more accurately modelled at arm_3. Only the reference is changed and the results will more accurately simulate the vertical movement loads.

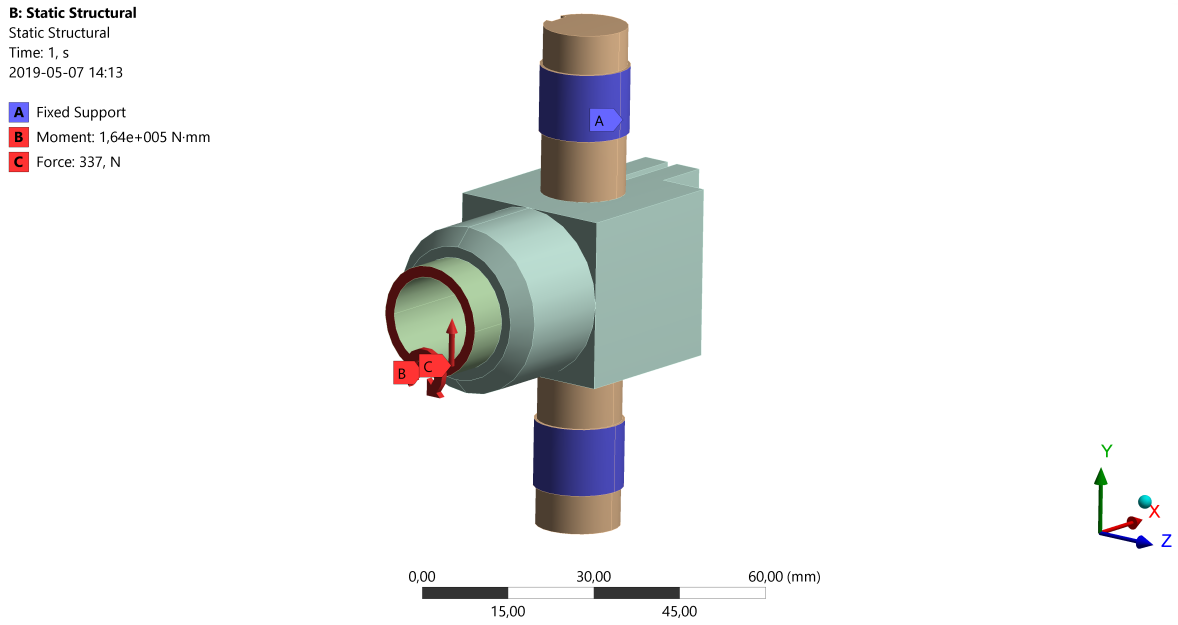

Figure C.9: Base vertical analysis setup

The horizontal movement is simulated with the same force as for the front, here it is applied at a 25 degree angle corresponding to the inner most angle.

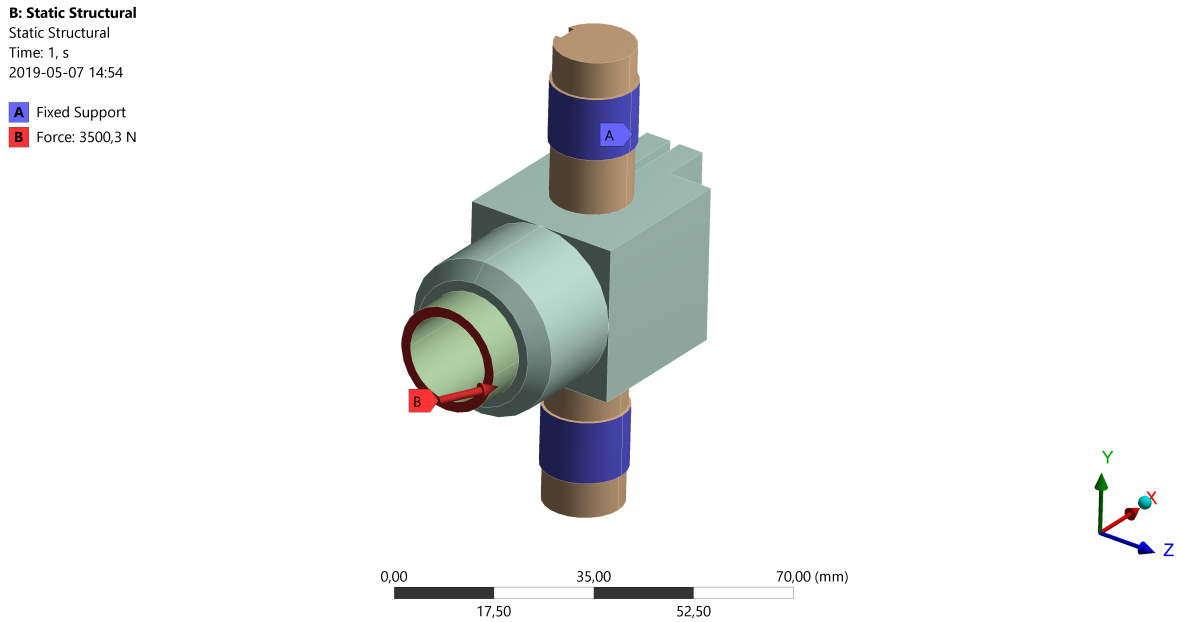

Figure C.10: Base horizontal analysis setup

Appendix D

Drawings

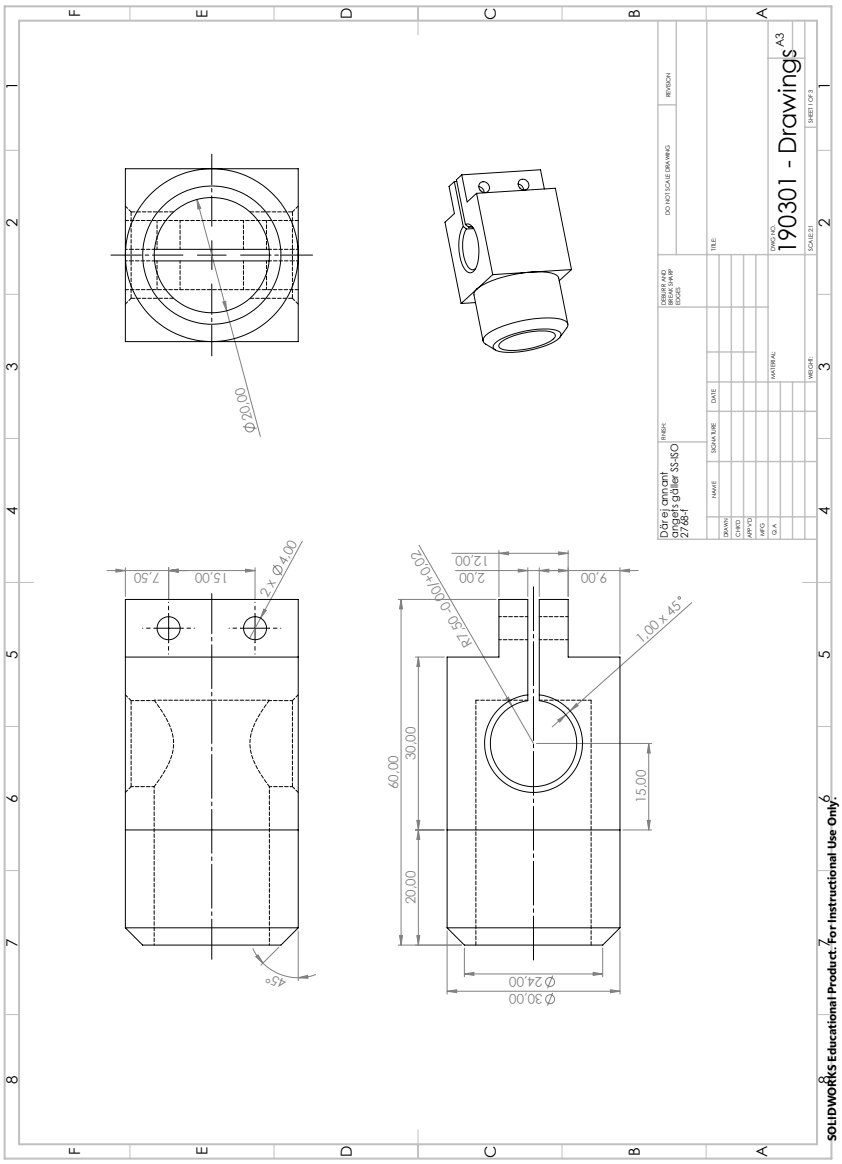

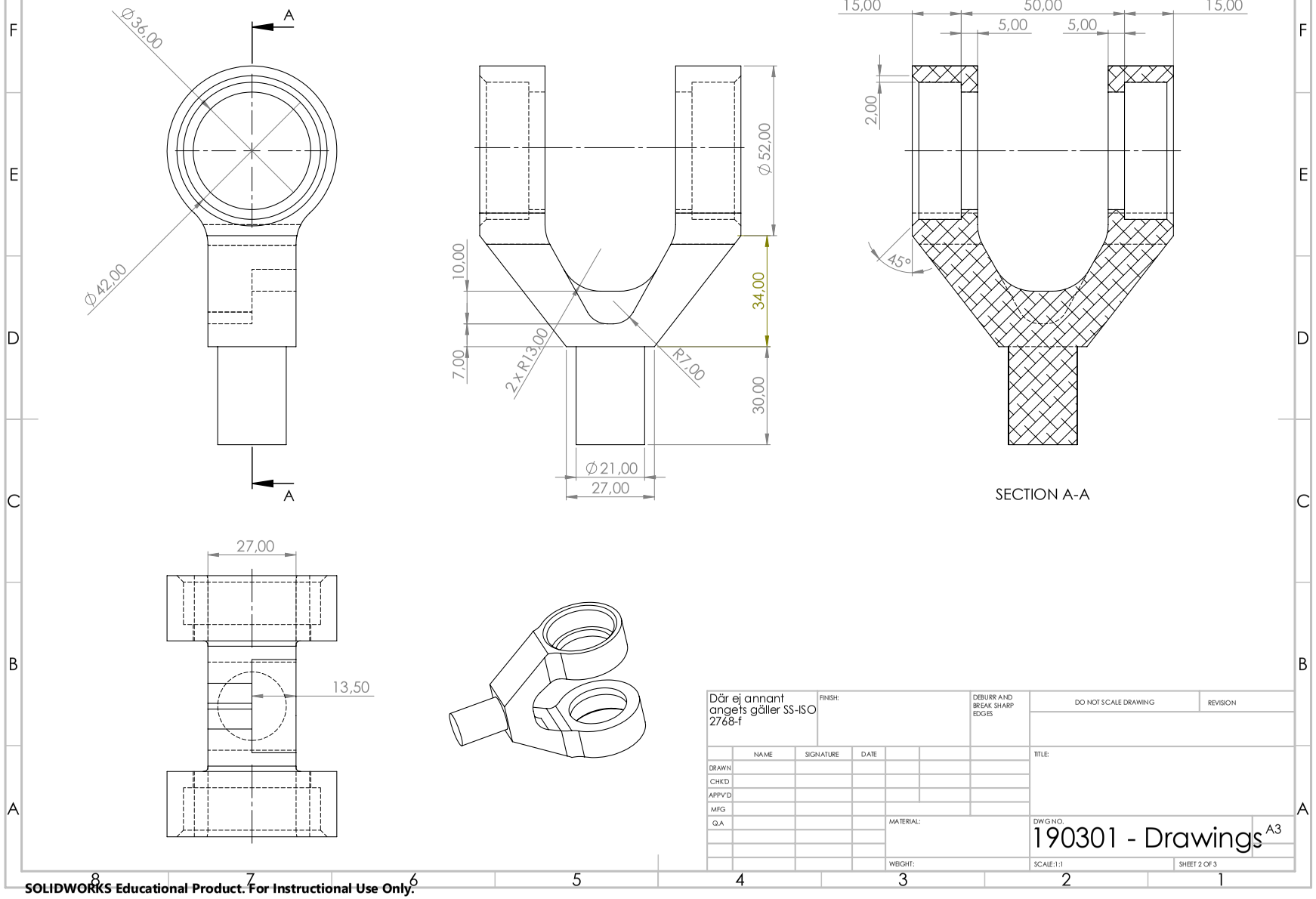

Appendix E

Kinematic code

Here the actual code describing the kinematics can be seen. A lot of other code has been written in order to test the solution but this is the core to the software project.

```
// Multiplication of "left" and "right" is stored in "res"
void matrix_multiplication(double left[][N],
                double right[][N],
                double res[][N]) {
        int i, j, k;
        for (i = 0; i < N; i++)
        {
                for (j = 0; j < N; j++)
                {
                        res[i][j] = 0;
                        for (k = 0; k < N; k++)
                                res[i][j] += left[i][k] * right[k][j];
                }
        }
}


// Passing a pointer to the matrix with doubles to be changed
void rot_x(double th, double M[][N]) {
        M[0][0] = 1;
        M[0][1] = 0;
        M[0][2] = 0;

        M[1][0] = 0;
        M[1][1] = cos(th);
        M[1][2] = -sin(th);

        M[2][0] = 0;
        M[2][1] = sin(th);
        M[2][2] = cos(th);

        M[3][3] = 1;
}
```

```
// Passing by value when parameters are cheap to copy
// Passing a pointer to the matrix with doubles to be changed
void rot_z(double th, double M[][N]) {
        M[0][0] = cos(th);
        M[0][1] = -sin(th);
        M[0][2] = 0;

        M[1][0] = sin(th);
        M[1][1] = cos(th);
        M[1][2] = 0;

        M[2][0] = 0;
        M[2][1] = 0;
        M[2][2] = 1;

        M[3][3] = 1;
}


// q is a list with 4 elements for joint rotation
// pos is the array which will be changed
int APKM_forward(const double q[4], double pos[4]) {
        // Parallell rod attachment point on base side pnt_ax2
        double pnt_ax2[3] = { ax2x + L3b * cos(q[1]),
                ax2y + L3b * sin(q[1]),
                0 };
        // Project to plane of axis3 and arm2 in order to get
        // 2d intersection problem
        double pnt_ax2_proj[3] = { pnt_ax2[0],
                pnt_ax2[1] * cos(q[2]),
                0 };
        // Vector from pnt_ax2 to elbox to solve for circle
        // intersection along
        double r_par_proj[3] = { L1 - pnt_ax2_proj[0],
                -pnt_ax2_proj[1],
                -pnt_ax2_proj[2] };
        // Length and angle relatived arm 1 of vector r_rap_proj
        double r_ang = atan2(r_par_proj[1], r_par_proj[0]);
        double d = sqrt(pow(r_par_proj[0], 2) + pow(r_par_proj[1], 2));
        // How long is the parallel rod component in the plane
        // and how far from plane
        double n_dist = pnt_ax2[1] * sin(q[2]);
        double Lpar_proj = sqrt(pow(Lpar, 2) - pow(n_dist, 2));

        // Intersect of two circles with centers on r_par_proj
        double x_int = (pow(L3, 2)
                - pow(Lpar_proj, 2)
                + pow(d, 2))
```

```
        / (2 * d);
if (x_int / L3 > 1) return -101;
// The angle of arm 2 in the place tilted by ax3
double q23 = PI / 2 + r_ang - acos(x_int / L3);

// Fwd kinnematics with transformation matrixes
double R1[4][4] = {             { 0, 0, 0, 0 },
                                { 0, 0, 0, 0 },
                                { 0, 0, 0, 0 },
                                { 0, 0, 0, 0 } };
rot_z(q[0], R1);
double T1[4][4] = {             { 1, 0, 0, 0 },
                                { 0, 1, 0, 0 },
                                { 0, 0, 1, 0 },
                                { 0, 0, 0, 1 } };
T1[0][3] = L1;
T1[1][3] = 0;
T1[2][3] = 0;
double R3[4][4] = {             { 0, 0, 0, 0 },
                                { 0, 0, 0, 0 },
                                { 0, 0, 0, 0 },
                                { 0, 0, 0, 0 } };
rot_x(q[2], R3);
double R23[4][4] = {            { 0, 0, 0, 0 },
                                { 0, 0, 0, 0 },
                                { 0, 0, 0, 0 },
                                { 0, 0, 0, 0 } };
rot_z(q23, R23);
double T2[4][4] = {             { 1, 0, 0, 0 },
                                { 0, 1, 0, 0 },
                                { 0, 0, 1, 0 },
                                { 0, 0, 0, 1 } };
T2[0][3] = 0;
T2[1][3] = L2 - d2;
T2[2][3] = 0;
double Tpc[4][4] = {            { 1, 0, 0, 0 },
                                { 0, 1, 0, 0 },
                                { 0, 0, 1, 0 },
                                { 0, 0, 0, 1 } };
Tpc[0][3] = 0;
Tpc[1][3] = L3;
Tpc[2][3] = 0;

// Pose for elbow
double pose_e[4][4] = {};
matrix_multiplication(R1, T1, pose_e);

// Pose for intersection between L2 axis and hinge axis
double pose_axh[4][4] = {};
double temp_result[4][4] = {};
```

```
        double temp_result_2[4][4] = {};
        matrix_multiplication(R23, T2, temp_result);
        matrix_multiplication(R3, temp_result, temp_result_2);
        matrix_multiplication(pose_e, temp_result_2, pose_axh);

        // Get direction of L2 in xy plane and add wrist
        // transforms, still rel ax1
        double dir2xy[2] = { pose_axh[0][3] - pose_e[0][3],
                pose_axh[1][3] - pose_e[1][3] };
        double dir2xyNorm = pow(pow(dir2xy[0], 2) + pow(dir2xy[1], 2),
                0.5);
        double dirw[2] = { dir2xy[0] / dir2xyNorm,
                dir2xy[1] / dir2xyNorm };
        double q21 = atan2(dirw[1], dirw[0]);

        double h2w[3] = { d2*cos(q21), d2*sin(q21), 0 };
        double w2f[3] = { 0, 0, -a2 };

        // Get to flange position and angle
        double trans[3] = { pose_axh[0][3] + h2w[0] + w2f[0],
                pose_axh[1][3] + h2w[1] + w2f[1],
                pose_axh[2][3] + h2w[2] + w2f[2] };
        double orient = q21 + q[3] - PI / 2;
        orient = orient - round(orient / (2 * PI)) * 2 * PI;

        for (size_t i = 0; i < 3; i++)
                pos[i] = trans[i];
        pos[3] = orient == -PI ? PI : orient;
        return 0;
}


// Pose is a list with 4 elements for x, y, z and rotation
// angles is the array which will be changed
int APKM_backward(const double pos[4], double angles[4]) {
        double x = pos[0];
        double y = pos[1];
        double z = pos[2] + a2;
        // Check if in range
        if (z > L2 - d2) return -201;

        // Find tilts of arms from z value(angle between L2
        // and xy - plane)
        double arm_tilt = asin(z / (L2 - d2));
        if (abs(arm_tilt) > restrAx3) return -202;
        //Projected length of L2 in xy-plane
        double L2proj = cos(arm_tilt)*(L2 - d2) + d2;

        // Solve for direction of L2 arm, from circles
        // intersect in local coordinates
```

```
double r = sqrt(pow(x, 2) + pow(y, 2));
double phi = atan2(y, x);
// Solve for intersection along r between L1 and
// projected L2
if (r > L1 + L2proj || r < L1 - L2proj) {
        //return -203;
}
double x_int = (pow(L1, 2) - pow(L2proj, 2)
        + pow(r, 2)) / (2 * r);
// Angle of arm 1 and 2
if (x_int > L1 || (r - x_int) > L2proj) return -204;
// L1_ang is zero parralell with x-axis
double L1_ang = phi - acos(x_int / L1);
// L2_ang is zero normal to L1
double L2_ang = -PI / 2.0 + acos(x_int / L1)
        + acos((r - x_int) / L2proj);
if (abs(L2_ang) > restrAx2 ) return -207;

// Elbow point location in baseframe
double pnt_e[3] = { L1*cos(L1_ang), L1*sin(L1_ang), 0 };

// Solve for parallell rods direction
// pnt_c is connection point between parallell rods and L2
double pnt_c[3] = { L1 - L3 * cos(arm_tilt)*sin(L2_ang),
        L3*cos(arm_tilt)*cos(L2_ang),
        L3*sin(arm_tilt) };
// Solve for circle intersection in local coords
// between pnt_c and base
// rotation point of ax2.
double cent_dist = sqrt(pow((pnt_c[0] - ax2x), 2)
        + pow((pnt_c[1] - ax2y), 2));
double cent_ang = atan2(pnt_c[1] - ax2y, pnt_c[0] - ax2x);

// Projected length of Lpar in xy - plane
double Lpar_proj = sqrt(Lpar*Lpar - pow(pnt_c[2], 2));
// Check if position is in reach for arm2 linkage
if (cent_dist > L3b + Lpar_proj) {
        // Handle the error
        return -205;
}
double x_int2 = (L3b*L3b
        - Lpar_proj * Lpar_proj
        + cent_dist * cent_dist)
        / (2 * cent_dist);
// Calculate angle of q2. zero is lever aligned with arm 1.
if (x_int2 > L3b) return -206;
double q2 = acos(x_int2 / L3b) + cent_ang;

// Axis 3 value
// Project L2 vector on a plane through elbow with ax3 as normal
```

```
        double orth_dist = cos(L2_ang)*(L2proj - d2);
        double q3 = atan(z / orth_dist);

        // Axis 4
        double q4 = pos[3] - L1_ang - L2_ang;

        double q1 = L1_ang;

        angles[0] = q1;
        angles[1] = q2;
        angles[2] = q3;
        angles[3] = q4;
        return 0;
}
```

Appendix F

Trajectory Graphs

This section includes graphs showing the Cartesian and joint acceleration, velocity and position of the test cycle in SI-units. Plots in Cartesian space is represented as X: red, Y: green, Z: blue, rotation around Z(axis 4): black. In joint space q_1: red, q_2: green, q_3: blue, q_4: black.

F.1 Test Cycle - Strict

In this section figures of the strict test cycle mentioned in Section 4.3.1 is shown. The robot will come to a complete stop at each of the specified points.

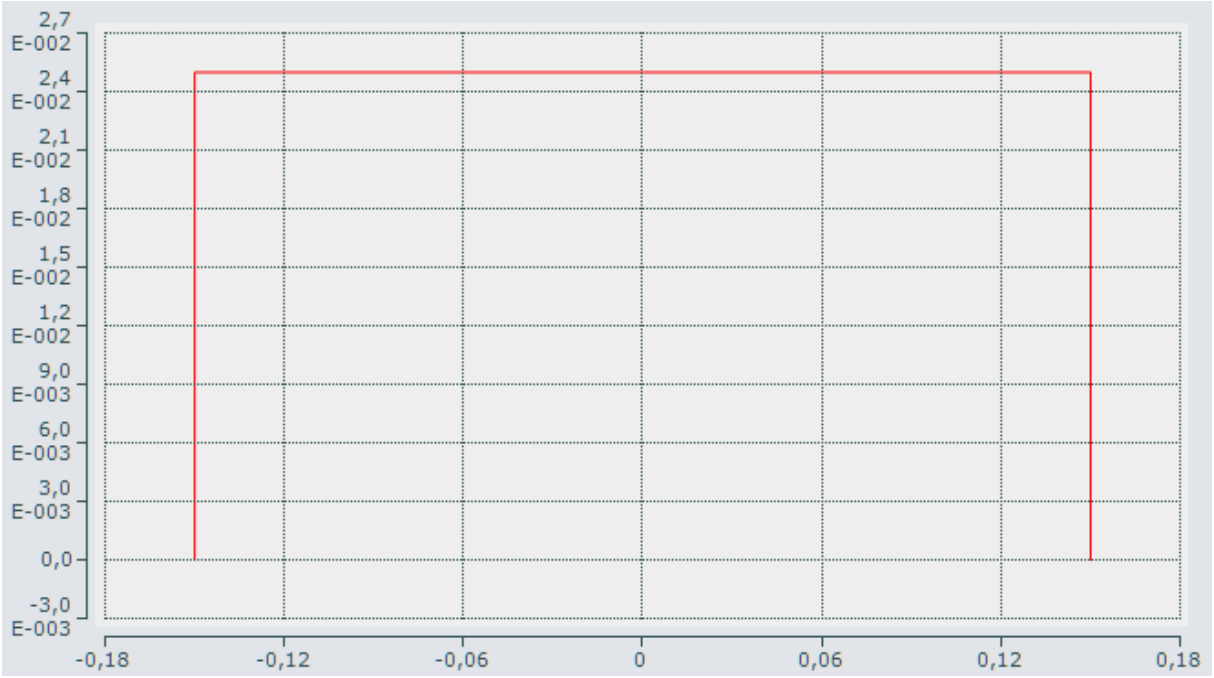

Figure F.1: The path of the end effector in X/Z-plane. The position in Y-axis is omitted since it is constant on 1.

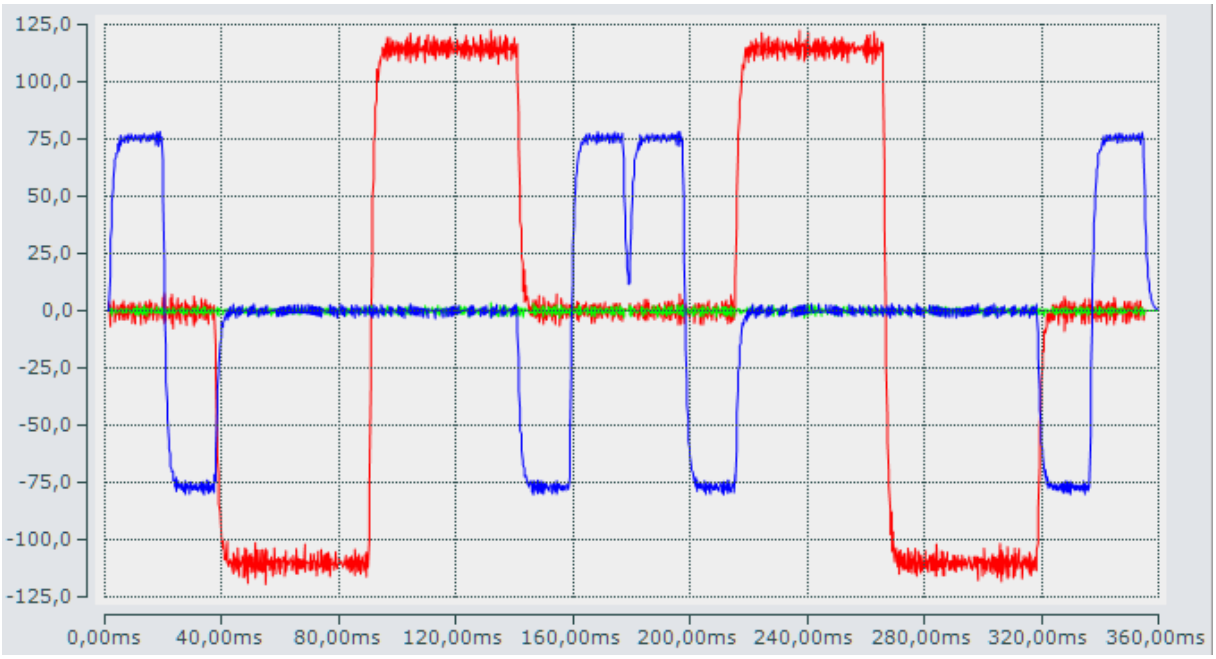

Figure F.2: Acceleration of the end effector in Cartesian coordinates, slightly filtered for readability due to instabilities in measurement data from the ISG kernel.

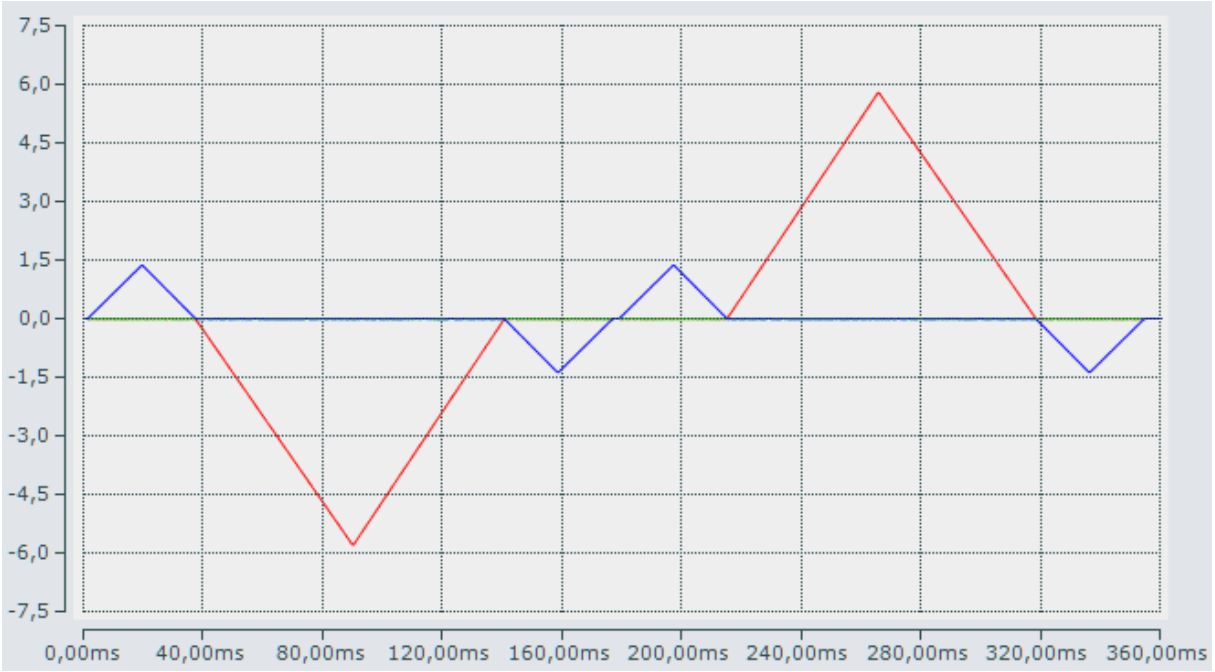

Figure F.3: Velocity of the end effector in Cartesian coordinates.

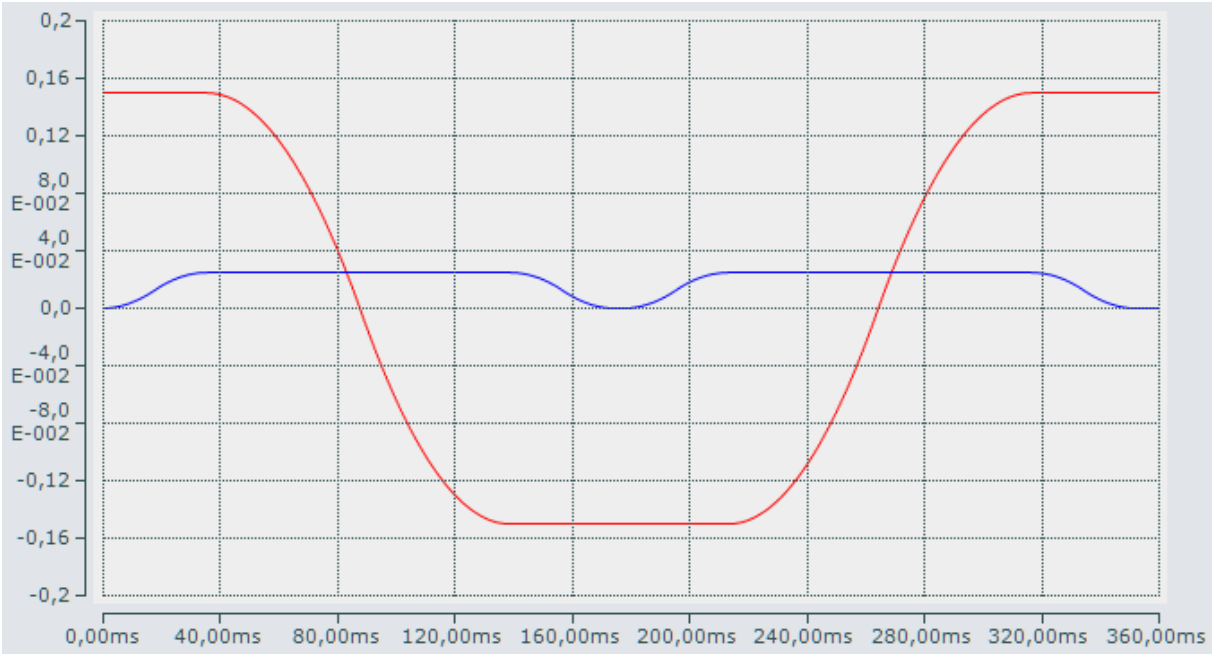

Figure F.4: Velocity of the end effector in Cartesian coordinates. The position in Y-axis is omitted since it is constant on 1.

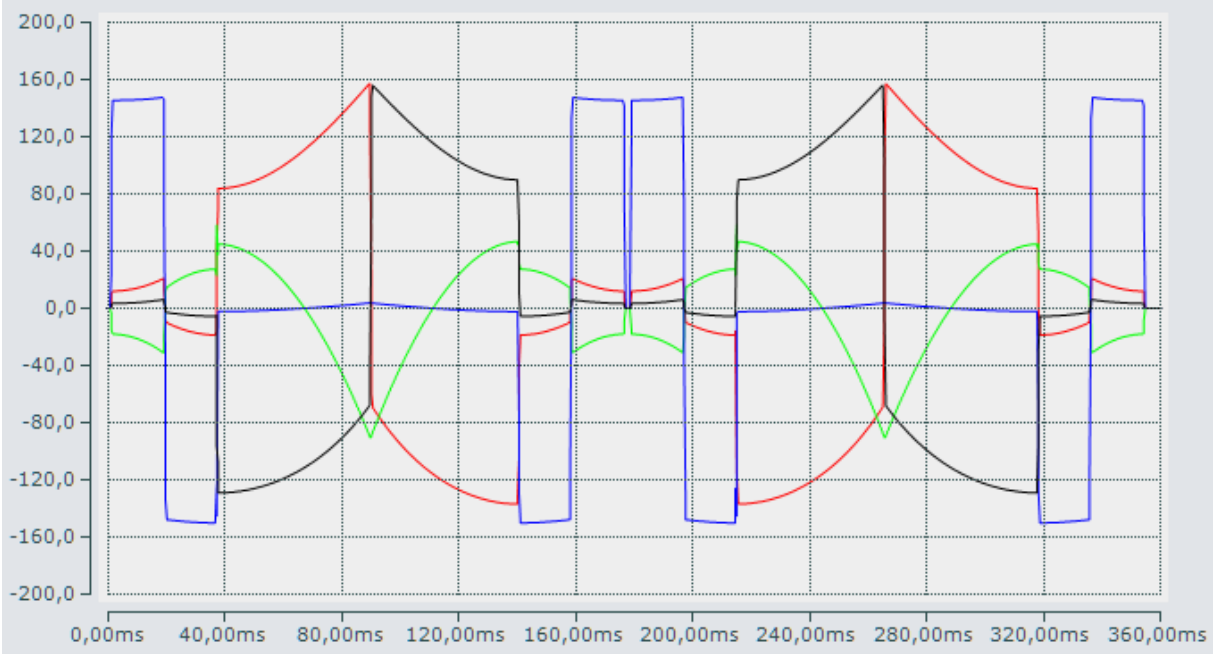

Figure F.5: Acceleration of each joint.

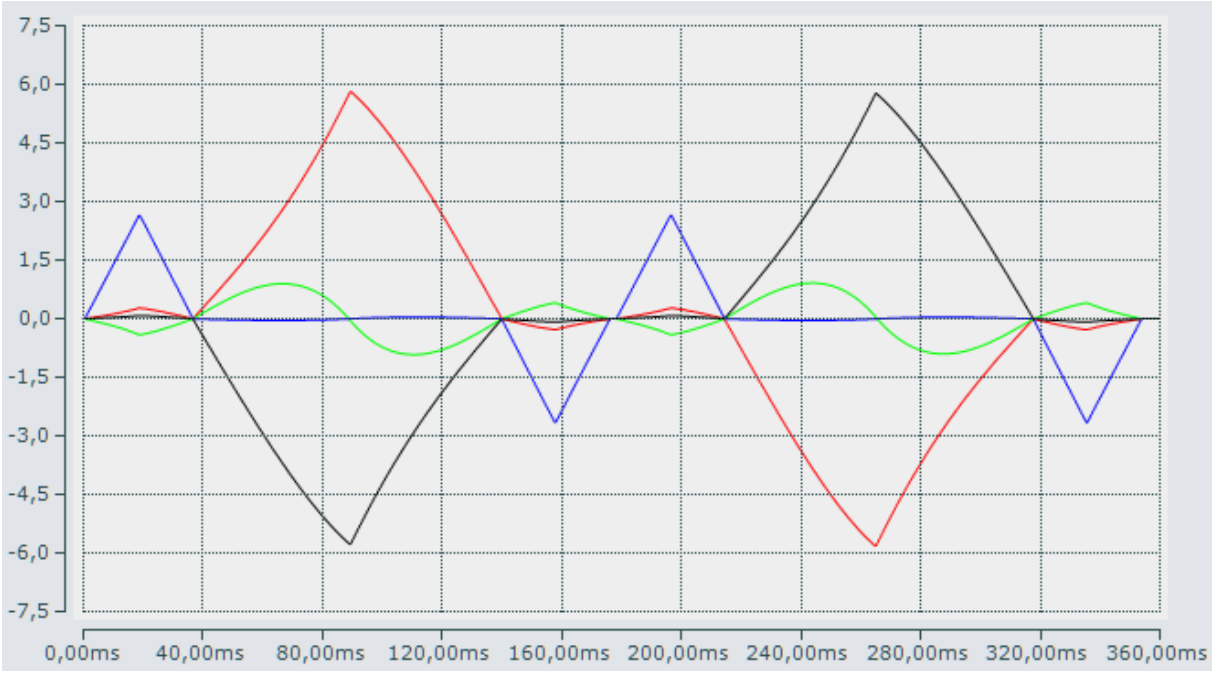

Figure F.6: Velocity of each joint.

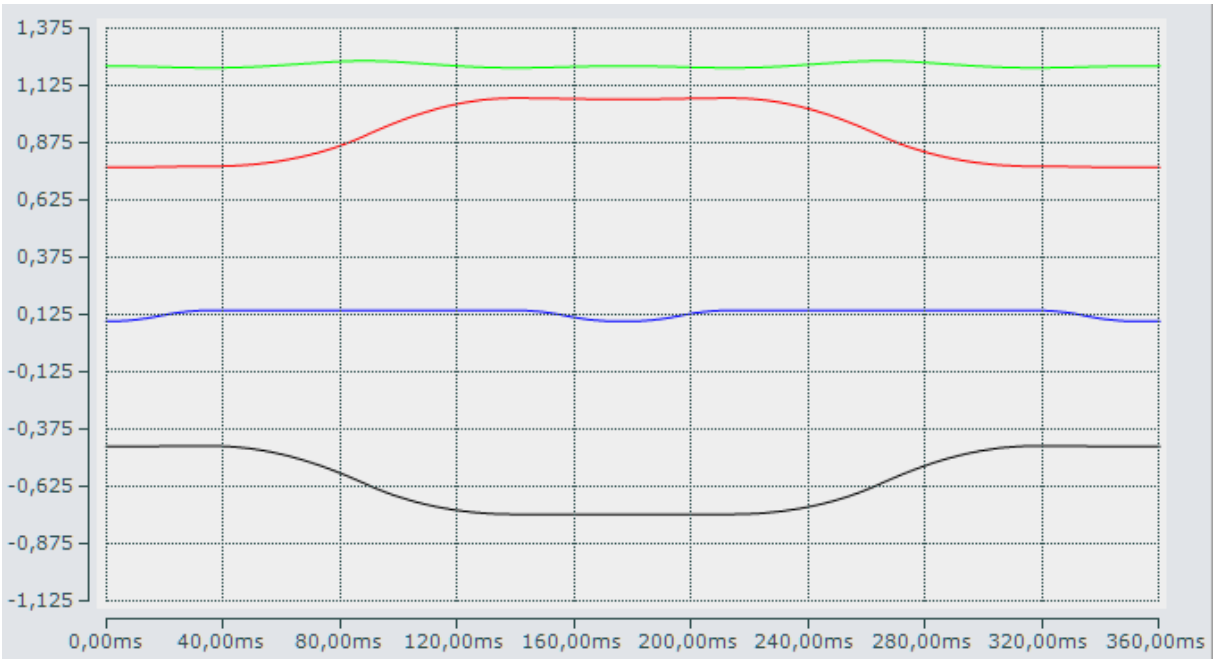

Figure F.7: Position of each joint.

F.2 Test Cycle - Blend

In this section figures of the test cycle with blended corners will be shown. The robot will not come to a complete stop at each of the specified points, but will instead cut the corners.

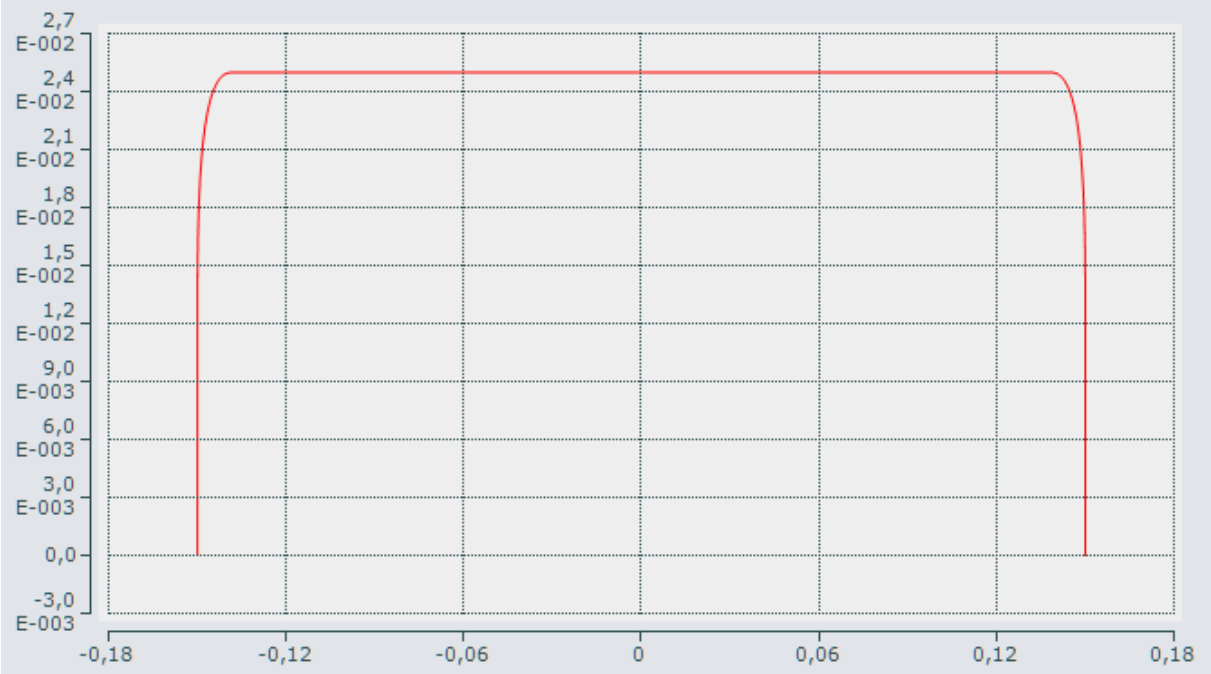

Figure F.8: The path of the end effector in X/Z-plane. The position in Y-axis is omitted since it is constant on 1.

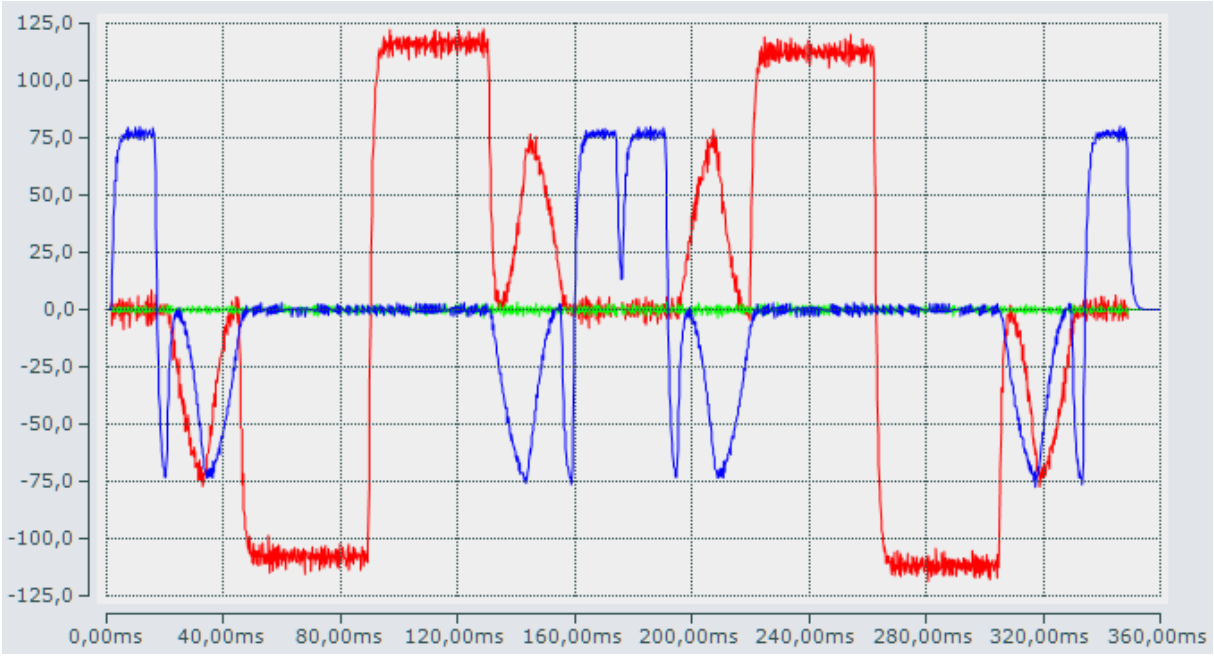

Figure F.9: Acceleration of the end effector in Cartesian coordinates, slightly filtered for readability due to instabilities in measurement data from the ISG kernel.

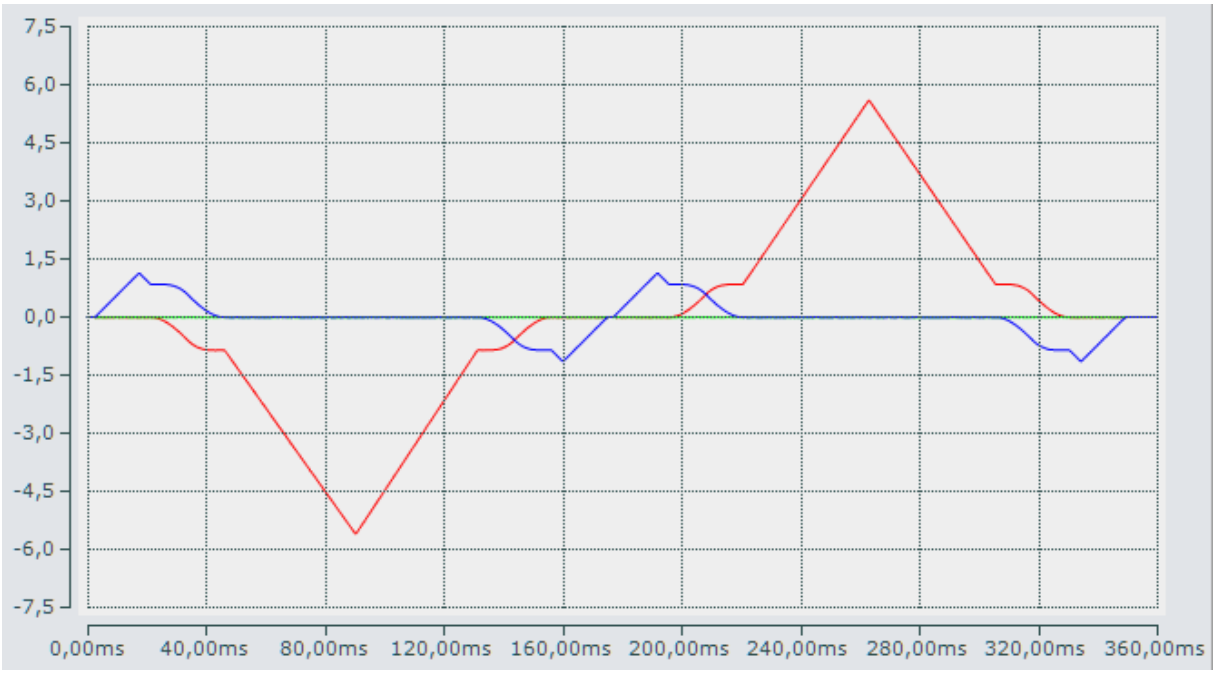

Figure F.10: Velocity of the end effector in Cartesian coordinates.

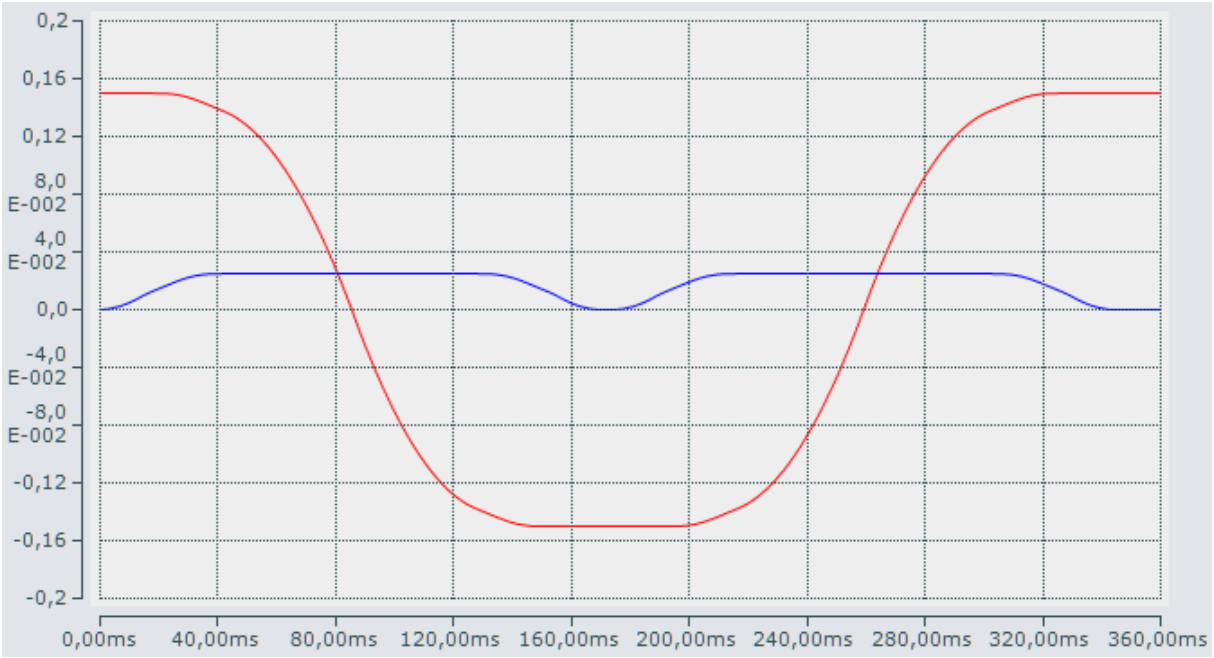

Figure F.11: Velocity of the end effector in Cartesian coordinates. The position in Y-axis is omitted since it is constant on 1.

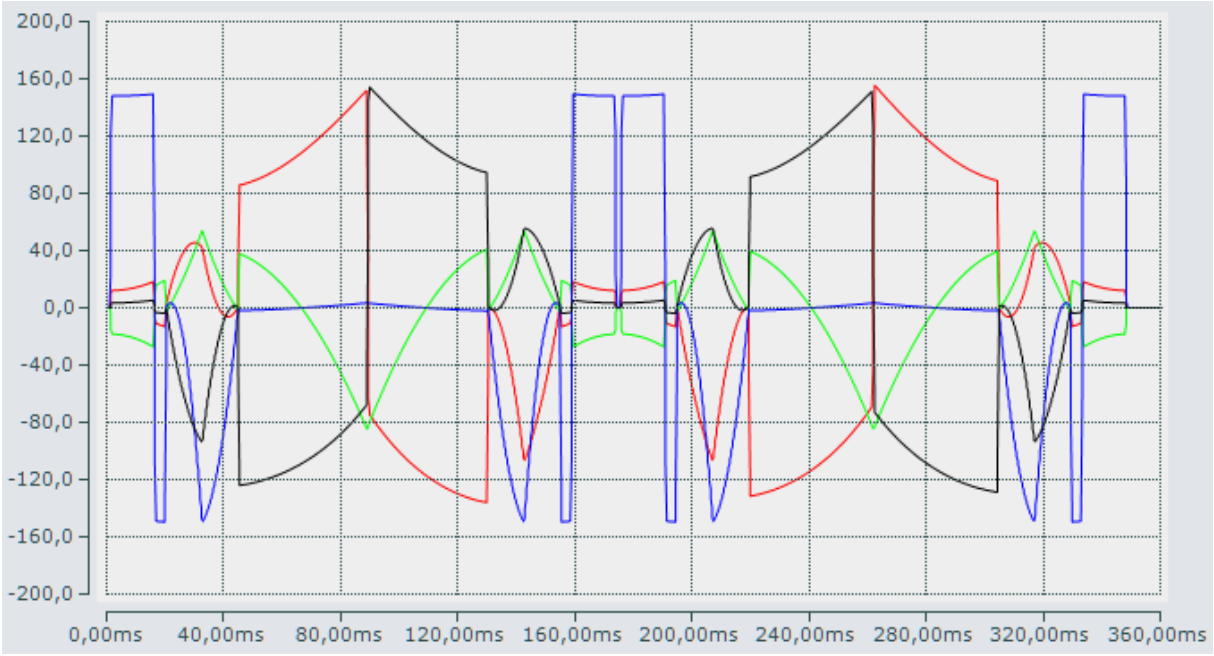

Figure F.12: Acceleration of each joint.

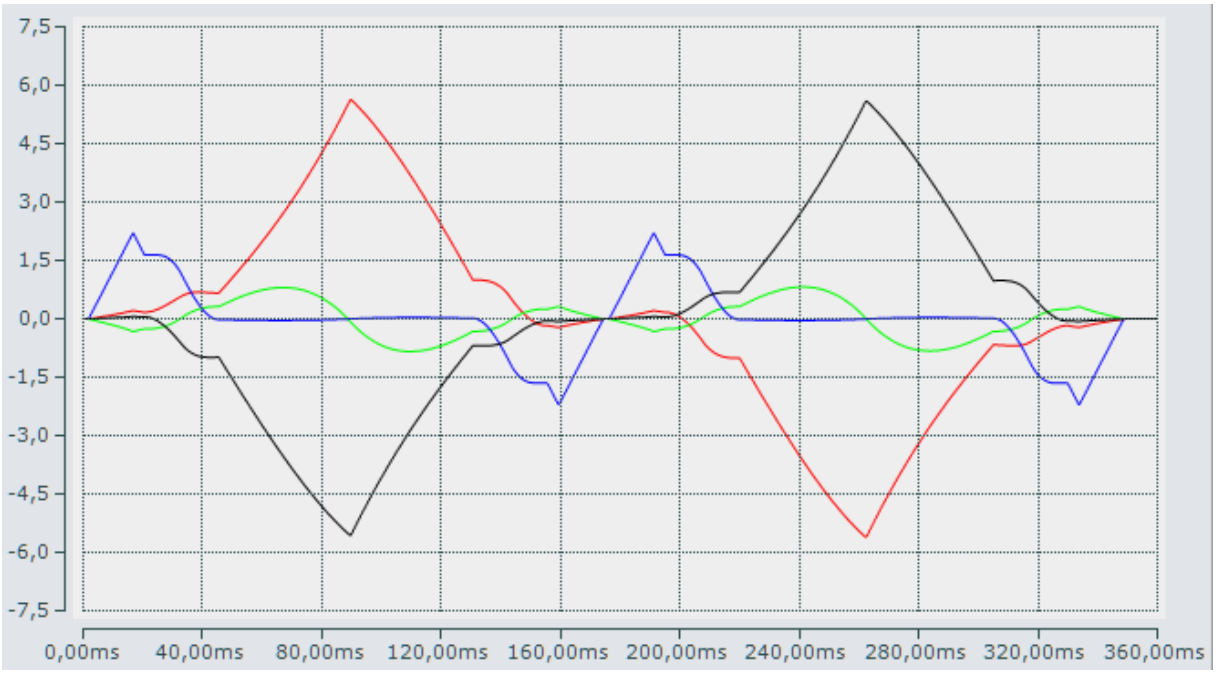

Figure F.13: Velocity of each joint.

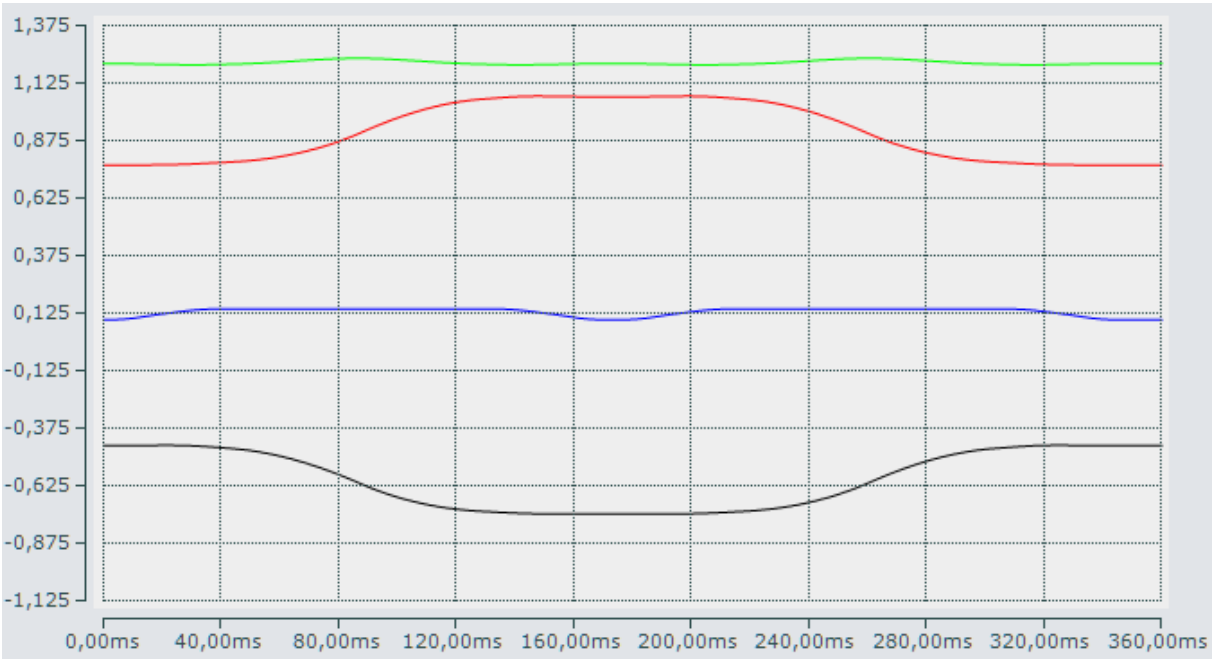

Figure F.14: Position of each joint.

F.3 Test Cycle - Rounded

In this section figures of a slightly rounded test cycle with blended corners will be shown. The robot will not come to a complete stop at each of the specified points, but will instead follow a rounded path based on the original test cycle and cut corners.

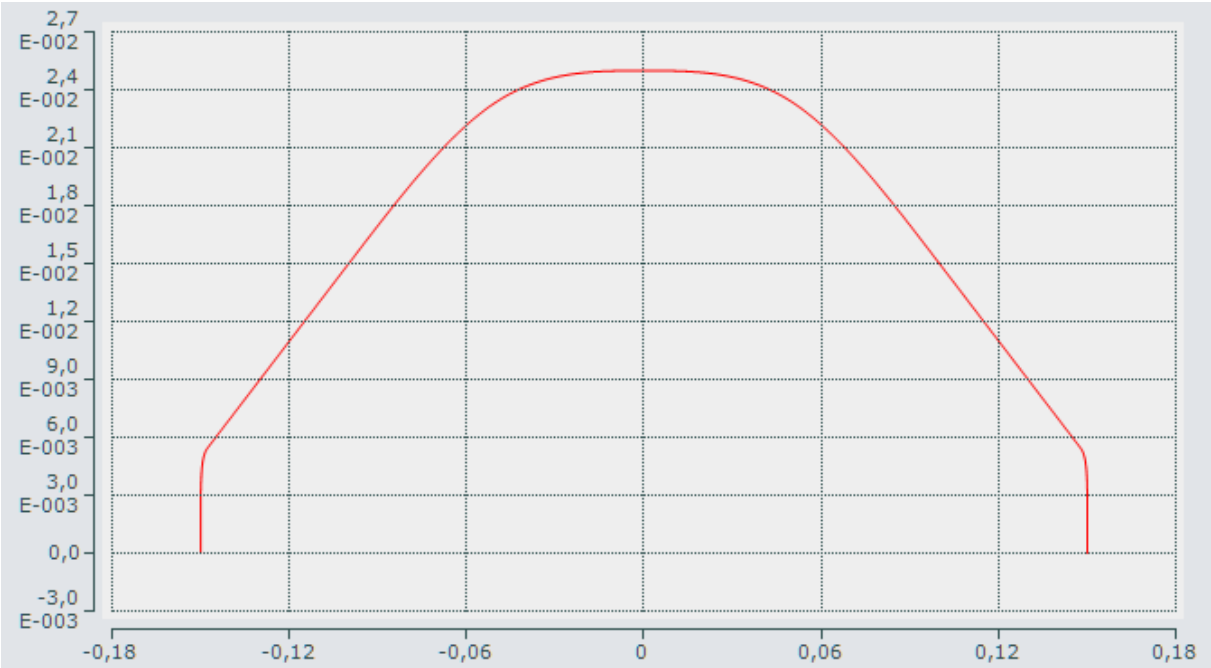

Figure F.15: The path of the end effector in X/Z-plane. The position in Y-axis is omitted since it is constant on 1.

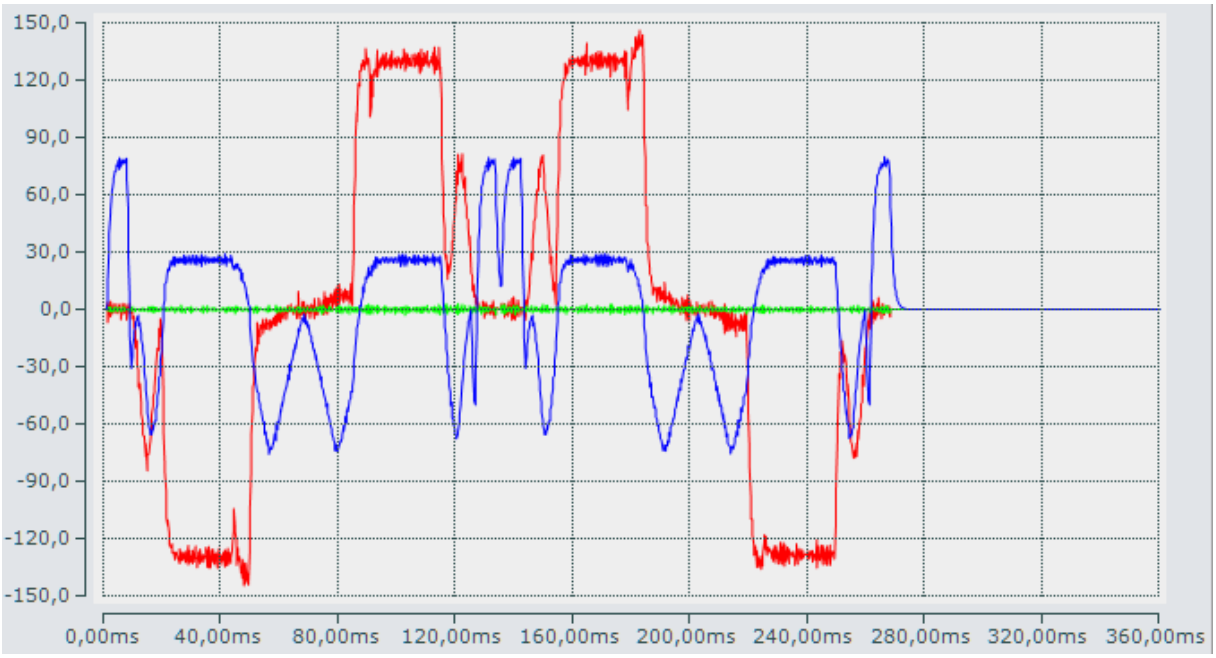

Figure F.16: Acceleration of the end effector in Cartesian coordinates, slightly filtered for readability due to instabilities in measurement data from the ISG kernel.

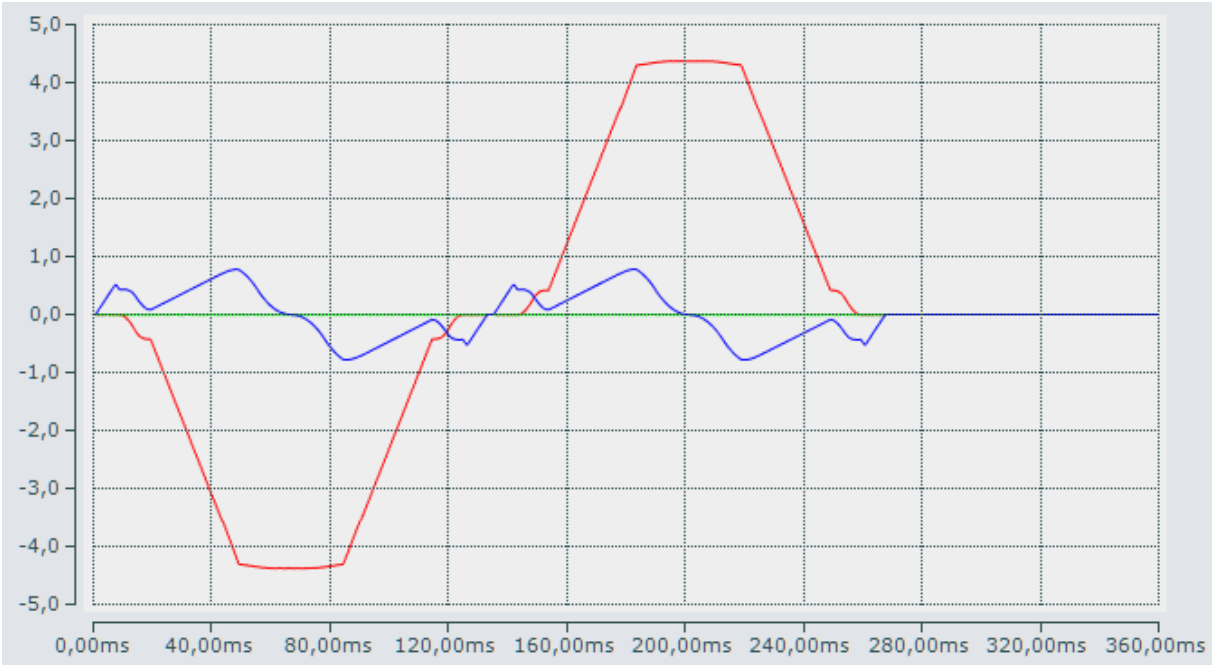

Figure F.17: Velocity of the end effector in Cartesian coordinates.

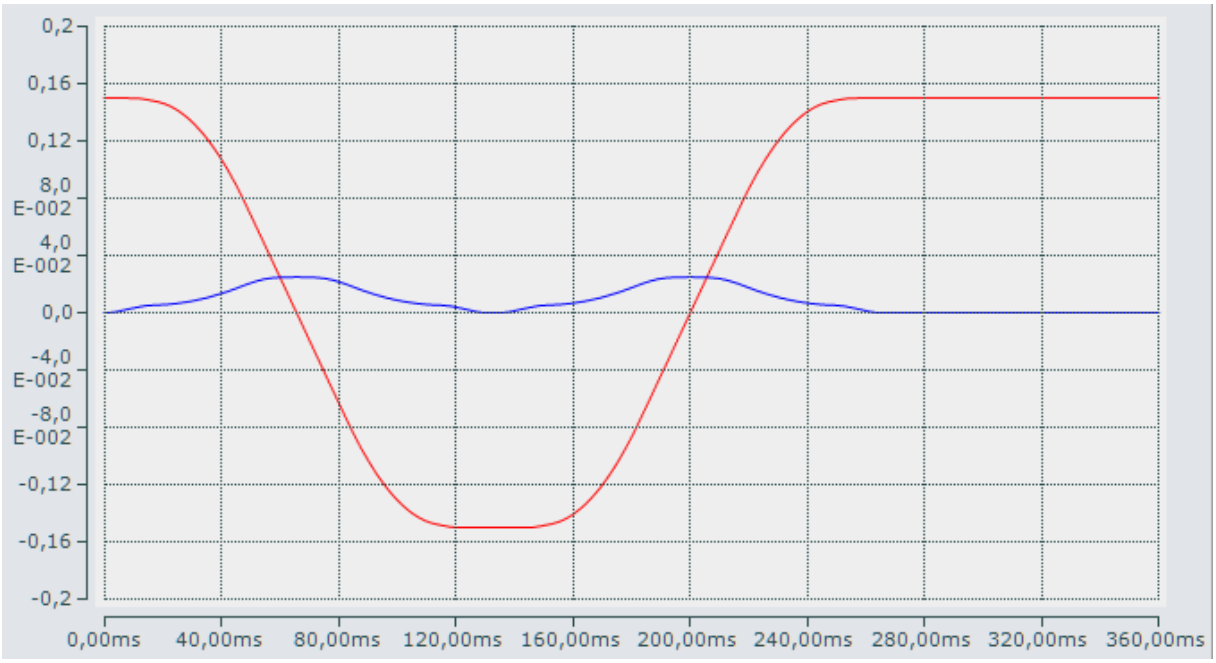

Figure F.18: Velocity of the end effector in Cartesian coordinates. The position in Y-axis is omitted since it is constant on 1.

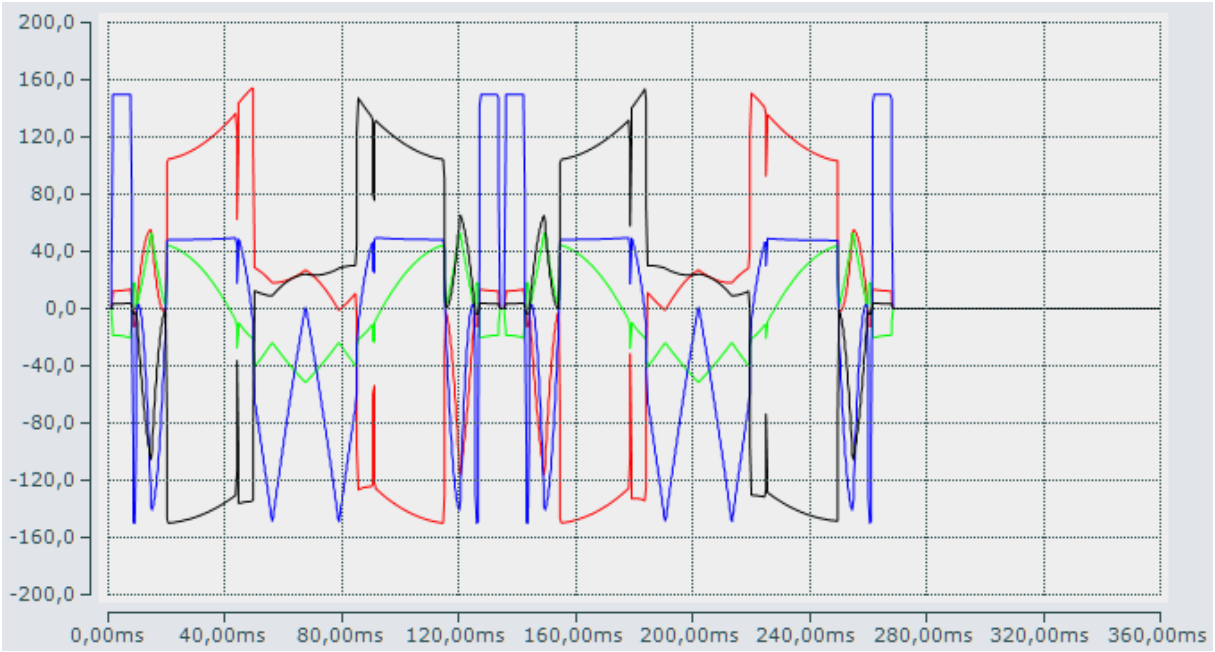

Figure F.19: Acceleration of each joint.

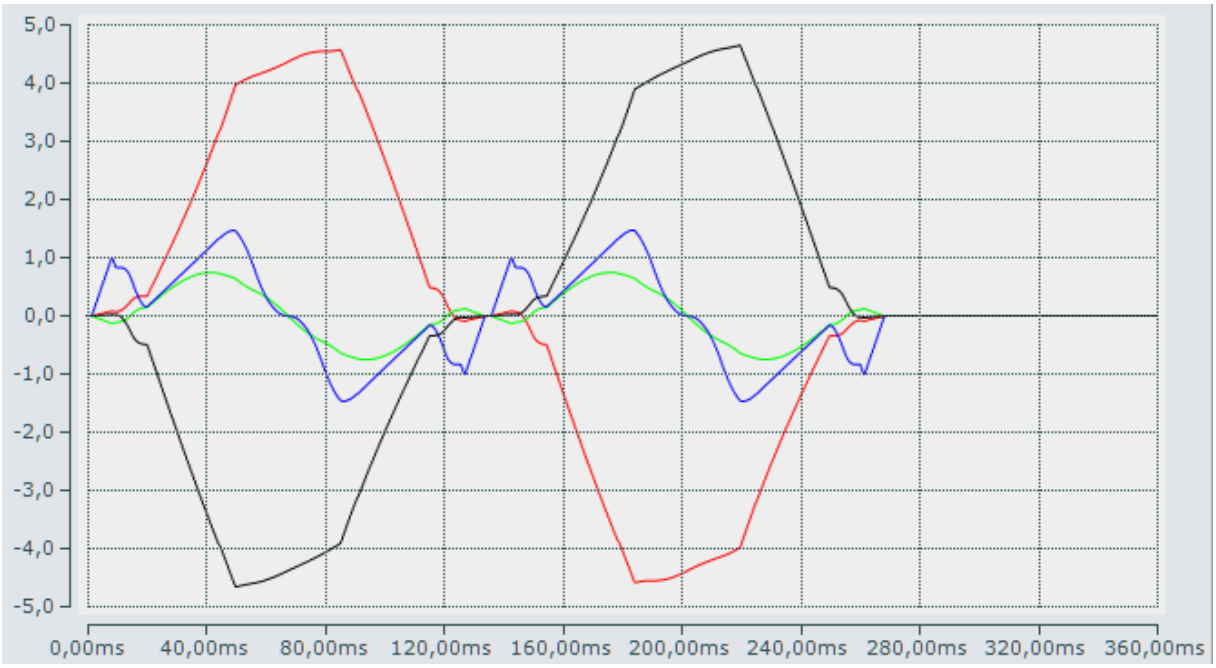

Figure F.20: Velocity of each joint.

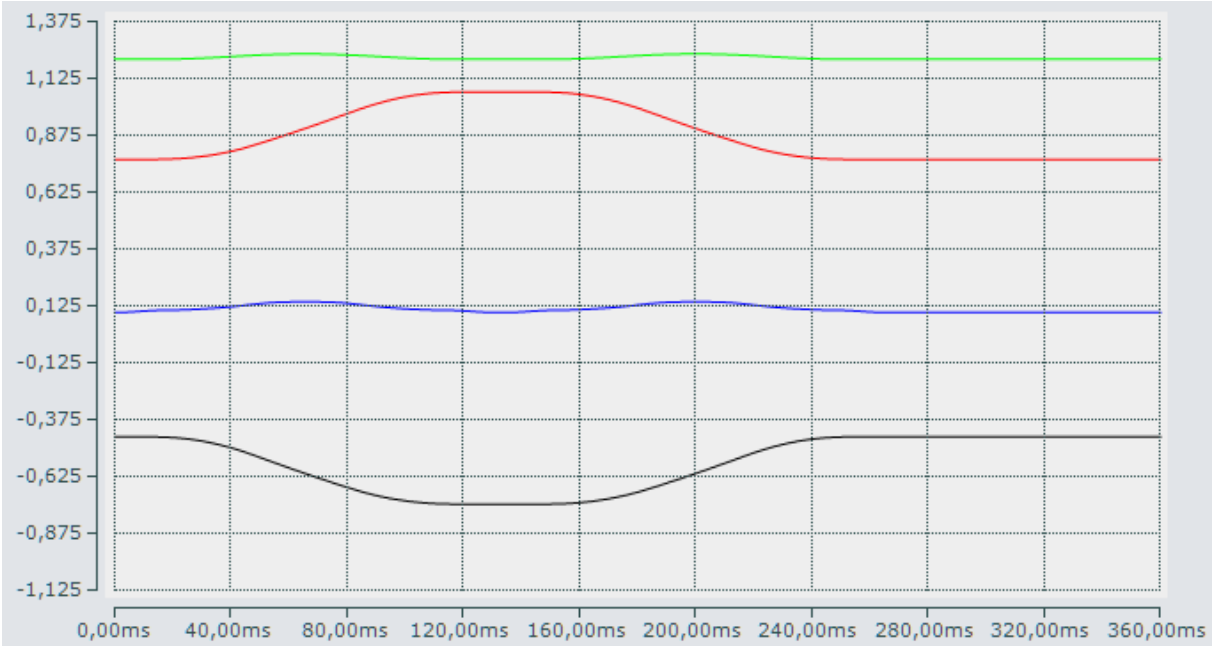

Figure F.21: Position of each joint.

References

[1] Connecting a kinematic transformation. May 2017.

[2] ABB. Product specification irb 910sc, December 2018. Accessed: 2019-04.

[3] ABB. Industrial robots. https://new.abb.com/products/robotics/industrial-robots/, 2019. Accessed: 2019-02.

[4] AST. Robotics & automation bearings. https://www.astbearings.com/robotics-and-automation-bearings.html, 2018. Accessed: 2019-03.

[5] Beckhoff. What's the isg motion control platform? Accessed: 2019-03.

[6] Beckhoff. Twincat - plc and motion control on the pc. https://www.beckhoff.com/twincat/, January 2019. Accessed: 2019-03.

[7] Gunnar Bolmsjö. *Industriell Robotteknik*. Studentlitteratur AB, 2006.

[8] K.S. Fu C.S.G Lee, R.C. Gonzalez. *Tutorial on robotics second edition*. IEEE Computer Society Press, 1986.

[9] Densorobotics. Technical specifications hm-40**/4a. https://www.densorobotics-europe.com/fileadmin/Products/HM-404A/HM_technical_Data_Sheet.pdf. Accessed: 2019-04.

[10] Steven D Eppinger and Karl T Ulrich. Product design and development. 1995.

[11] Grainger. 303 stainless steel shaft collar. https://www.grainger.com/product/RULAND-MANUFACTURING-303-Stainless-Steel-Shaft-45WU15. Accessed: 2019-04.

[12] Mechanicalc INC. Stresses & deflections in beams. https://mechanicalc.com/reference/beam-analysis, 2019. Accessed: 2019-05.

[13] WEN Technology Inc. Power-torque, 2002. Accessed: 2019-02.

[14] ISG. Prospect isg kernel. Accessed: 2019-04.

[15] Richard W. Armstrong Jr. Load to motor inertia mismatch: Unveiling the truth. https://pdfs.semanticscholar.org/f1d3/f1eee2a1a3380eb5cdbc3a605a21c6058bfd.pdf, 1998. Accessed: 2019-02.

[16] makeitfrom. 6061-t6 aluminum. https://www.makeitfrom.com/material-properties/6061-T6-Aluminum/, August 2018. Accessed: 2019-04.

[17] Isaac Maw. The what, why and how of delta robots. https://www.engineering.com/AdvancedManufacturing/ArticleID/16651/The-What-Why-and-How-of-Delta-Robots.aspx, March 2018. Accessed: 2019-02.

[18] Misumi. Precision pivot pins - flanged, threaded with lock nut. https://us.misumi-ec.com/vona2/detail/110300095930/, 2019. Accessed: 2019-05.

[19] B. Nysten, J.-P. Issi, R. Barton, D. R. Boyington, and J. G. Lavin. Determination of lattice defects in carbon fibers by means of thermal-conductivity measurements. *Phys. Rev. B*, 44, Aug 1991.

[20] Erik Oberg, Franklin D Jones, Holbrook L Horton, Henry H Ryffel, and James H Geronimo. *Machinery's handbook*, volume 200. Industrial Press New York, 2004.

[21] PCT. 050611. PCT/EP2019/050611, 2019. Accessed: 2019-01.

[22] PLCopen. Iec 61161-3, 2013. Accessed: 2019-03.

[23] Bosch Rexroth. Synchronous servo motors. https://md.boschrexroth.com/, November 2017. Accessed: 2019-02.

[24] RockWestComposites. 3m scotch-weld epoxy adhesive. https://multimedia.3m.com/mws/media/669980/3m-scotch-weld-epoxy-adhesive-dp420-dp420-ns-dp420-lh.pdf. Accessed: 2019-04.

[25] Mark E Rosheim. *Robot evolution: the development of anthrobotics*. John Wiley & Sons, 1994.

[26] SKF. 7302bep. https://www.skf.com/group/products/bearings-units-housings/ball-bearings/angular-contact-ball-bearings/single-row-angular-contact-ball-bearings/single-row/index.html?designation=7302%20BEP&unit=metricUnit. Accessed: 2019-05.

[27] SKF. Arrangements and their bearing types. https://www.skf.com/group/products/bearings-units-housings/principles/bearing-selection-process/bearing-type-arrangement/arrangements-and-their-bearing-types/index.html. Accessed: 2019-03.

[28] SKF. Bearing preload. https://www.skf.com/binary/12-299896/0901d1968065f1f4-Bearing-preload_tcm_12-299896.pdf. Accessed: 2019-05.

[29] SKF. Bearing selection process. https://www.skf.com/group/products/bearings-units-housings/principles/bearing-selection-process/index.html. Accessed: 2019-03.

[30] SKF. Cast iron plummer block housings. https://www.skf.com/ph/products/bearings-units-housings/bearing-units/ball-bearing-units/y-bearing-plummer-block-units/housing-designs/Cast-iron-pl-bl-hsg/index.htmll. Accessed: 2019-04.

[31] SKF. Tapered roller bearings, single row 30202. https://www.skf.com/group/products/bearings-units-housings/roller-bearings/tapered-roller-bearings/single-row-tapered-roller-bearings/

single-row/index.html?designation=30202&unit=metricUnit. Accessed: 2019-03.

[32] SnDProducts. Heavydutyhinges. https://www.sdproducts.com/heavy-duty-hinges.html, 2019. Accessed: 2019-05.

[33] Outdoor Pro Store Store. Carbon bicycle headset cap. https://www.aliexpress.com/item/Carbon-Bicycle-Headset-Cap-Hanging-Core-Fork-Top-Mountain-Road-Bike-Fork32870806381.html?spm=2114.search0302.3.10.7662626arOO7J8&ws_ab_test=searchweb0_0,searchweb201602_0_453_454_10618_536_317_537_319_10059_10696_10084_10083_10821_10887_10307_321_322_10902_10065_10068_10301_10103_10884_10303_10820,searchweb201603_0,ppcSwitch_0&algo_pvid=bae2f816-fd0e-44f8-bc3f-349e5465c473&algo_expid=bae2f816-fd0e-44f8-bc3f-349e5465c473-1. Accessed: 2019-04.

[34] Technavio. Major types of industrial robots. https://www.technavio.com/blog/major-types-of-industrial-robots, Aug 2018. Accessed: 2019-01.

[35] THK. Sk. https://www.thkstore.com/sk.html. Accessed: 2019-04.

[36] Wilfried Voss. *A comprehensible guide to servo motor sizing*. Copperhill Media, 2007.

[37] Wikipedia. File: Schematic diagram of jerk, acceleration, and speed.svg. https://en.wikipedia.org/wiki/File:Schematic_diagram_of_Jerk,_Acceleration,_and_Speed.svg, January 2016. Accessed: 2019-03.

[38] TB Woods. Tb woods sure-grip bushing. https://www.amazon.com/TB-Woods-Sure-Grip-Bushing-Length/dp/B003H057GW/ref=pd_day0_hl_328_3/141-6862278-8992249?_encoding=UTF8&pd_rd_i=B003H057GW&pd_rd_r=4c6405e6-472b-11e9-b0ce-1582fe71c4d3&pd_rd_w=2ORHg&pd_rd_wg=hUVsc&pf_rd_p=ad07871c-e646-4161-82c7-5ed0d4c85b07&pf_rd_r=DTAA18089MVHVV3DG5MF&psc=1&refRID=DTAA18089MVHVV3DG5MF. Accessed: 2019-03.

[39] P. S. Engineering Works. 2 inch pipe clamp. https://www.indiamart.com/proddetail/2-inch-pipe-clamp-9789302491.html. Accessed: 2019-04.